SYNTHESIS AND APPLICATION OF ORGANIC THIN FILM MODIFIED SURFACES

by

CHANG XU

A dissertation submitted to the Graduate Faculty in Chemistry in partial fulfillment of the requirements for the degree of Doctor of Philosophy, The City University of New York

2005

This manuscript has been read and accepted for the
Graduate Faculty in Chemistry in satisfaction of the
dissertation requirement for the degree of Doctor of Philosophy.

4/28/05 — Date
Chair of Examining Committee

4-28-05 — Date
Prof. Herold Koeppl (ukm.)
Executive Officer

Prof. Charles Michael Drain

Prof. James D. Batteas

Prof. Alexander Couzis
Supervision Committee

THE CITY UNIVERSITY OF NEW YORK

Abstract

SYNTHESIS AND APPLICATION OF ORGANIC THIN FILM MODIFIED SURFACES

by

Chang Xu

Advisor: Professor Charles Michael Drain

The theme of this dissertation is surface modification with thin organic films. In particular, this thesis focuses on self-assembled monolayers and polymer brushes, which are elaborated in the introduction. Following the introduction, tribology behaviors of OTE SAMs on a nanometer scale asperity are presented in chapter 2. Despite most tribology study of SAMs based on atomic flat surface, surfaces naturally occurring are rarely flat. Most surfaces in contact are composed of nanometer scale asperities. Interaction between those asperities dominates the tribology behaviors between surfaces. With silica nanoparticles and AFM tips as mimic of asperities, our work provides new insights of how the underlying surface geometries will affect the SAMs tribology behaviors.

The majority of this thesis is focus on surface modification with polymer brushes. Chapter 3 introduces micro-channel confined surface initiated polymerization (μSIP), a versatile method of engineering surface initiated polymerization. μSIP enables the formation of polymer brushes of complex surface structure. Micrometer level polymer brush patterns were generated with μSIP. This

method was further exploited to synthesize statistic polymer brushes gradient on surface.

Chapter 4 focuses on the synthesis and characterization of gradient statistical copolymer brushes of MMA and HEMA. Gradient statistical copolymer brushes with gradual increase of HEMA segment concentration from surface was synthesized by gradual addition of HEMA to a MMA polymerization solution. The gradient nature of the polymer brushes is evidenced by the gradual change of surface water contact angle measurement. The solvent responsibility of the gradient polymer brushes was also studied.

A combinatorial approach to study the properties of block copolymer brush is detailed in Chapter 5. A serial of block copolymer brush gradients were synthesized. Base on those gradient substrates, we explored how the thickness of each block affects the solvent responsibility of the polymer brushes.

Chapter 6 expands our research from surface modification and characterization to application. The interaction between surface and porphyrin nanoparticle was studied. It was found that the aggregation behavior of porphyrin on surface in greatly affected by surface energy. The strong interaction between porphyrin nanoparticles and surface results in breaking down and collapse of nanoparticles on hydrophilic surface.

This thesis is dedicated to my parents,

Xiuhua Xu and Junyu Wang

and

especially to my wife, Qian Cai,

for all their love and support

BIOGRAPHY

Chang Xu was born in Wuwei, China on July 31, 1977, the second son of Xiuhua Xu and Junyu Wang. He obtained his Bachelor of Science (B.S) in July 1996 from University of Science and Technology of China (USTC), majoring in Biology. In the fall of 1999, he enrolled in the Department of Chemistry of the City University of New York (CUNY), where he began his Ph.D research on polymer and surface science under the direction of Dr. James D. Batteas and Dr. Charles Micheal Drain.

Currently, Chang Xu is working as a Guest Researcher at National Institute of Standards and Technology (NIST). He lives with his beloved wife, Qian Cai, to whom he married in 1999.

ACKNOWLEDGMENTS

I would like to express my sincere gratitude to my mentors, Professor Charles Michael Drain and Dr. James D. Batteas, who gave me the wonderful opportunity to be involved in the field of polymer and surface chemistry and guided me in my every growth step. I would like to acknowledge to Dr. Kathryn L. Beers, who supervised my last year work at the Combinatorial Methods Center of the National Institute of Standards and Technology (NIST).

I thank Alexander Couzis. As my committee members, he gave me sound advice and strong supports.

I would like to give my special thanks to my fellow lab mates, Drs Tao Wu and Ying Mei, they shared a wonderful time and experiences with me.

I also want to give my thanks to my wife, Qian Cai and my parents, Xiuhua Xu and Junyu Wang. It is their love and strong support that enables me to concentrate on my research.

TABLE OF CONTENTS

CHAPTER V: SURFACE-GRAFTED BLOCK COPOLYMER BRUSH GRADIENTS SYNTHESIS AND THEIR APPLICATION IN COMBINATORIAL STUDY OF THE BLOCK COPOLYMER BRUSH PROPERTIES

List of Figures

List of Table and Schemes

Chapter I

Introduction and thesis goal

1.1 Surface modification with organic thin films

Controlling surface properties of materials is of great importance.[1,2] Surfaces and interfaces of solid materials dominate the interactions between solid materials and their surroundings. Numerous methods have been applied to modify surfaces.[3] Coating the surface with organic thin films, such as self-assembled monolayers (SAMs) and polymer brushes, has attracted significant interest since last decade.[3,4] The presence of SAMs or polymer brushes on surface, a layer of chemically bounded molecules or macromolecules, may completely change surface properties such as wetting, conductivity, friction, and biocompatibility.

SAMs are two-dimensional molecular assemblies spontaneously formed on surfaces.[5] A typical molecule that self-assembly on surface possess a head group and a linear alkyl chain, to the end of which often attaches functional groups. While the interaction between the head group and substrate determines the formation and stability of SAMs, the interfacial properties of SAMs mostly rely on their end functional groups. A variety of functional groups have been incorporated into SAMs, ranging from simple organic groups to complex bioactive DNA and protein segments.[6,7]

SAMs modified surfaces have been subject to extensive studies for applications ranging from micro-electro-mechanical system (MEMS) to biotechnology. For their well-defined structure, wide range of end functional groups, and simple preparation methods, SAMs are model systems for the studies of organic and biological interfaces. With recent development in lithographic techniques, SAMs can be patterned on surface with

dimensions down to tens of nanometer, which can further be utilized as templates to construct complex two or three-dimensional structures on surface.[8]

Grafting surface with polymer brushes provides another method to modify surface properties.[4] Polymer chains can either be pre-synthesized in solution before attaching to the surface or propagate from initiating sites anchored on surface. With recent development of surface-initiated polymerization, high-density polymer brushes have been synthesized from SAMs that have initiator moieties as end functional groups.

Taking advantage of the well-established polymerization methods, surface-initiated polymerization have been used to synthesize polymer brushes with various functional groups, controlled grafting densities and thicknesses.[4] Polymer brushes are robust and chemically versatile. The mechanical properties of the polymer brushes can be easily tuned by adjusting their grafting density, thickness and cross-linking density. With living/controlled polymerization, block copolymer brushes were synthesized with surface-initiated polymerization.[9]

Surface-initiated polymerization allows surface modification with advantages of both SAMs and polymeric materials. For example, patterned polymer brushes can be easily fabricated from patterned initiator SAMs.[10] With mixed SAMs of two different initiators, mixed polymer brushes were generated from different polymerization methods.[11] The responsive nature of the polymeric material provides means to construct smart surfaces.[12] With the wide range of functional monomers and well-designed architecture, surface properties can be easily manipulated with polymer brushes.

1.2 Alkylsilane self-assembled monolayers

One way to modify surface properties is through the formation of self-assembled monolayers (SAMs) on surface, which are uni-directional molecular assemblies formed by spontaneous organization of molecules on solid surfaces. Since the discovery of the self-assembly of disulfides on gold by Nuzzo and Allara,[7] studies in self-assembled monolayers have witnessed tremendous growth and propelled advances in numerous other scientific areas.[5]

1.2.1 Structure of self-assembled monolayers

Generally, molecules form SAMs on surface can be divided into three parts (Figure 1.1): active head group, alkyl chain, and end functional group. The strong interaction between the active head group and corresponding substrate provide driving force for the formation of SAMs. The van der Waals forces between alkyl chains also provide additional energy for the formation and stabilization of the SAMs, and become more and more important with increase of alkyl chain length. The properties of the surface were mostly determined by the end functional groups, which either be synthesized prior to the self-assembly or derive from chemical modification of the other end groups after the formation of SAMs. The wide range of end functional groups available, along with the formation of mixed SAMs, provides a convenient way to design and fine tune surface with wide range of properties.

A variety of SAMs have been prepared with different combinations of molecules and substrates. Examples of SAMs include alkylsilane on silicon oxide,[13,14] alkanthiol, dialkyl

sulfide, or dialkyl disulfide on gold,[7, 15,16] carboxylic acids on aluminum oxide[17] or silver[16] *etc.*

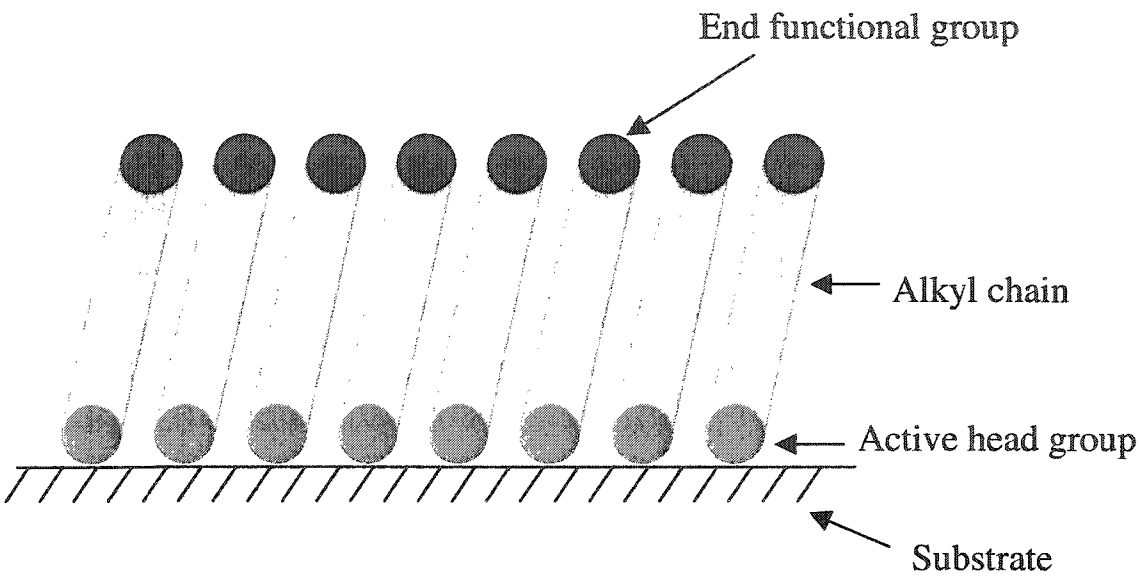

Figure 1.1 Structure of self-assembled monolayers

1.2.2 SAMs of alkylsilane

Among various types of SAMs, SAMs of alkylsilane attract great interests. Alkylsilane self-assemble on various substrates including mica, silicon, glass, poly-dimethyloxysilane and metal oxides *etc.*[5] Alkylsilane SAMs are robust and stable. Due to the covalent nature of the Si-O-Si network between the alkylsilane molecules and surface, alkylsilane SAMs can tolerate high temperature and chemically mechanically robust. In contrary, molecules inside orgnaothiols SAMs on gold constantly exchange

with other organothiols in solution. Once heated above 70°C, molecules begin to dissociate from surface.

1.2.3 Preparation method of alkylsilane SAMs

Alkylsilane SAMs are prepared by the reaction between alkylsilane derivatives R_nSiX_{4-n} (R - alkyl chain, X – Cl, or OR, $1 \leq n \leq 3$) and hydroxylated surfaces. Generally, there are two methods to prepare alkylsilane SAMs on surface: solution method and vapor method.[18] In solution method, the formation of SAMs is accomplished by the immersion of the substrate into a solution of alkylsilane molecules. In vapor method, volatile alkylsilane molecules are first vaporized before they reach the surface. Very often, this evaporation process is facilitated by vacuum or elevated temperature. Despite minimized the deposition of alkylsilane micelles in vapor method, due to limited amount of volatile alkylsilane available and complex experimental setup, most alkylsilane SAMs are prepared with solution methods.

Alkylsilanes typically used to form SAMs can be divided into two categories according to their surface-active head groups: chlorosilane and alkoxysilane. As Si-Cl bond is more active towards surface hydroxyl group and moisture than Si-OR bond, preparation conditions of SAMs differ for those two groups of alkylsilanes. Generally, SAMs formation with trichlorosilane is handled at or below room temperature. However, for the less active alkoxysilanes, high temperature or pre-hydrolysis is required before they self-assemble onto the surface.

The formation SAMs is a condensation process among alkylsilane molecules and surface hydroxyl groups promoted by the trace amount of water absorbed on surface.[19-21] For the formation of silane SAMs on surface, it is required that the surface is hydroxylated. Moreover, the amount of water present in solution is crucial to the synthesis of SAMs on surface. There are two competing processes during the formation of SAMs. A hydrolyzed alkylsilane can reacts with the surface hydroxyl groups to form SAMs or other alkylsilane to form polymer in solution. While formation of monolayers is incomplete in the absence of water,[22] excess water accelerates the polymerization of alkylsilanes, resulting in the formation of micelles on the surface.[23]

Alkylsilane is covalently bounded to the underlying surface and further stabilized by the Si-O-Si networks among alkysilane molecules (Figure 1.2).[3] Thus, alkylsilane SAMs are mechanical robust and chemically stable. It is stable under most organic solvent and acid conditions. For the hydrolysis of Si-O bonds, SAMs are not stable in basic environments. Once deposited on surface, molecules insides SAMs will not be replaced by other molecules in solution. The cross-linking Si-O-Si networks among alkylsilane SAMs are essential to the stability of SAMs. For example, immersed in ethanol, SAMs of trichlorosilane undergoes much less material loss than that of monochlorosilane, where the Si-O-Si network is absent.[24]

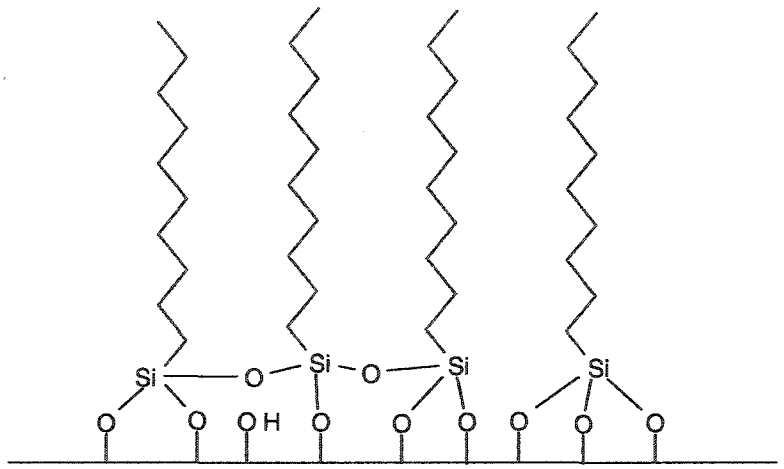

Figure 1.2 Schematic illustration of alkylsilane SAMs

1.2.4 Nanotribology with SAMs

Studying interactions, such as friction, wear and lubrication, between surfaces in relative motion, tribology is an area subject to extensive focus for it practical significance.[25] With the continuous demands of minimizing device sizes in the semiconductor industry and micro-electro-mechanical systems (MEMS),[26] it is required to understand tribology at nanometer scale.

The advent of atomic force microscopy (AFM) greatly accelerated tribology studies.[27] Probing forces between small tips and substrates, atomic force microscopy (AFM) provides a versatile tool to probe surface properties with atomic level resolution. Originally used to probe surface topography by maintaining a constant force between the tip and substrate, AFM is quickly extended to study the adhesion and friction force between the tip and surface at atomic scale and becomes an important tool in the field of nanotribology: the study of tribology at nanometer scale.[28-31] With AFM tip and sample

surface modified by various SAMs, it is easily to study how different parameters, such as end functional groups,[32] alkyl chain length,[33] and environment,[34] affect surface tribology behaviors.

With AFM, it was notified that the surface friction and adhesion of SAMs depends on its end functional groups. Investigation of phase separated mixed SAMs shows that surface with different functional groups can be differentiated in friction images.[32] The alkyl chain length of the SAMs also affects its tribology properties. SAMs of long chain alkylsilane have much lower friction than that of short chain alkysilane.[33] This phenomenon is explained by the relatively conformational disorder in the SAMs of short chain alkylsilane. For the same reason, it was explained why mixed SAMs or SAMs of unsymmetric molecules has much higher friction and adhesion than those of uniform SAMs.

Adhesion between surfaces greatly depends on its environments.[34] Generally, adhesion can be measured in vacuum, liquid or ambient conditions. In high vacuum, the work of adhesion corresponds only interactions between solid surfaces. Under ambient conditions, condensation of water forms capillary around contact area and interferes the measured adhesion force. As a result, adhesion force was affected by air humidity. To overcome this problem, adhesion between two surfaces were measured inside solvent. In this case, the solvation of the surfaces upon the break of contact contributes to the work of adhesion.

The adhesion force between surfaces results in deformation of surfaces, which is best described by JKR or DMT theory of continuum contact mechanics.[35]

$$F_{ad} = n\pi R W_{SMT} \qquad (1)$$

$$W_{SMT} = \gamma_{SM} + \gamma_{TM} - \gamma_{ST} \qquad (2)$$

In the above equation, F_{ad} is the adhesion force between the tip and surface when the tip is separated from surface. n is 3/2 for JKR theory and 2 for DMT theory. R is the radius of the tip. γ_{SM} and γ_{TM} are the surface free energies of surfaces and tip in contact with the medium, respectively. γ_{ST} is the interfacial energy between tip and surface.

1.3 Surface modification with polymer brushes

1.3.1 Synthetic strategies of polymer brushes

Immobilizing polymer brushes on surface can be achieved through either physisorption or chemisorption of polymer chains on surface. Physisorption of polymer brushes on surface relies on strong absorption between surface and polymers (Figure 1.3A).[36-38] Typical polymer brushes physisorpted on surfaces have two functional layers: a bottom anchoring layer that strongly interacts with the surface and a top layer that stretches from surface and forms brushes.

As non-covalent interaction between polymer brushes with the surface is weak, the polymer brushes physisorpted on surface are inherently fragile. Polymer brushes are susceptible to small molecule and polymer contaminants in the environment and thermally unstable.[39,40] Desorption of polymer brushes is inevitable once they are exposed to a good solvent of the anchoring layer.

To overcome above-mentioned deficiencies, a "grafting to" technique were developed to form polymer brushes chemisported on surfaces through covalent bonds (Figure 1.3B).[41-44] In this approach, polymers are first synthesized with functional groups that are capable to react with corresponding functional groups chemically bonded to the surface. The molecular weight and polydisperity of the polymer chains can be pre-designed before they are anchored to the surface. In addition, after deposition, the grafting density of the polymer chain can be calculated from resulting polymer film thickness. However, the polymer initially attached to the surface will establish a diffusion barrier to hinder the reactive chain end of other polymer chains to migrate to the surface. Therefore, synthesizing high grafting density polymer brushes often fails with "grafting to" approach.

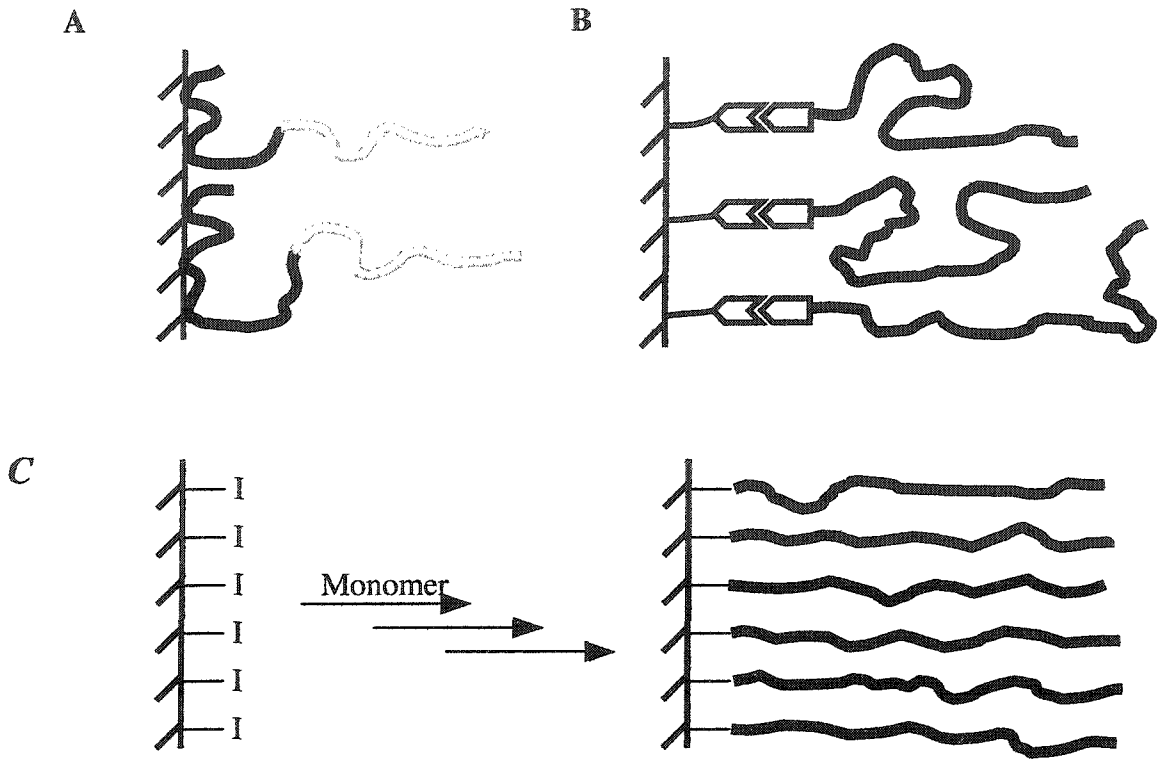

Figure 1.3. Schematic illustration of polymer brush preparation methods: A) physisorption, B) "grafting to" and C) "grafting from" or surface-initiated polymerization.

The latest development in synthesizing polymer brushes covalently attached to surface is surface-initiated polymerization ("grafting from" technique, Figure 1.3C).[4] In this approach, initiator moieties are first immobilized on surface. Subsequent polymerization from surface results in the formation of polymer brushes on surface. Since the monomer is much smaller and has much faster diffusion rate than polymer, it is

more accessible to the surface reactive sites. As a result, polymer brushes with relatively high grafting-densities can be synthesized.

1.3.2 Surface-initiated polymerization

With initiator tethered on surface, surface-initiated polymerization was successfully adopted to growing polymer brushes from various substrates, such as colloid particle[45], carbon nanotube,[46,47] and planar surface.[9,11] For their simple preparation method and high-density packing, self-assembled monolayers were extensively used to introducing initiating sites on planar substrates and colloid particles. For this purpose, molecules contain both surface anchoring head groups and initiator moieties were utilized.[48,49] In an alternative approach, initiator moieties were introduced to the surface through SAMs' active end functional groups after SAMs' formation.[50] Radical, anionic, cationic and ring-opening metathesis polymerizations were all demonstrated to form polymer brushes on surface.

Conventional free radical polymerization has been widely used to synthesize polymers at industrial scale. Since the first example reported by Boven *et al.*,[51] free radical polymerization have been successfully exploited to form PSt, PMMA, MePVP, BuPVP, PAA brushes on surface.[4] With free radical polymerization, a variety of functional polymers were synthesized with controlled grafting densities. However, due to the termination and competing side reaction, the molecular weight of the resulting polymer cannot be controlled. Moreover, conventional radical polymerization failed to produce copolymers with well-defined structures and block copolymer.

To provide control over the growth of polymer chains, surface-initiated living anionic and cationic polymerizations were introduced. With anionic polymerization, Jordan *et al.* synthesized PSt brushes on gold substrate.[52] In a later work by Advincula *et al.*, the living nature of the polymerization was demonstrated by the formation of block copolymer brushes of PSt b-polyisoprene and polybutadiene-b-polystyrene.[53] Zhao *et al.* utilized carboncationic polymerization to prepare PSt brushes.[54,55] The polymerization was proven to be living as further growth of PSt was successful upon reinitiating the polymer chain ends. Despite their living nature, the vigorous polymerization condition and limited monomer functionality prevent anionic and cationic polymerization from wide application in surface-initiated polymerization.

Controlled/living radical polymerizations (CRP), especially atom transfer radical polymerization (ATRP), are extensively utilized in surface-initiated polymerization. In the past decade, CRP techniques, such as nitroxide-mediated radical polymerization (NMP),[56] reversible addition-fragmentation chain transfer (RAFT),[57] ATRP,[58] underwent tremendous development and have prepared a large varieties of materials.

Among all living polymerization techniques, for its mild polymerization conditions, wide range of functional monomer, ATRP is mostly used to grow polymer brushes from surface.[4]

1.4 Surface-initiated atom transfer radical polymerization

As one of the most important advance in polymerization strategies within last decade, ATRP is used to synthesize polymers with controlled molecule weight and narrow molecular weight distributions. A variety of monomers, such as styrenes, acrylates, methacrylates, and acrylamides, have been successfully polymerized with ATRP.[59,60] With initiator moieties immobilized on surface, surface-initiated ATRP immediately became the most versatile method to synthesize polymer brushes from surface.[61]

1.4.1 Mechanism of atom transfer radical polymerization

In traditional radical polymerization, the radical concentration is so high that extensive bimolecular radical coupling and disproportionation lead to the termination of propagating chain ends. In ATRP, those chain termination processes are minimized by the "persistent radical effect".[62] A typical ATRP system is composed of monomer, initiator, transition metal species and ligand. Figure 1.4 showes a general mechanism of ATRP. The transition metal complex undergoes reversible one-oxygen oxidation by abstraction of a halogen atom from a dormant species, R-X, to form an active radical species and an oxidized transition metal complex (persistent radical). The propagation of polymer chain is accomplished by addition of monomer to the active radical species. The active species can also reacts with the oxidized transition metal complex and regenerate the dormant species. At the beginning of the polymerization, active radical species undergoes fast irresversible bimolecular coupling and disproportionation. Therefore, the active radical concentration decreases and persistent radical concentration increases. The trend continues until the concentration of the active radical is so low that the active

radical reacts much faster with persistent radial to form dormant species than other active radicals.

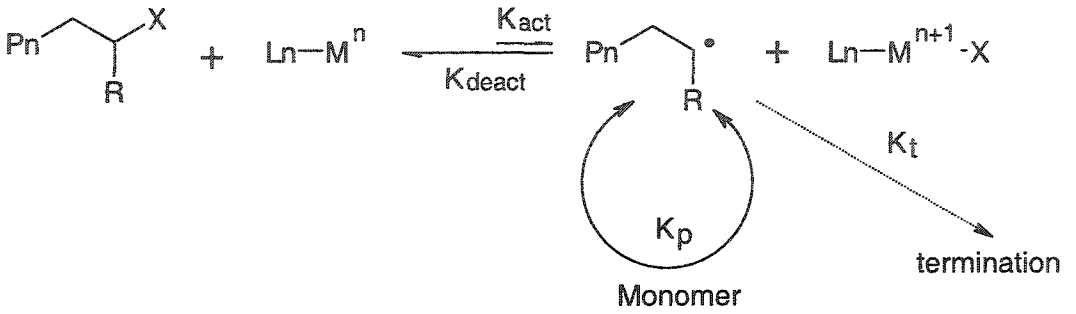

Figure 1.4 Mechanism for atom transfer radical polymerization

ATRP can be carried out in bulk, solution or emulsion.[59,60] For the radical nature of the polymerization, protic solvent such as alcohol and water can be used. The selection of protic solvent often is necessary to dissolve polar monomers and their polymers.

1.4.2 Copolymer synthesis with ATRP

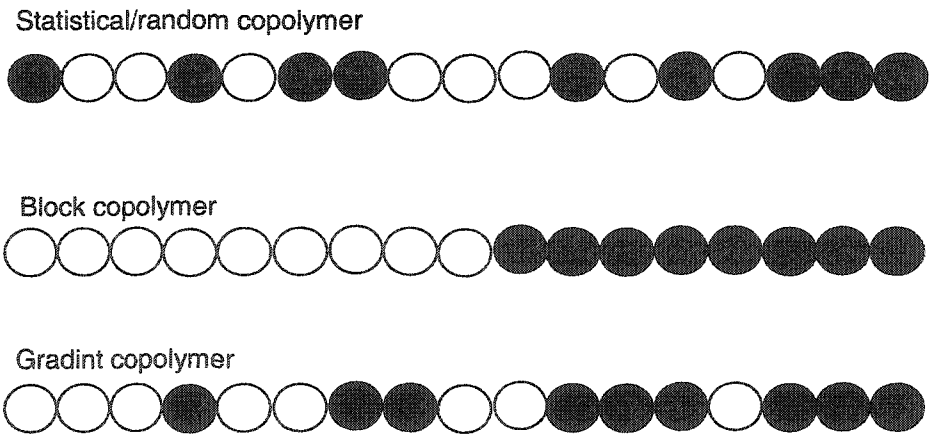

Figure 1.5 Copolymer synthesized with ATRP

Exploiting the "living" nature of ATRP, a variety of copolymers have been synthesized (Figure 1.5). As almost all propagating chain ends stay reactive throughout the polymerization, any variation of composition inside the polymerization solution will affect all polymer chains. Therefore, the composition of each monomer along the polymer chains can be easily controlled. In one case, by gradual change monomer composition from one to the other, gradient copolymer can be synthesized.[63] In ATRP, the propagating chain ends remain active after polymerization, allowing subsequent polymerization of a second monomer and formation of block copolymers.[64,65]

1.4.3 Surface –initiated atom transfer radical polymerization

In ATRP, the success of the polymerization depends on the equilibrium established between dormant species and active radical species. One challenge for surface initiated polymerization is the trace amount of initiating sites available on surface. To circumvent this problem, free initiator is added to the polymerization solution.[56] After the polymerization, the free polymer could be analyzed with conventional methods. It is found that resulting polymer brush thickness increases linearly with the molecular weight of the free polymer in solution, suggesting that the polymerization is controlled.

Later, it was demonstrated by Matyjaszewski and co-workers that surface initiated ATRP can be controlled even without the addition of free sacrificial initiator.[62] In their approach, the polymerization equilibrium was established through the extra Cu(II) species added to the polymerization solution as deactivator. The controlled aspect of their polymerization was evidenced by the linear increase of polymer brush thickness with polymerization time. Since there are no free polymer chains formed in solution, the

resulting polymer brushes can be easily cleaned by simply rinsing the surface with solvent. In contrary, for polymer brushes formed with the presence of free initiator, long time solvent extraction is necessary to remove the entangled free polymer chains from polymer brushes.

After the initiator moieties containing molecules (Figure 1.6) self-assembled on surface, surface-initiated ATRP was successfully carried out with conditions similar to that in solution ATRP upon the addition of free sacrificial initiator or deactivator. Most surface-initiated ATRP reported so far are catalyzed by copper based system. For example, PSt brushes were synthesized at 100 °C with bipyridine. PMMA brushes were synthesized at 70 °C with PMDETA.[62] With Me_4Cyclam, PMMA brushes were synthesized at room temperature.[66] Polymerization at low or room temperature allows the formation of polymer brushes on temperature sensitive materials.

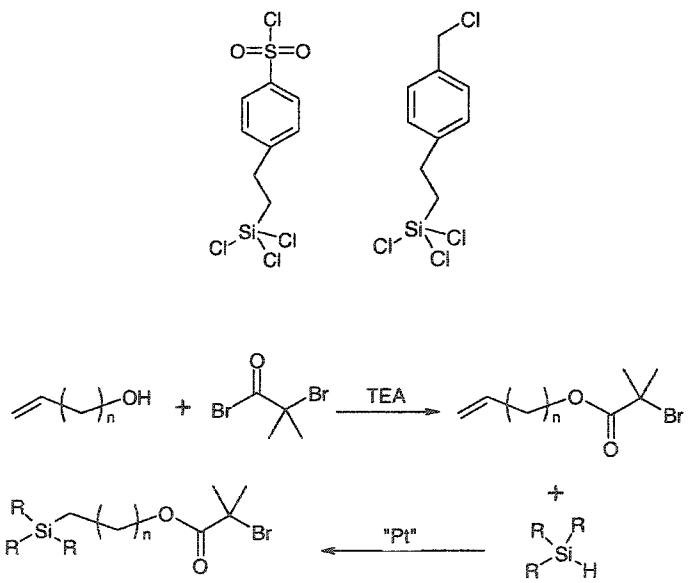

Figure 1.6 Commercial and lab synthesized chemicals to immobilizing ATRP initiator moieties on surface through self-assembled monolayers.

Water accelerated ATRP was also adopted into surface initiated polymerization.[67,68] Huck *et al.* reported the fast growth of thick PGMA brushes on surface in water at room temperature. With methanol as co-solvent, fast growth of PMMA brushes thickness was observed at room temperature with bipyridine as ligand. Here, an interesting observation was that even the polymerization was carried out in non- solvent of the resulting polymer, the polymerization proceeds in a controlled fashion with thickness of polymer brushes increase linearly with polymerization time.[67] Water accelerated polymerization was also utilized to synthesize extreme thick PHEMA brushes (thickness up to 700 nm) with polymerization time extended overnight.[69]

The living nature of surface-initiated ATRP was exploited to synthesize block copolymer brushes. Bruening *et al.* synthesized PHEMA-b-PDMAEMA.[70] With addition of excessive amount of Cu(II) species to the polymerization solution, high retention of the end-functional group for the re-initiation of the second block was achieved. Further extension of this approach results in ABC and ABA type triblock copolymers.

Monomers successfully utilized for surface-initiated ATRP include styrenes, (meth)acrylates and acrylamides. Surface-initiated ATRP has also been expanded to grow polyelectrolyte brushes on surface. Huck *et al.* showed that polyelectrolytes brushes could be directly synthesized from ionic monomers in a controlled fashion.[71] Through room temperature polymerization of ethylene glycol dimethacrylate (EDGMA), Huang *et al.* synthesized cross-linked polymer brushes on surface.[72] With functional monomers, the resulting polymer brushes can be further modified. For example, through esterification of the hydroxyl groups, a variety of functional groups were attached to the

poly (2-hydroxyethyl methacryalte) brushes; pH sensitive poly (methyl methacrylic acid) brushes were derived from hydrolysis of poly (tert-butyl methacrylate) brushes;[62] non-fouling positive charged brushes were synthesized from quantanization of poly ((2-dimethyl amino)ethyl methacrylate) brushes.[73]

1.5 Surface engineering with polymer brushes

1.5.1 Responsive polymer brushes

Polymer can response to the environmental stimuli such as pH, temperature, electric field and solvent. Therefore, polymer brushes can form responsive surfaces. The simplest responsive surfaces are constructed from responsive homo-polymers brushes. One example of such polymers is PNIPAM, a well-studied thermal responsive polymer. Once heated above its LCST, PNIPAM undergoes reversible transition from hydrophilic to hydrophobic. Huck *et al.* reported the swelling behavior of PNIPAM brushes in water.[68] As the system is heated up, a decrease in PNIPAM brush thickness was observed around its LCST, suggesting collapse of polymer brushes. Jiang et al applied PNIPAM brushes to control the wettablity of the surface.[74] The modified surface is hydrophilic below PNIPAM's LCST while hydrophobic above PNIPAM's LCST.

Responsive behaviors were also observed from block copolymer brushes and mixed polymer brushes (Figure 1.7). Brittain *et al.* reported the responsive behavior of copolymer brushes is PSt-PMMA brushes with selective solvent treatment.[75] After treating the surface with dichloromethane, a good solvent for PMMA and non-solvent for

PSt, the surface was featureless under AFM and surface water contact angle was close to that of PMMA. After treating the surface with cyclohexane, a theta solvent for PSt and non-solvent for PMMA, irregular wormlike structure appeared and surface water contact angle became close to that of PSt. This switch of surface properties is attributed to the rearrangement of the each block inside the polymer brushes during solvent treatment. During cyclohexane treatment, PSt segments swell and migrate to the surface while PMMA segments collapse. This process is reversed when the surface is treated with dichloromethane. As a result, the surface properties switch back and forth with selective solvent treatment. Based on the same mechanism as block copolymer brushes, surface with switching properties were synthesized with mixed polymer brushes of PSt and PMMA.

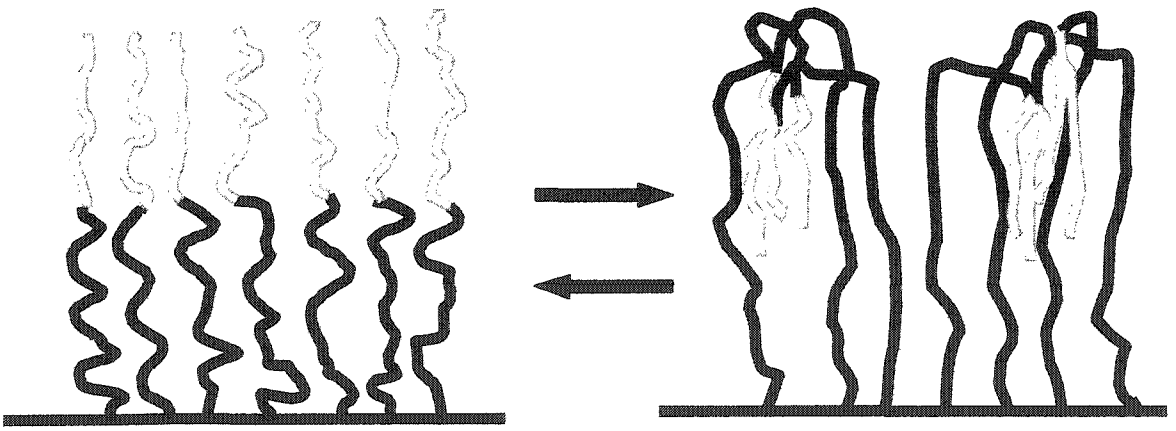

Figure 1.7 Schematic illustration of solvent response of block copolymer brushes

1.5.2 Polymer brush gradients

Improving efficiency and reducing cost, combinatorial studies have permeated into numerous areas of scientific studies. In particular, surface composition gradients have allowed fast screening the properties the modified surface, such as biomaterial-cell interaction,[76] thin polymer film phase behavior[77] and nanoparticle deposition.[78]

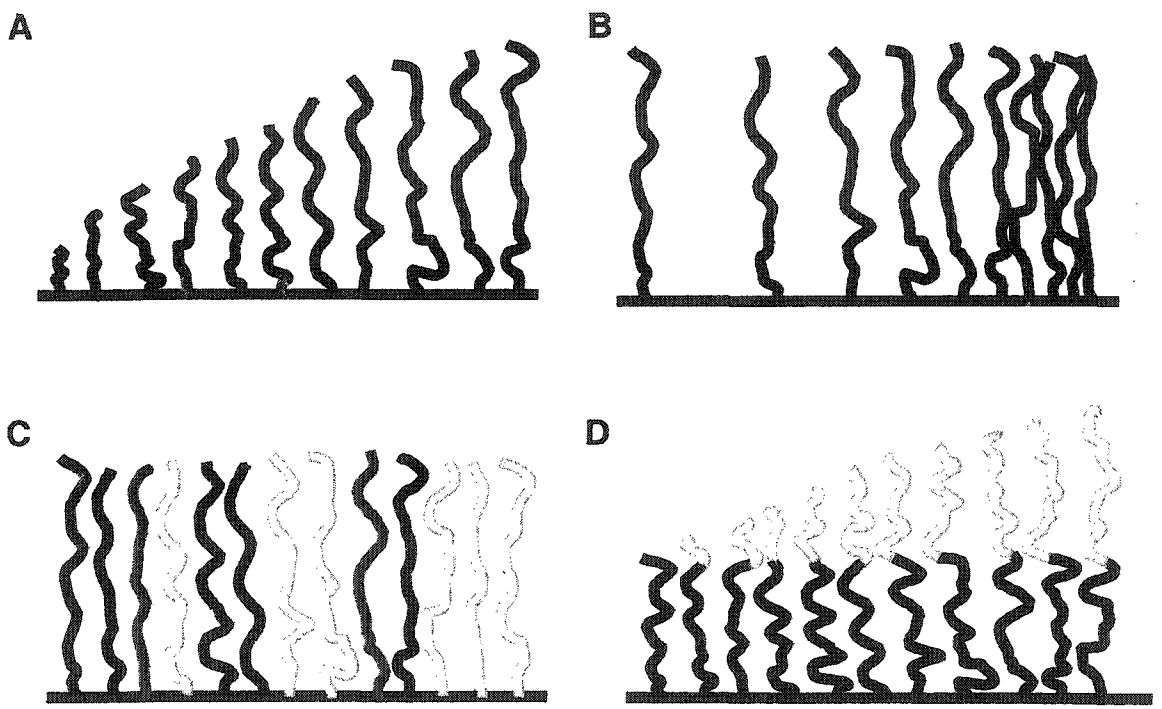

Figure 1.8 Surface gradient synthesized from polymer brushes. A) Molecular weight gradient; B) Grafting density gradient; C) Mixed gradient polymer brushes; D) Block copolymer gradient.

Several methods have been developed to produce composition gradient on surface with different length scales.[79] With recent development in polymer brushes synthesis, especially surface-initiated polymerization, various polymer brushes gradient have been

synthesized.[80-83] For example, slowly removed from the polymerization solution, surface with polymer brush molecular weight gradient was synthesized (Figure 1.8a).[80] With same approach, reinitiating from synthesized polymer brushes resulted in block copolymer gradient surface (Figure 1.8d).[81] Through a surface initiator concentration gradient SAMs on surface, surface with polymer brushes grafting density gradient was prepared (Figure 1.8b).[82] From mixed SAMs of two different initiators that have opposition gradient profile to each other, mixed polymer brushes gradient was synthesized by sequential surface-initiated polymerization with different polymerization methods (Figure 1.8c).[83]

1.6 Thesis goals and objectives

The theme of this dissertation is surface modification with thin organic films. In particular, self-assembled monolayers and polymer brushes are the focuses of study.

Tribology behaviors of OTE SAMs on a nanometer scale asperity are presented in chapter 2. Despite most tribology study of SAMs based on atomic flat surface, surfaces naturally occurring are rarely flat. Most surfaces in contact are composed of nanometer scale asperities. Interaction between those asperities dominates the tribology behaviors between surfaces. With silica nanoparticles and AFM tips as mimic of asperities, our work provides new insights of how the underlying surface geometries will affect the SAMs tribology behaviors.

Chapter 3 introduces micro-channel confined surface initiated polymerization (μSIP), a versatile method of engineering surface initiated polymerization. μSIP enables the formation of polymer brushes of complex surface structure. Micrometer level polymer brush patterns was generated with μSIP. This method was further exploited to synthesize statistic polymer brushes gradient on surface.

Chapter 4 focuses on the synthesis and characterization of gradient statistical copolymer brushes of MMA and HEMA. Gradient statistical copolymer brushes with gradual increase of HEMA segment concentration from surface was synthesized by gradual addition of HEMA to a MMA polymerization solution. The gradient nature of the polymer brushes is evidenced by the gradual change of surface water contact angle

measurement results. The solvent responsibility of the gradient polymer brushes was also studied.

A combinatorial approach to study the block copolymer brush properties is detailed in Chapter 5. A serial of block copolymer brush gradients were synthesized. Base on those gradient substrates, we explored how the thickness of each block affects the solvent responsibility of the polymer brushes.

Chapter 6 expands our research from surface modification and characterization to application. The interaction between surface and porphyrin nanoparticle was studied. It was found that the aggregation behavior of porphyrin on surface in greatly affected by surface energy. The strong interaction between porphyrin nanoparticles and surface results in breaking down and collapse of nanoparticles on hydrophilic surface.

Chapter II

Tribology behavior of OTE SAMs on surface with nano-sized curvature

2.1 Introduction

For the past several years there has been a significant interest in the use of self-assembled monolayers (SAMs) as lubricants for the micro-electro-mechanical systems (MEMS) devices.[1-4] As such the details of friction, adhesion and wear for SAMs on Si surface can be investigated as model systems to explore the trobological properties of these materials.[2] With AFM, it is possible to establish the relationship between the structure of SAMs and their tribology behaviors with molecular level details.[2] For example, the effect of, changing the end-functional group chemistry, inter-chain lateral interactions, chain length, chain entanglement, and head groups all impact the triboogical behaviors in such systems.[5-10]

Many nanotribological studies have used AFM to examine SAMs on atomically flat surfaces with the AFM tip acting as a model for the nanoscopic asperities encounters in real contacts. Surfaces that appear smooth on the macroscopic scale, upon closer inspection are found to typically consist of nanometer scaled asperities (typical on the order of 10 nanometers) whose intentional or accidental interactions ultimately control adhesion, friction and wear at the contacting interfaces.[11] The size of these asperities becomes particularly important when one considers that the true contact area between interfaces for the distribution of load is localized through asperity-asperity interactions where extremely high-pressures can be produced as they contact each other, sharply increasing local stress fields that can cause materials to yield and shear as they encounter each other during sliding and intermittent contact. In addition to load distribution at nanoscale asperity-asperity contacts, their size will influence surface wetting and

adhesion due to capillary forces localized at the contacts.[12] Additionally, the structure of applied lubricant films will be highly dependent upon asperity curvature and may significantly differ from those on flat surface. Additionally, in MEMS devices, surface roughness may be intentionally introduced to reduce the stiction between surfaces in contacts.[12] However, these same asperities however must later resist wear during controlled or accidental contact during device operation. Functioning as a protective protect lubricant layer in such systems, self-assembled monolayers (SAMs) of alkylsilane and fluorosilane compounds with chain lengths ranging from C_{10}-C_{18} have been shown to be useful in the reduction of friction and adhesion in MEMS. It is essential to understand the tribological behavior of SAMs on such nanoscopic asperities. In most studies, SAM modified AFM tips are frequently used and it is assumed that the SAMs on AFM tip are identical in structure to those on a flat surface.[13-22] Such an assumption however may be completly invalid, especially for AFM tips with sub-10 nm radius of curvature.

In this chapter, the triboloigcal behavior of OTE SAMs on asperities with nano-sized curvature were studied and compared with OTE SAMs on flat Si surfaces. To achieve this goal, AFM tips and silica nanoparticles were exploited to mimic nanoscale asperities. The adhesion and friction between OTE SAMs and bare silica surface was investigated under aqueous environments. Additionally, time dependent behavior of the measured adhesion between silica surfaces was studied, which may provide essential information toward understanding the nature of the monolayers used in these studies.

2.2 Experimental Section

2.2.1 Materials.

H_2O_2 (30% reagent grade) and concentrated NH_4OH, tetrahydrofuran (THF) were ordered from Fisher. Colloidal silica OX-50 was obtained from Degussa and dispersed in a sol at ~ pH 13. Octadecyltriethoxysilane (OTE), $CH_3(CH_2)_{17}Si(OCH_2CH_3)_3$ was purchased from Gelest. All chemicals were used as received without further purification. High purity water was obtained using a Barnstead EASYpure RF system with resistivity no less than 18.2 MΩ·cm.

2.2.2 Formation of OTE SAMs on surfaces.

Si(100) substrates (Virginia Semiconductor) and AFM tips (Veeco) were cleaned and hydroxylated in a 4:1:1(v:v:v) mixture of H_2O, 30% H_2O_2 and NH_4OH at 80°C for 10 minutes. The substrate were then thoroughly rinsed with high purity H_2O and dried. Thin films of colloidal silica were formed by spin-coating (Headway Research, Garland, TX) onto cleaned and oxidized Si(100) wafers. Monolayer films of OTE were prepared on cleaned and oxidized Si(100), silica nanoparticle films and cleaned and oxidized Si AFM tips through self-assembly. The OTE monolayers were prepared using a stock hydrolysis solution composed of 0.25g OTE, 0.75 ml of ~ 6M HCl and 20ml THF. The solution is then stirred for a minimum of 4 hrs prior to use. Film formation is carried out in a Wheaton staining jar, using 1ml of the stock OTE solution and 20 ml of cyclohexane. After 3 hours, the substrates and/or tips are removed, sonicated in THF and placed under vacuum at ambient temperature overnight.

Prior to the AFM measurements, the OTE film quality on each sample substrate was checked with sessile contact angle using a homebuilt system incorporating a sample stage and a digital camera interfaced with a PC to allow for digital analysis of the contact angle. For ideal OTE films on Si(100) and nanoparticle surfaces we typically observe water contact angles of ~ 110° and 120° respectively. As a comparison, clean hydroxyl terminated Si(100) and silica nanoparticle surfaces in both cases show contact angles less than 10°.

2.2.3 Tribology study with AFM

AFM images and force-distance measurements were made with a Molecular Imaging PicoSPM (Phoenix, AZ) coupled with RHK Technology SPM 1000 Electronics Revision 8 (Troy, MI). The experiments employed commercially available Si cantilevers (Silicon MDT, Tallinn, Estonia), with a nominal force constant of ~ 0.12N/m and average tip radii of ~ 10 nm. All data are collected in high purity water at pH 2 - 3 and room temperature (22 ± 3 °C). The pH value of the solution was adjusted with HCl and NaOH. This pH was slected as this is the isolectric point for the native oxide on Si ad allows for the exposed rsgions of the surfaces to remain fully hydroxylated. The adhesion forces between the AFM tip and surface were determined from pull-off forces of the force-distance curves. A minimum of xx force distance curves were obtained for each measurement. The rates of the measurements were controlled both by variation of the approach and retract rate as well as the residence time of the tip on the surface or off the surface during a single F-z sweep.

2.3 Results and discussion

2.3.1 Adhesion between OTE SAMs

First, the adhesion between octadecyltriethoxysilane (OTE) modified AFM tips and OTE modified substrates were investigated. To eliminate capillary forces induced by humidity in air, all measurements were carried out in water at pH 3. Two different systems were studied according to the substrates used to immobilize OTE SAMs. In System 1 (S1), a Si(100) substrate was used while in System 2 (S2), a nanoparticle film composed of spin coated silica nanoparticles was employed. Following the formation of OTE SAMs on the surface, topographic images were collected by AFM. Despite some micelles deposition on the surface, most surface areas on OTE modified Si(100) substrate are flat with RMS roughness less than 0.1 nm, as revealed by AFM topographic image of the surface. During force measurements, areas with micelles were avoided and only flat surface areas were studied. In contrast, the OTE modified nanoparticle films, surfaces are rough and individual particles can clearly be identified in the AFM images (Figure 2.1). For the adhesion measurements on the nanoparticles, only the highest particulate asperities in the topographic images were selected for acquisition of force-distance data to eliminate interference from neighboring particles on a given particle-tip interaction. Re-imaging of the surface following force-distance data acquisition, indicated that the nanoparticles were not displaced by any of the measurements.

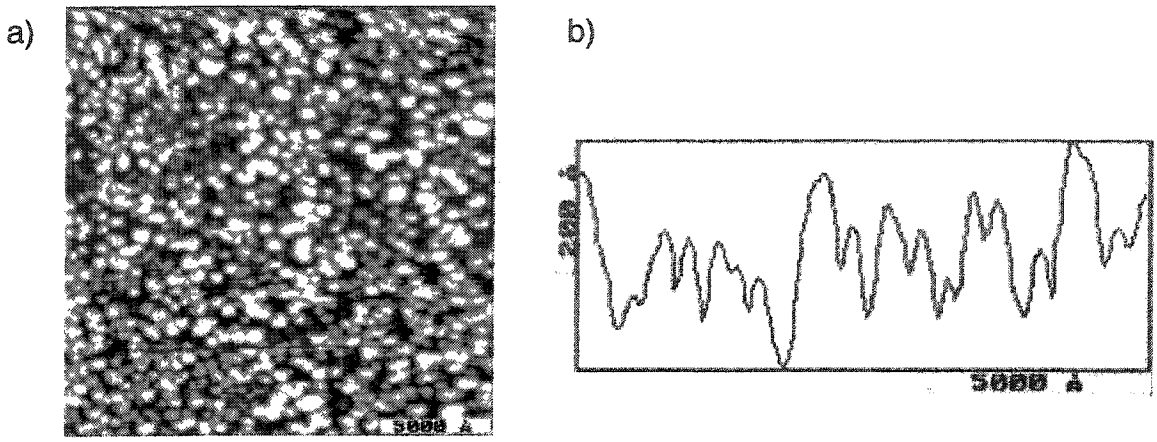

Figure 2.1 AFM topographic images of OTE modified nanoparticle surface.

Figure 2.2 shows the measured adhesion forces for each class of sample. In both cases, the same OTE modified tip was used. More than 15 times the adhesion force was measured on OTE modified flat Si surface than on OTE modified silica particle surface. Moreover, the adhesion forces on the OTE modified silica nanoparticle surfaces clearly show a dependence on the tip approach/retract rate used during F-Z data acquisition whereby higher adhesion forces were always observed when slower tip approach /retract rates were used. Based on the JKR model, the adhesion force between the two surfaces are directed proportional to their reduced radius.

$$F_{ad} = -4/3\pi W_{ad} R$$

where $R = R_1R_2/(R_1 + R_2)$ and R_1 and R_2 is the respective radii of two surfaces in contact. Considering that the nominal dimension of the AFM tip is ~ 10 nm and average diameter of the silica nanoparticles is ~ 50 nm, the reduced radius of the tip on nanoparticle surface is ~ 30 % less than that on flat surface, The small difference in reduced radius

alone cannot explain the large discrepancy in the adhesion forces. Therefore, most of the reduction in adhesion must be rooted from the molecular nature of the OTE SAMs on surfaces.

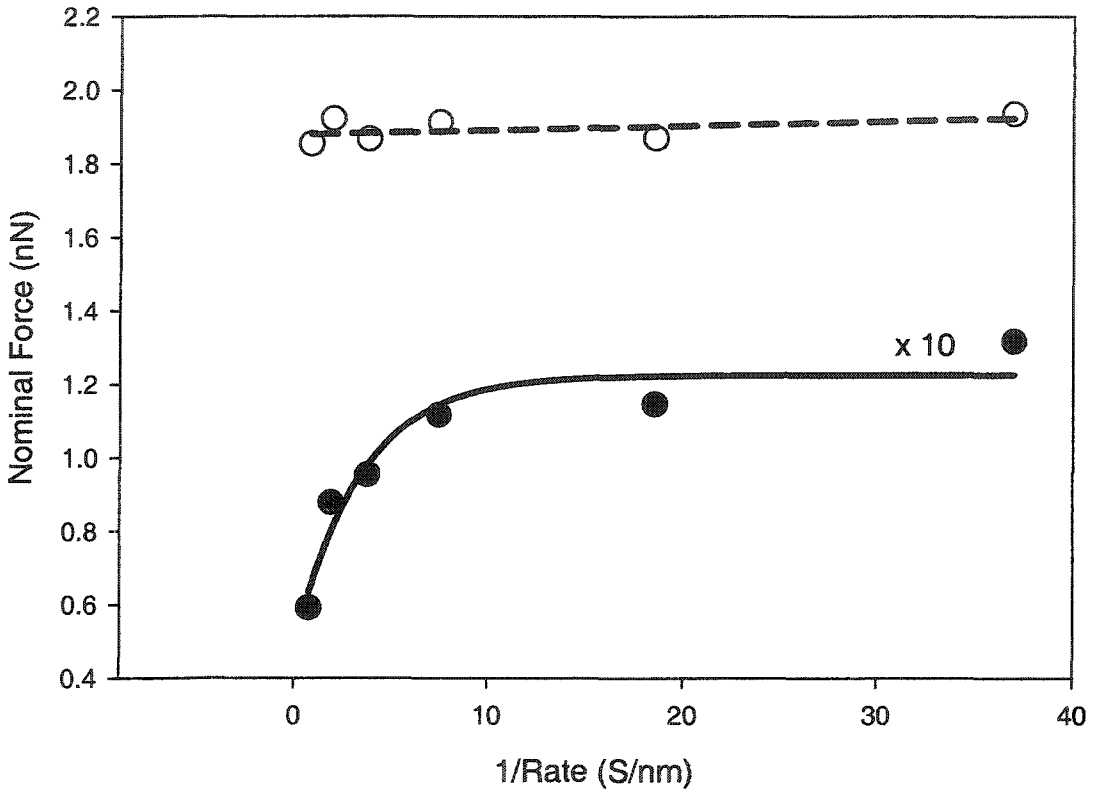

Figure 2.2 Adhesion forces between OTE modified AFM tip and surfaces.

2.3.2 Tribology behaviors between OTE SAMs and bare silica surfaces

The above results indicate that surface curvature has strong impact on the adhesion between OTE SAMs. To further address this issue, we explored the tribology behavior of two more systems: System 3 (S3) a cleaned and hydroxylated silicon AFM tip and an OTE SAM on a flat Si surface and System 4 (S4) and OTE coated Si tip and flat cleaned and hydroxylayed silicon surface (Fig. 2.3). In both systems, the interaction is between a hydrophobic OTE SAMs surface and a hydrophilic hydroxylated Si surface. The only difference is which surface is functionalized with OTE, was on the flat surface in S3 and on the curved surface of the AFM tip in S4. During force measurements, identical experimental conditions were used for each system.

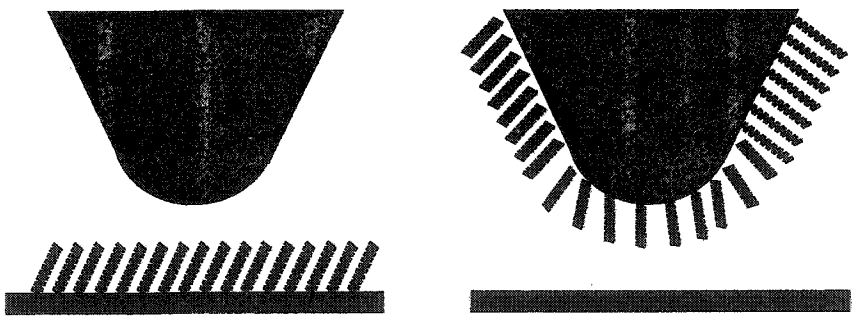

a b

Figure 2.3 Two systems studied in this experiment for friction and adhesion. a) Silicon tip and OTE coated flat surface; b) OTE coated tip and flat silicon surface

Compared with the first two systems, these two have some advantages experimentally. First, as the OTE modifies only one side of the surfaces in contact, there no OTE chain entanglements can occur during the force measurements. Second, in both cases, the substrate surfaces are atomic flat and therefore allow measurement and comparison of friction forces between the two systems. This was not possible for the nanoparticle films as the particulatre studes of the surface inadvertently couples lateral force and topographic signals in the AFM measurements.

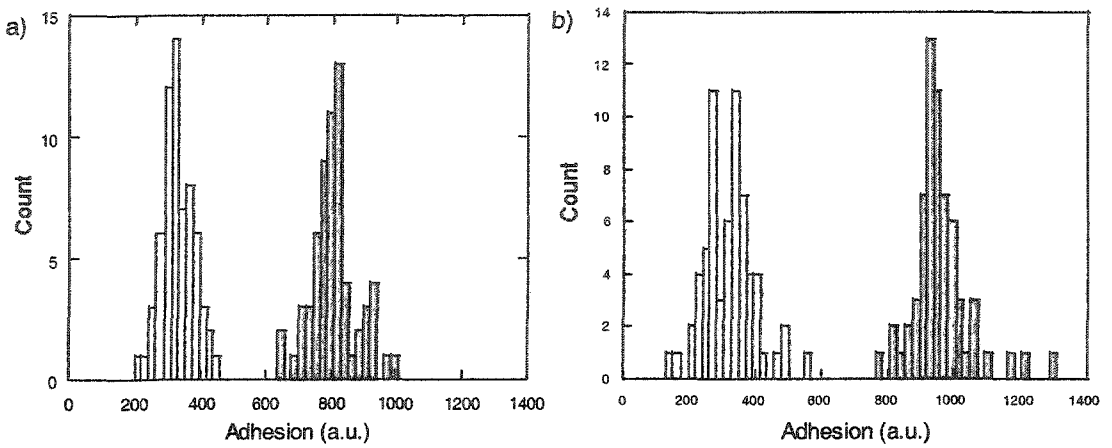

Figure 2.4 Adhesion measured before and after friction measurement. ▨: Si tip and OTE covered surface; □: OTE covered tip and Si surface;

To make data comparable, each in experiment, the same AFM tip was used for the measurements in both systems. First, the tips were cleaned and hydroxylated and. then used for investigation of S3. Following thorough rinsing with water, the AFM tip was dried and immersed in OTE solution for SAM formation. Then it was used again for force measurements in S4. Prior to friction and adhesion measurement, topographic image were acquired for both hydroxylated Si surfaces and OTE modified surfaces. On both surfaces, similar surface roughnesses of ~ 0.1 nm.

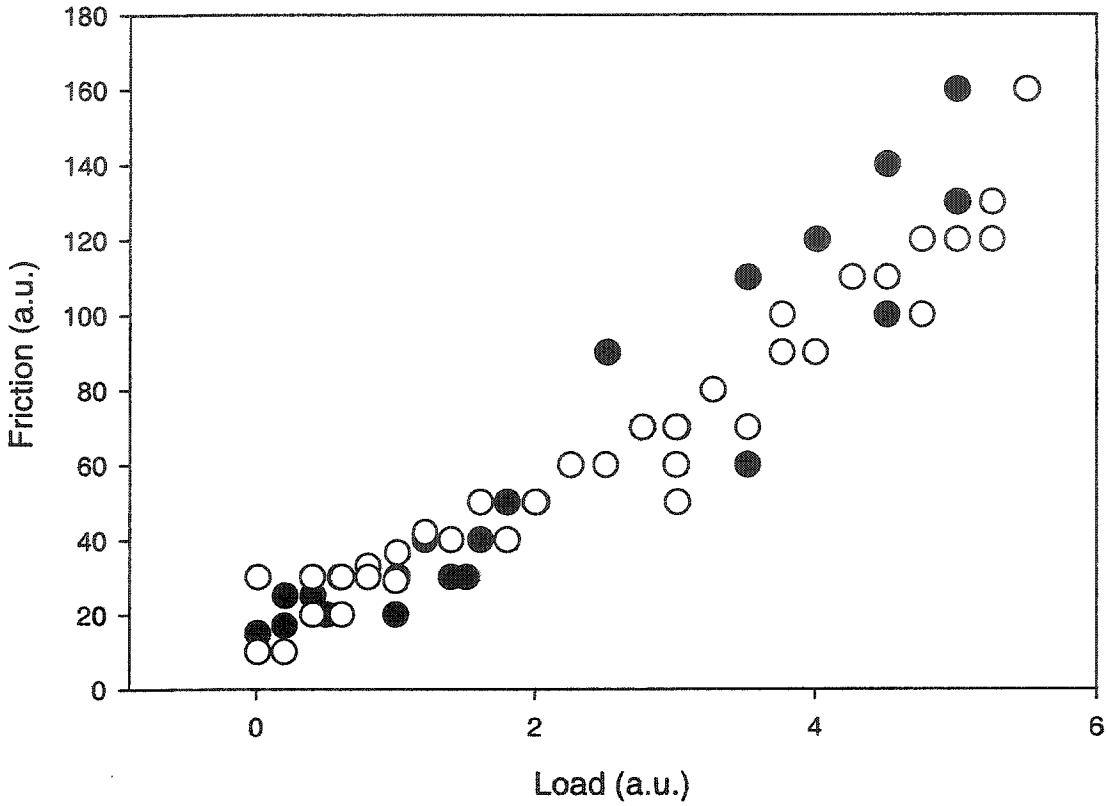

Figure 2.5 Friction force at different load in the 2 systems: ○ Si tip and OTE coated surface and ●: OTE coated tip and Si surface

Even though the same trend was observed for the 5 tips used, for clarity here we only present data gathered from a single tip. Adhesion measurements were made at different positions on the surfaces and were collected while tip scanned over the surface. Each set of data presented in Figure 2.4 is composed of adhesion from 64 different points. Adhesion force in S3 was found to be ~ 3 times that in S4. Compared with the friction between cleaned and hydroxylated Si/Si surfaces, the friction in both systems was greatly reduced (Fig. 2.5). Interestingly, unlike the difference in adhesion forces, the frictional forces in both systems were similar over the range of applied load.

The differences in adhesion cannot be explained soley by variation in contact area. Here one must also consider the details of the OTE filsm formed on the AFM tip and the Si surface. For an AFM tip of xx nm radius of curvature, the packing density of the OTE SAMs (~ 2 molecules/nm^2) {ref, check Bai reference on mica for this value} would be lower than on an atomically flat surface. This acts tolower the packing desntiy on the tip and will reduce chain-chain hydrophobic interactions on the tip that would laterally stabilize the films. Thus in principle, one would expect that the OTE films on the tip would be softer than those on the atomically flat Si surface. Additionally, if we consider the lower packing density at the free end of OTE SAMs on tip than on flat surface and the presence of water during force measurement. On flat surfaces, SAMs molecules are orderly packed. However, due to the curvature of the surface, the free end of OTE molecules on AFM tip or silica particles has much more mobility. Once the SAMs are immersed in water, its molecules have to arrange themselves to minimize their contact with surrounding water. One possible arrangement is the formation of island of OTE SAMs circumvented by channels of water. Therefore, the effective contact area of the OTE SAMs is reduced. Moreover, when the OTE modified tip is separated from the other surface in contact, the water inside the channel destabilizes the contact area. At the separation point of the contact, the overall OTE SAMs are stretched, resulting in increased contact area between the OTE and the water inside channel. When the tip is separated from surface, the effective change of contact area between OTE SAMs and water is also reduced. The other possible arrangement is the collapse of OTE molecules, which exposed more polar methylene group to the surface and make the surface less hydrophobic. In both rearrangements, the adhesion force is reduced.

The formation of SAMs on tip can further protect tip from wearing. Comparing the adhesion force before and after friction measurement in system 1, we can find increased adhesion force after the friction measurement, which suggest the wear of tip during friction measurement and increased tip radius. However, in system 2, adhesion remained same after tip experienced friction measurement with same applied force range. Also there is no evidence showing the wear of Si surface after we zoom out, acquire and compare topographic image over a larger surface area.

2.3.3 Time dependent adhesion between silica surfaces.

Another phenomenon that we interested in was the time dependence behavior of the adhesion force measured by AFM. To address this, silica-silica interaction in pH = 3 water was investigated.

Generally, to measure adhesion force, first AFM tip is retracted to a certain initial position (p_i) and out of contact from surface for a controlled amount of time (ΔT_1) (Fig. 2.4a). Then the tip is approaching toward surface at controlled speed and jump in contact with surface (t_1). After push the tip to a certain indentation (p_f), tip is retracted again at the same speed as approaching. The tip is separated from the sample surface when the exerted force (pull-off force) on the tip exceeds adhesion force between tip and sample surface (t_2).

In this case, the contact time ΔT_c is:

$$\Delta T_c = t_1 - t_2$$

If the indentation of the tip into sample surface (D) is constant, the contact time is in reverse proportional to the approaching-retracting rate (v):

$$\Delta T_c \propto 1/v$$

The out-of-contact time ΔT_o is:

$$\Delta T_o = \Delta T_1$$

Before the force measurement, topographic image of treated Si surface were obtained with AFM in contact mode, which showed that Si surface is smooth with RMS roughness less than 1Å. To eliminate the impact of tip indentation on adhesion, we controlled the indentation of the tip into the sample surface the same in all force measurement.

The measured adhesion force is affected by both the out-of-contact time and tip approaching/retracting rate (Fig. 2.6). The highest adhesion force is observed at the low approaching-retracting rate and low out-of-contact time. If out-of-contact time is 0, measured adhesion force increases with increase of tip approaching/retracting rate. However, for measurement with extended out-of-contact time ($\geq$ 16 s), the adhesion force increase with increase of tip approaching/retracting rate. For measurement with fast tip approaching/retracting rate (2.1 μm/s), adhesion forces decreases with increase of out-of-contact time. When the tip approaching/retracting rate becomes smaller and smaller, this trend becomes less and less significant. For tip approaching/retracting rate less than 0.1 μm/s, adhesion force is no longer depends on the out-of-contact time.

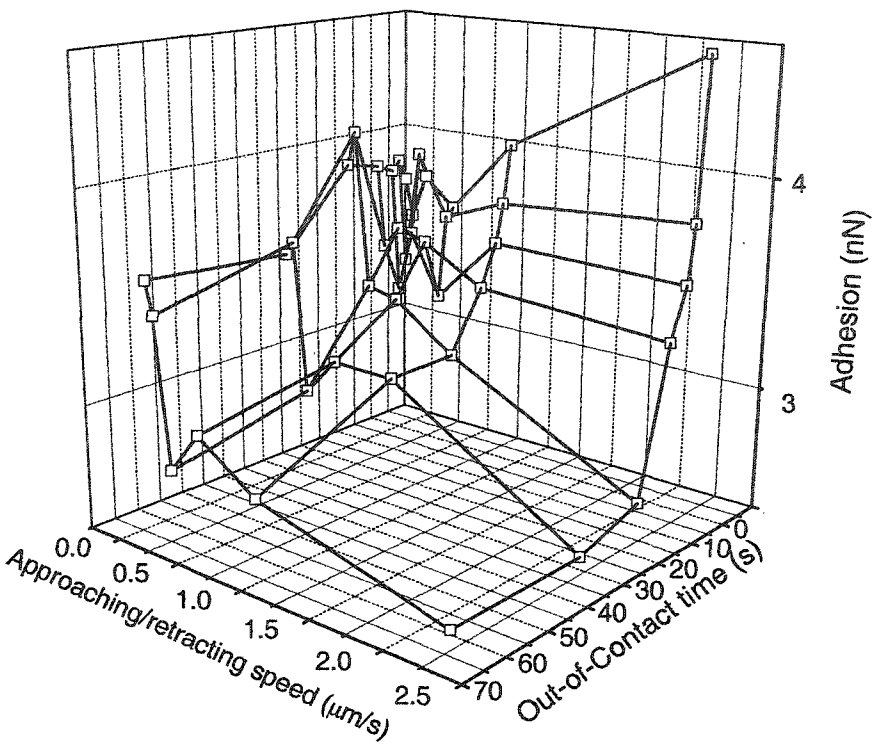

Figure 2.6 Influence of contact time and out-of-contact time on force measurement.

In our experiment, the tip approaching/retracting rate determines not only how fast the tip is separated from the surface but also how long the contact is established and maintained. It is reported that the adhesion forces increase with increase of tip retracting rate, which agrees well with adhesion forces measured with 0 out-of-contact time. The other time-dependent behaviors in Figure 2.6 can be explained by the equilibrium process during the force measurement.

Two distinct states were assumed during the force measurement: one is in-contact state (S_c), associated with an equilibrium system configuration (C_c), and the other is out-of-contact state (S_o), associated with an equilibrium system configuration (C_o). During

the force measurement, the system configuration switches between C_c and C_o. If the surfaces are in contact, the system will gradually equilibrate toward C_c. In contrary, if the surfaces are separated, the system will equilibrate toward C_o. At the point where the contact is broken, if the system configuration is close to C_c, large pull-off will be necessary; if the system configuration is close to C_o, little pull-off force will be required. In our study, if the out-of-contact time is long, the system configuration is close to that of C_o. Therefore, small adhesion force is observed. At low tip approaching/retracting rate, since the contact time is long and the system has enough time to equilibrate toward C_c, measured adhesion force is insensitive to the out-of-contact time. For measurement with long out-of-contact time, the system start at a configuration very close to C_o, during the contact, the system configuration gradually change toward the C_c. The transition is more complete in measurements with slower tip approaching/retracting rate (longer contact time), resulting in larger adhesion forces.

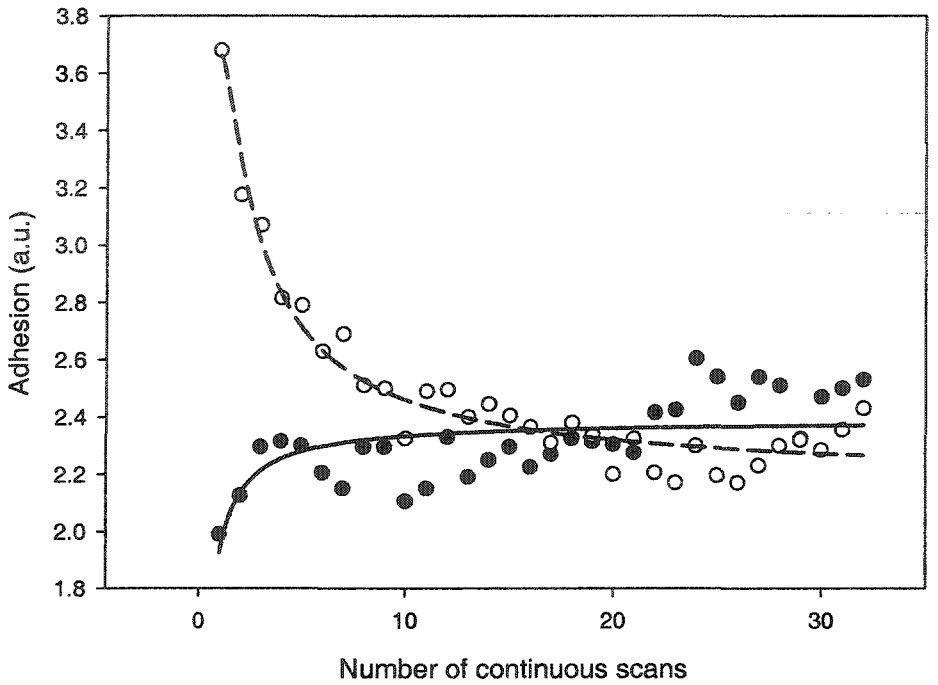

Figure 2.7 Change of adhesion force during 32 consecutive scans. ●: Tip is out of contact with the surface 32 seconds before 1st measurement ○: Tip resides on surface 32 seconds before 1st measurement;

To further test the existence of equilibrium process during force measurement, adhesion forces during consecutive force measurements were monitored. In this process, one force measurement is immediately followed by another. Before force measurement, the AFM tip is either brought in or out of contact with the surface for 32s. As shown in Figure 2.7, after the tip resides on surface for 32s, the adhesion force is high and gradually decreases with increased number of measurement. In contrary, after the tip stand in solution for 32s, the adhesion force is low and gradually increases with increased number of measurement. After ten repeating measurements, the adhesion forces become stabilized and similar adhesion is observed in both cases. The history of adhesion forces

during these two consecutive measurements strongly evidences the existence of equilibrium process during force measurement.

2.4 Conclusions:

In summary, using AFM tip and nanoparticles, we studied the tribology behavior of OTE SAMs on surfaces with nano-sized curvature in water. With OTE modified AFM tips, it was found that adhesion of SAMs on nanoparticle surfaces is much smaller than that of SAMs on flat surface. Moreover, adhesion of SAMs on nanoparticle surfaces is time dependent and increases with decrease of tip approaching/retracting rate. To further study the tribology behavior of SAMs on asperities, we compared the adhesion forces in the following two systems: 1) bare AFM tip and OTE SAMs on flat surfaces, and 2) OTE SAMs on AFM tip and flat silica surface. In both systems, the presence of OTE SAMs reduces friction between two Si surfaces. However, in system 2, adhesion force is much smaller than that in system 1, which is explained as the rearrangement of OTE molecules on AFM tip in water.

The time dependent behavior in adhesion measurement is further studied between two silica surfaces in water. The results indicate the presence of equilibrium process during the force measurement, resulting in different adhesion forces measured with different out-of-contact time and tip approaching/retracting rate. The existence of equilibrium during the force measurement is further evidenced by repeated force measurement after certain tip-surface contact and out-of-contact times.

Chapter III

Microchannel confined surface-initiated polymerization

3.1 Introduction

Surface initiated polymerization is an attractive method used with increasing frequency to modify surfaces with grafted polymer brushes.[1-8] Among many types of polymerization techniques available, atom transfer radical polymerization (ATRP)[9-11] is of special interest because it is versatile, robust, well controlled, and possesses a living nature. The use of grafted polymer to control surface chemistry has become so appealing[12-14] that research to understand the behavior of tethered chains at interfaces has become extensive. Recently, combinatorial methods have been demonstrated as tools to better understand the effects of graft density[15, 16] and molecular weight[17, 18] on polymer brush surfaces.

Use of microchannels as unique reaction environments has also become increasingly popular.[19, 20] In microchannels, only small volumes of reagents are necessary and the solutions can be manipulated rapidly into or out of the channels. Microchannels can also be used to impose certain lateral control of the reaction mixture within the channel depending on the flow conditions and fluid dynamics. Laminar flow inside microchannels has enabled spatial control of reaction mixtures, enabling microfabrication of structures much smaller than the width of the channel.[21]

While ATRP in microchannels has been carried out previously to provide uniform coverage of surfaces,[22] we are unaware of any use of the unique environment of microchannels to manipulate monomer/catalyst solutions on a flat surface and produce gradient and patterned specimen for further investigating the physical behavior of

polymer brush layers. In this work, we report a microchannel confined surface initiated polymerization (μSIP) technique.

3.2 Experimental Section

3.2.1 Materials and measurement methods

Deionized H_2O was obtained from a Barnstead EASYpure system. 2-hydroxyethyl methacrylate (HEMA, ophthalmic grade, 99.5+ %, Polysciences), bipyridine (Aldrich, 99+ %) copper (II) bromide ($CuBr_2$, 99 %, Aldrich), Copper (I) chloride (CuCl, 99+ %, Aldrich), methanol (ACS grade, Aldrich), optical adhesive (NOA 81, Norland Products), and polydimethylsiloxane (PDMS, Sylgard 184, Dow Corning) were used as received. BS-8000 programmable syringe pump (Braintree Scientific, Inc.) was used to control the injection rate of the reaction mixture. Polymer brush thickness was measured using a J. A. Woollam Co. Inc. VASE. BMA, NIPAM and DMAEMA,

3.2.2 Preparation of initiator modified silicon surface

The initiator, 11-(2-bromo-2-methyl)propionyloxyundecenyltrichlorosilane, was synthesized according to the literature procedure.[1] A freshly cut silicon wafer was rinsed with acetone, treated with UV-Ozone for 30 min, and quickly immersed into an initiator toluene solution overnight. Following rinsing with toluene and acetone, the initiator-modified substrate was dried under a flow of nitrogen.

3.2.3 Fabrication of PDMS microchannel stamp

Two different types of PDMS stamps were used in this study. The first type of stamp (large stamp) is a 4.5 cm by 0.8 cm well of 300 μm thickness. The procedure for fabrication of this type of microchannel was adopted from the literature.[25] Briefly, NOA 81 was first patterned onto glass plates. A typical pattern formed is 4.5 cm long, 0.8 cm wide and 300 μm high. A prepolymer mixture of PDMS (10:1 mass ratio of base to curing agent) was poured onto the top of the glass plate. After curing at 75 °C for more than an hour, the formed PDMS stamp was separated from the patterned surface. Holes were punched in the stamp for tubing connections. The second type of stamp (small stamp) used has repeating line pattern of 900 nm high and 3 mm long, with width ranging from a few microns to 30 microns. The distance between two adjacent lines various also from a few to 20 microns. This type of stamp is mold directly against an etched silicon mask.

3.2.4 Preparation of polymerization solution

The feed ratios of the polymerization solutions were adopted from the literatures and were summarized in table 1.[23, 24] Solid contents were added to a flask fitted with a rubber septum and underwent three cycles of evacuation and backfilling with argon, followed by addition of degassed solvents and monomer. The reaction mixtures were stirred at room temperature for 1 h.

Polymerization solution	Monomer (mL)	Solvents			Ligand		Catalyst		
		Water (mL)	iPOH (mL)	MeOH (mL)	PMDETA (mL)	Bpy (mg)	CuCl (mg)	CuBr (mg)	$CuBr_2$ (mg)
HEMA	8	8	-	-	-	488	110	-	72
BMA	5	0.5	4.5	-	-	46.4	-	19.2	3.3
DMAEMA	5	0.5	4.5	-	-	46.4	-	19.2	3.3
NIPAM	12.6*	6.3	-	6.3	0.7	-	-	0.16	-

* gram

Table 3.1 Feed ratios of the polymerization solutions.

3.2.5 μSIP with large PDMS stamps

The reaction mixture was transferred into a nitrogen-purged syringe and placed on a syringe pump. Microchannel was formed through the conformal contact between the PDMS stamp and initiator modified silicon substrate (Scheme 3.1). The deoxygenated stamp was inverted and clamped onto an initiator modified silicon wafer and submerged in a bath of argon. The surface/stamp assembly was deoxygenated by three vacuum-argon backfill cycles prior to use. The polymerization solution was dispensed into the stamp at a controlled rate through a tube between the syringe and the inlet of the microchannel.

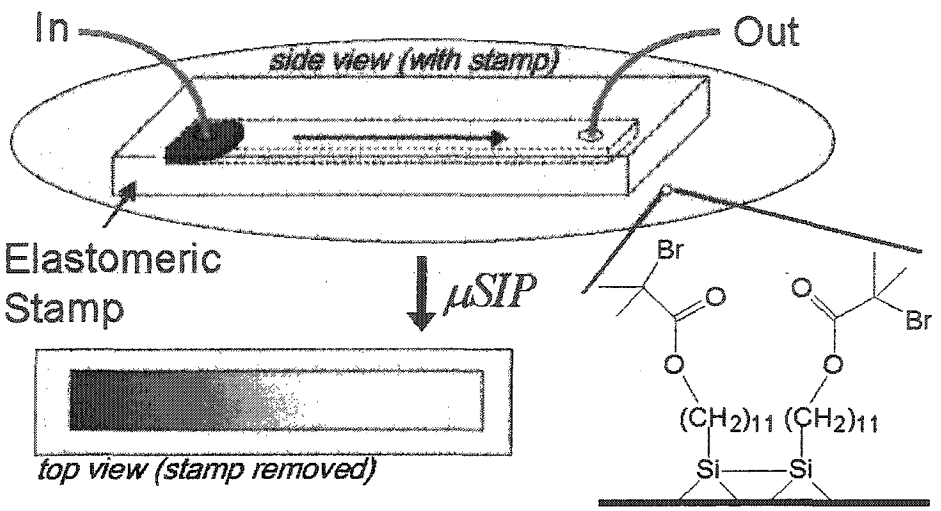

Scheme 3.1 Microchannel confined surface-initiated polymerization (μSIP).

3.2.6 μSIP for statistic copolymer gradient synthesis.

First two syringes containing polymerization solutions with different monomers were mounted on two syringe pumps. To ensure the complete mixing of the solutions, a passive microfluidic mixer with two inlets and one outlet was fabricated. Each inlet of the passive mixer was connected to one syringe and the outlet was connected to the glass vial. A glass vial was designed with two openings, a big top opening that allows silicon slides to be inserted into the vial and a small bottom opening connects to the passive mixer and serves as inlet for the polymerization solution. The dimension of the inner space of the vial is 1 x 2 x 6.5 mm^3. Before the polymerization, a 0.5 x 1.8 x 7 mm^3 initiator modified single side polished silicon substrate was inserted into the vial. The silicon slide was placed so that it closely attached to one side of the vial with its polished face open to the space. As a result, the effective spacing between the substrate and the other side of the vial is 500 μm. The passive mixer and the vial were placed in a sealed

tank and underwent three cycles of vacuum and backfilling with argon. Surface-initiated polymerization was started by fast pumping the reaction mixture into the reaction flask through its bottom opening. The injection period was fast,

Here two polymerization solutions were prepared. The only difference between these two solutions is that one (A) had BMA the solvent and the other (B) had DMAEMA as the solvent. Solution was added by first pumping solution A into the channel. Then the pumping rate of solution A was gradually decreased while the pumping rate of solution B was simultaneously increased. Through the course of infusion, the overall infusion rate was kept constant; however, the channel was filled quickly in this case (less than 2 min), such that the difference in exposure time along the channel was no longer a factor in the experiment and polymerization time was constant across the surface. Before the mixture entered the channel, it passed through a micro-stirrer to ensure complete mixing of the solution. After 40 min of polymerization, the substrate was quickly removed from polymerization mixture, thoroughly rinsed with DMF and ethanol, and dried under a flow of nitrogen.

3.2.7 Surface patterning with small PDMS stamps

Scheme 3.2 illustrates the setup for surface patterning with small PDMS stamps. The PDMS stamp (small stamp) was cut so that both ends of the channel are open. The stamp was then put on an initiator SAMs modified substrate. The whole setup was placed in a flask sealed with septum. Following three cycles of vacuum and backfilling with argon, the polymerization solution was placed next to the opening of the channel and the

polymerization quickly filled the channel. After a certain period of time, the PDMS stamp was removed and the substrate was thoroughly rinsed with DMF.

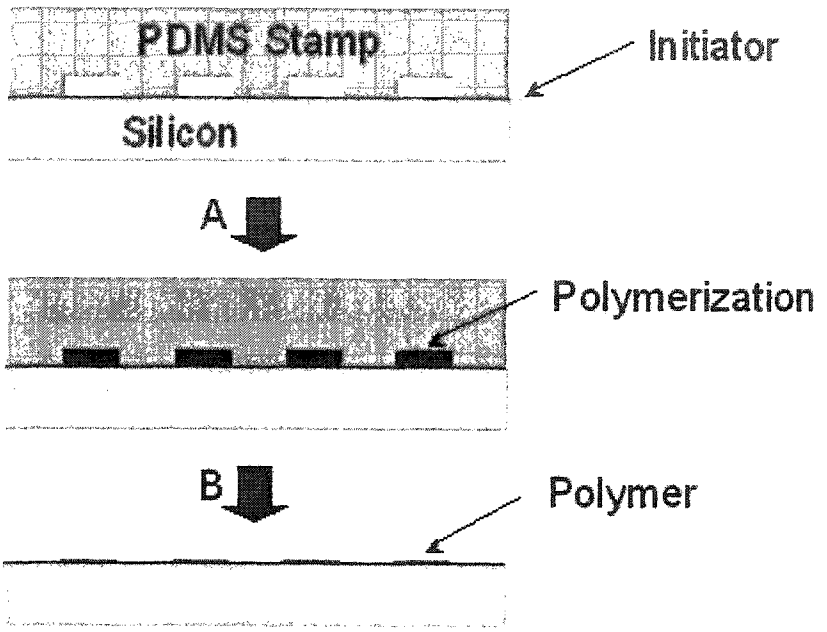

Scheme 3.2 Surface patterning with microchannel confined surface initiated polymerization

3.3 Results and discussion

3.3.1 Kinetics of polymer brushes growth inside microchannel

Aqueous ATRP of 2-hydroxyethyl methacrylate (HEMA) was chosen as a model system to validate of this technique.[23] At current polymerization conditions, controlled polymerization of HEMA from surface was reported with linear growth of polymer brush thickness with polymerization time.

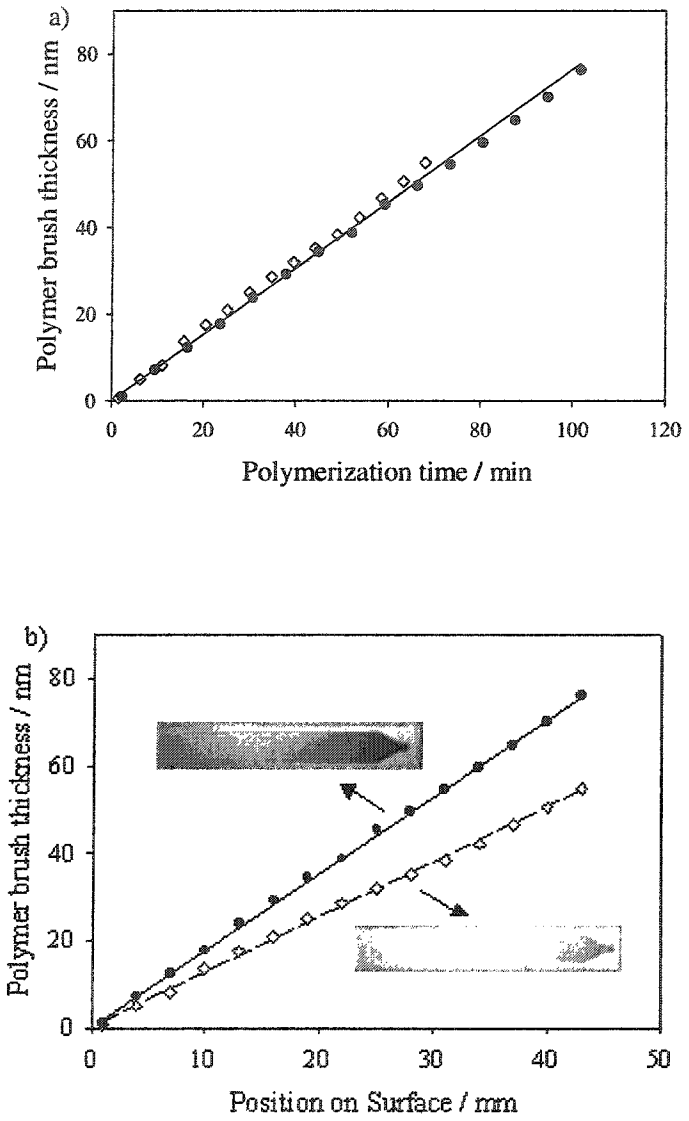

Figure 3.1 Kinetics of poly-(hydroxyl ethyl methacrylate) brush growth with microchannel confined surface-initiated polymerization (μSIP) and the formation of a gradient polymer brush on a surface: (a) profile of thickness across the gradient (insets are digital images of the gradient films), (b) brush thickness as a function of time as determined by the exposure time to the monomer/catalyst solution. Solution front advancing rate: ● = 0.423 mm/min, ○ = 0.634 mm/min. Two standard deviations in the ellipsometry measurements are ± 1 nm.

To study the kinetics of brush growth on the surface inside microchannel, a solution with constant concentration of monomer and catalyst was gradually pumped into the channel at a fixed rate from the inlet, located at one end of the channel. After the reaction mixture reaches the outlet, the PDMS stamp was quickly removed and the silicon substrate was thoroughly rinsed with DMF. As a result, different regions on the surface have different polymerization times, which is directly proportional to the distance from the outlet and the time of surface exposure to the monomer solution. Ellipsometry data taken along the length of the final specimen show that the thickness of the polymer brush increases linearly with their distance from the outlet (Figure 3.1a) and polymerization time (Figure 3.1b).

By filling the channel at a slower rate, we were also able to generate polymer brushes with a steeper thickness gradient on the surface. The slope of the thickness gradient can be tuned, therefore, by adjusting the filling rate of the reaction mixture. As shown in Figure 3.1b, the thickness of the film as a function of exposure time is independent of the filling rate of the reaction mixture. Atomic force microscope images of the surfaces, confirming local coverage and uniformity of the resultant polymer layer are available in the supporting information. The entire region of the silicon wafer exposed to the monomer/catalyst solution was covered with grafted polymer.

3.3.2 Consecutive μSIP

During μSIP, the initiator-functionalized regions are either exposed to the reaction mixture or in contact with PDMS. To evaluate the polymerization behavior of the surface after contact with PDMS and the re-initiation efficiency of the grafted layer, a channel

was placed on the surface and quickly filled with the polymerization mixture. After 60 min of polymerization, the first PDMS stamp was removed and the surface was rinsed with DMF. The channel was then reapplied to the surface, but with its position shifted, such that the newly formed channel now covered part of the area that was previously in contact with the PDMS and part of the area that was inside the previous channel. Then the channel was again filled with the reaction mixture for 30 min. Three distinct regions are formed as a result of these two consecutive polymerizations (Figure 3.2). Region A was exposed during the first polymerization and subsequently covered by PDMS during the second, while region B was exposed for both polymerizations, and region C was first covered by the PDMS and then exposed inside the second channel. Thus, the net polymerization times for regions A, B, and C were 60 min, 90 min, and 30 mins, respectively. From ellipsometry measurements, the resulting thickness of the polymer brushes formed in regions A, B, and C were 43 nm, 65 nm, and 24 nm, respectively. Thus, it is clear that the surface covered by the PDMS stamp retains its initiating capacity.

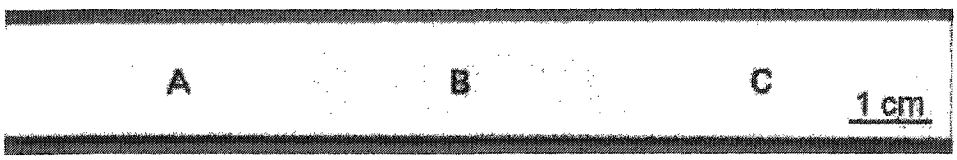

Figure 3.2 Consecutive microchannel confined surface-initiated polymerization (μSIP) on surface. The first channel includes region A and B, polymerization for 60 mins. The second channel includes region B and C, polymerization for 30 mins. Polymer brush thickness in region A, B, and C are 43 nm, 65 nm, and 24 nm respectively.

This result suggests that multiple polymer brushes and/or multi-layer copolymer brushes could be easily achieved with consecutive μSIP steps by re-initiating the polymer-functionalized surface, without multi-step patterning of different initiator segments, or the use of multiple polymerization chemistries, which may limit the types of polymers that can be produced.[24] Hence, μSIP will enable patterning arrays of polymer brushes with a simplicity and uniformity not readily available with other techniques.

3.3.3 μSIP for combinatorial study of surface-initiated polymerization conditions

After the microchannel is filled with solution and the flow is stopped, the only mixing will be diffusive. In a channel with a gradient in composition, if the gradient is shallow enough, it is possible for the reaction to finish before any significant change in the composition profile can occur. Thus, by analyzing the tethered polymer brushes on the surface, we can continuously study the influence of a solution composition gradient on surface initiated polymerization.

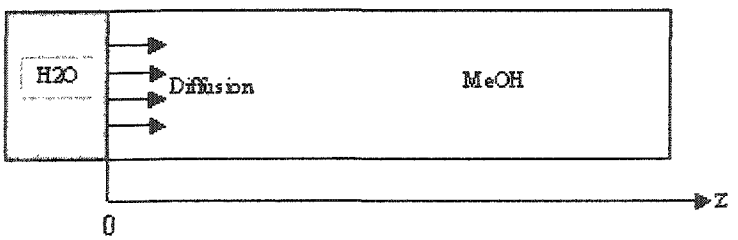

Scheme 3.3 Water diffusion in methanol solution

To approximate the diffusion along the channel, we used a simple model to illustrate the diffusion profile, as shown in Scheme 3.3. In the model, water and methanol are separated at the beginning, with the initial condition of

$$z > 0,\ x_{H2O} = 0$$

We also assume there is no diffusion of MeOH into water, so the concentration of water, x, at $z = 0$ remains as the highest value, x_0, which is equal to 1 for pure water. With this assumption, we could affirm to obtain the farthest water-diffusing profile.

The boundary conditions were defined as,

$$\text{at } t > 0, \quad z = 0,\ x_{H2O} = x_0$$

$$z \to \infty,\ x_{H2O} = 0$$

Solving for the rate of change of the concentration,

$$\frac{\partial x}{\partial t} = -D_{AB}\frac{\partial^2 x}{\partial z^2} - N_A\Big|_{z=0}$$

where D_{AB} is the diffusivity of A in B, yields

$$\frac{x}{x_0} = \frac{1 - erf\left(\frac{z}{\sqrt{4D_{AB}t}} - \varphi\right)}{1 + erf(\varphi)}$$

where φ is a dimensionless molar average velocity related to x_0 as,

$$x_0 = \frac{1}{1+[\sqrt{\pi}(1+erf\varphi)\varphi \exp\varphi^2]^{-1}}$$

The literature value of the diffusivity of methanol in water as 1.26×10^{-9} m^2/s at 288 K.[26]

Figure 3.3 shows the solution to this equation for two concentration profiles, a pure water source ($x_0 = 1$) and a low concentration of water in the source ($x_0 = 0.25$) at two times, 0.5 h and 1 h, respectively. From the profiles, we notice that for the extreme case of pure water, there is only 5 mm to 7 mm diffusion during our reaction time. For the gradient system, the initial condition of x_0=0.25 is more realistic. In this case, the diffusion is limited to 1 mm to 2 mm, in a 45 mm long channel. So we conclude that the surface polymer reaction under a gradient solution composition is complete before any significant change in the gradient profile can occur.

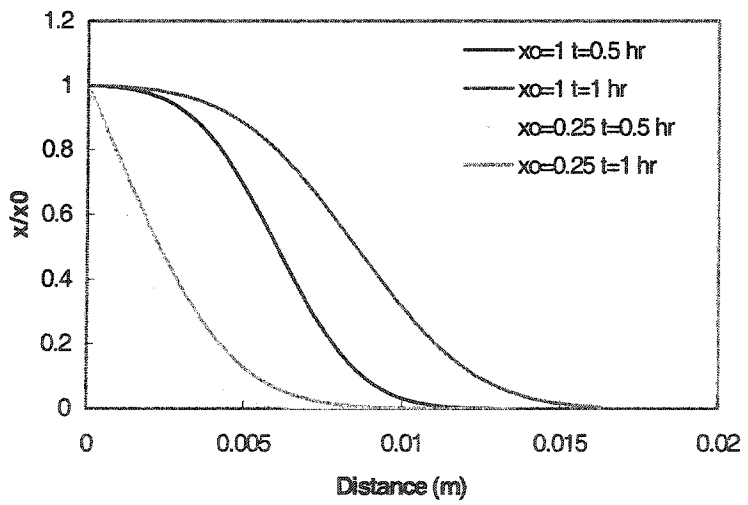

Figure 3.3 Water concentration profile inside methanol

We employed μSIP to investigate how the addition of methanol affects the polymerization throughout the channel. For ATRP of HEMA, it is known that the addition of methanol to the reaction mixture will reduce the polymerization rate.[24] Here two polymerization solutions were prepared. The only difference between these two solutions is that one (A) had methanol/water (50/50 by volume) as the solvent and the other (B) had water as the solvent. Solution was added by first pumping solution A into the channel. Then the pumping rate of solution A was gradually decreased while the pumping rate of solution B was simultaneously increased. Through the course of infusion, the overall infusion rate was kept constant; however, the channel was filled quickly in this case (less than 2 min), such that the difference in exposure time along the channel was no longer a factor in the experiment and polymerization time was constant across the surface. Before the mixture entered the channel, it passed through a micro-stirrer to ensure complete mixing of the solution. Before the experiment, the volume of the solution required to fill up the channel was calculated and the pumping rate of the two pumps was programmed so that a linear methanol concentration gradient was established from one end of the channel to the other.

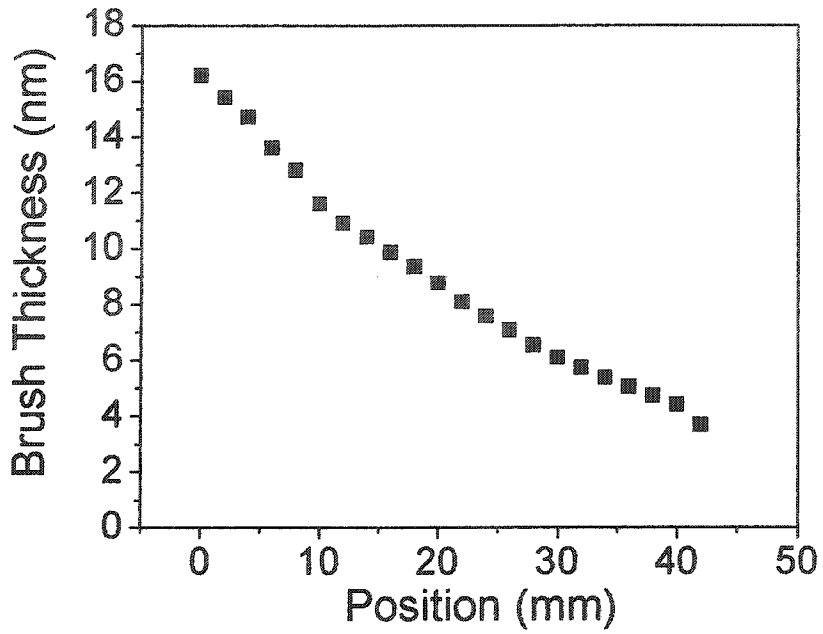

Figure 3.4 Influence of solvent composition on polymerization. The inlet of the channel was at 0 mm. Methanol content in the monomer/catalyst solution is highest at positions far from the inlet.

Figure 3.4 shows the result after 25 min of polymerization. The thickness of the polymer brush decreased from the channel end rich in water to the end enriched with methanol (50/50 v/v). Therefore, with a single μSIP experiment, we confirmed that the substitution of methanol to water in the polymerization solution does slow the growth rate of polymer brushes from a surface and show that a concentration gradient within the solution can be trapped such that local regions of the surface are exposed to different polymerization solutions. It is precisely the ability to trap the solution as a gradient that remains a challenge using existing techniques and makes μSIP unique.

3.3.4 μSIP for statistic copolymer gradient synthesis.

Taking advantage of the limited mixing inside microchannel, we further explored μSIP to synthesize statistical copolymer gradient. Statistical copolymerization of BMA and DMAEMA was selected as model system in this study. For their close reactivity ratios, BMA and DMAEMA can readily go through copolymerization. In a separate work, utilizing the same polymerization conditions, controlled surface-initiated polymerizations of both BMA and DMAEMA were demonstrated: polymer brush thickness grows linearly with polymerization time. The resulting polymer brushes thickness was first characterized by ellipsometry. As shown in Figure 3.5a, polymer brushes with thickness no less than 10 nm was formed on surface.

Surface water contact angle measurement was used to access the gradient profile of the surface. PBMA and PDMAEMA brushes have distinct surface hydrophilicities. For homopolymer brushes of BMA and DMAEMA synthesized under the same conditions, the surface water contact angles are 90° and 64°, respectively. As shown in Figure 3.5b, the water contact angle measurement results clearly reveal the gradient properties of the surface. From the bottom to the top of the substrate, the water contact angle smoothly changes from characteristic value of PDMAEMA to that of PBMA. Atom force microscopy (AFM) measurement of the surface shows uniform coverage of polymer brushes with surface roughness less than 0.5 nm. Therefore, Cassie equation could be applied to evaluate the surface chemical composition: $\cos\theta = \varphi \cos\theta_A + (1-\varphi) \cos\theta_B$, where θ is water contact angle of the statistical copolymers brushes at a given location on surface, φ is the composition of DMAEMA units inside the polymer brushes. θ_A and θ_B are the water contact angle for homopolymer brushes of PDMAEMA and PBMA. It is

clearly that the composition of the surface gradually changes from PDMAEMA rich at one end to PBMA rich at the other.

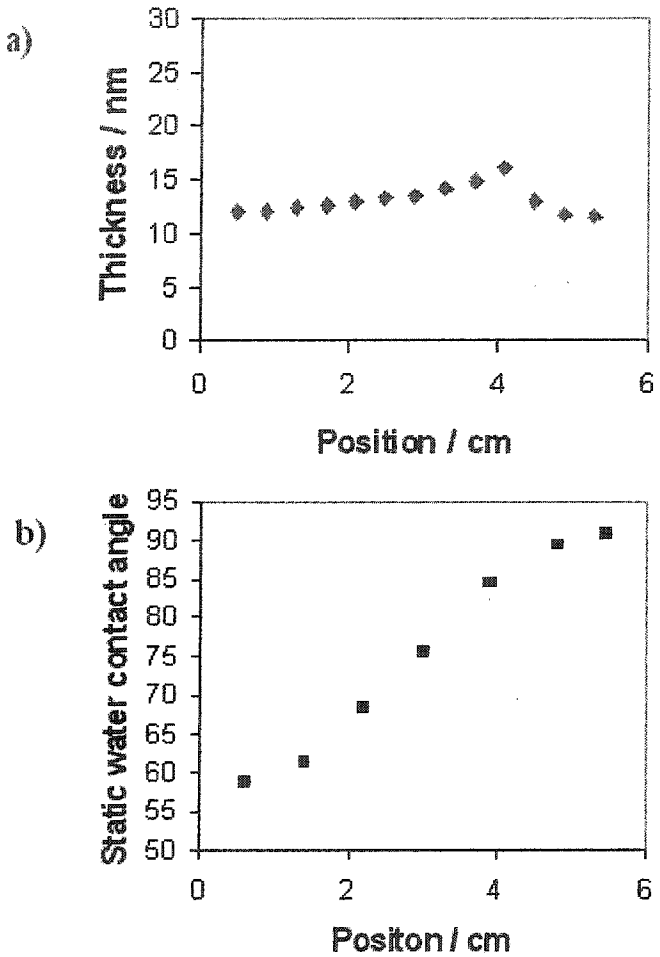

Figure 3.5 Thickness (a) and contact angle (b) profiles of the statistical copolymer brushes gradient of BMA and DMAEMA

The surface composition gradient was further characterized with Near Edge X-ray Absorption Fine Structure (NEXAFS). As shown in Figure 3.6, peaks corresponding to $\sigma_{N\text{-}C}$ of DMAEMA gradually decrease from the bottom to the top of the substrate, which further proves the formation of statistical copolymer brush gradient on surface.

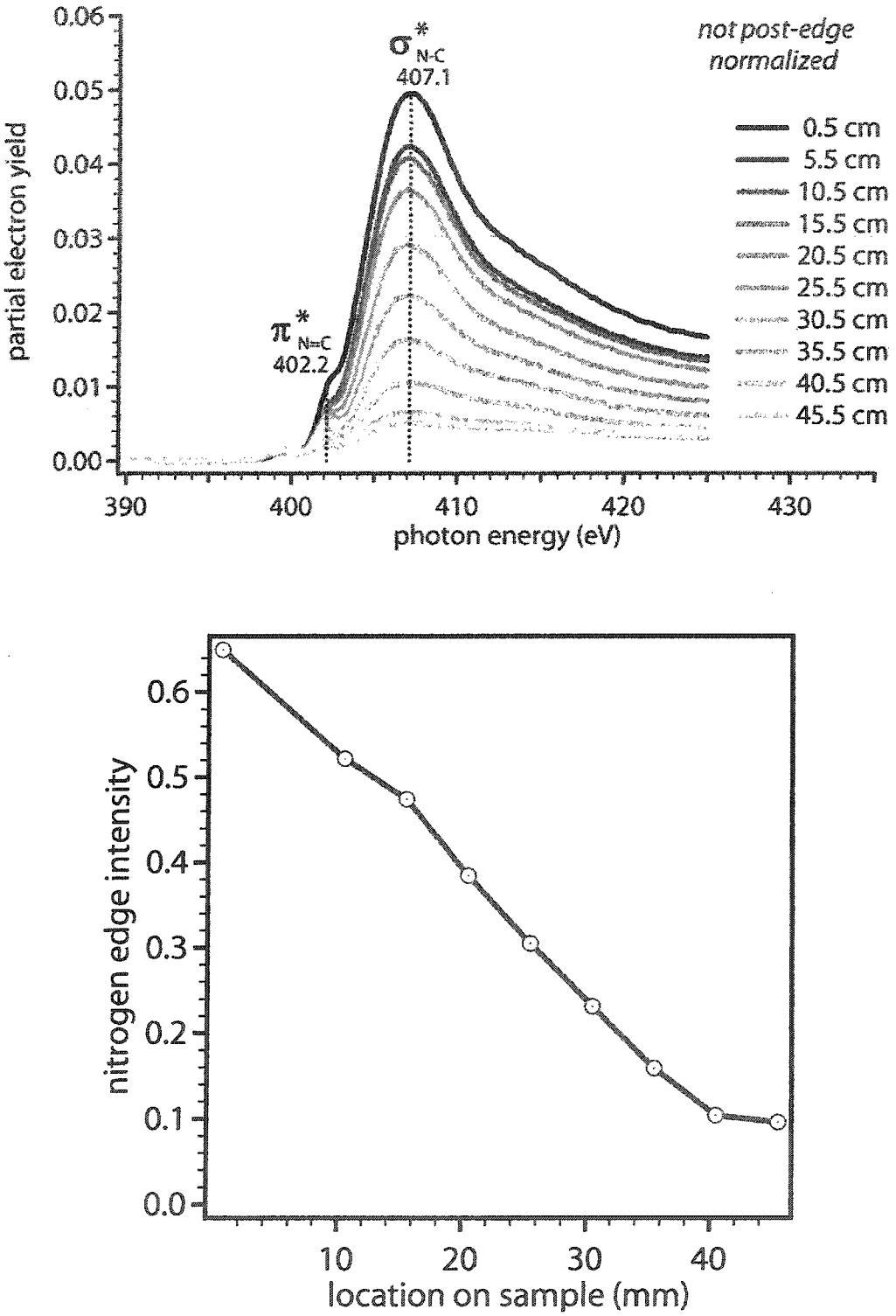

Figure 3.6 NEXAFS analysis of the statistical copolymer gradient of BMA and DMAEMA

3.3.5 Surface patterning with μSIP

During μSIP, polymer brushes formed only on surface areas in direct contact with polymerization solution. Therefore, with micro-patterned PDMS stamps (small stamps), μSIP was explored to generate patterned polymer brushes on surface at micron level. Once the polymerization solution was placed next to one end of the microchannel, it was drawn into the channel by capillary forces.

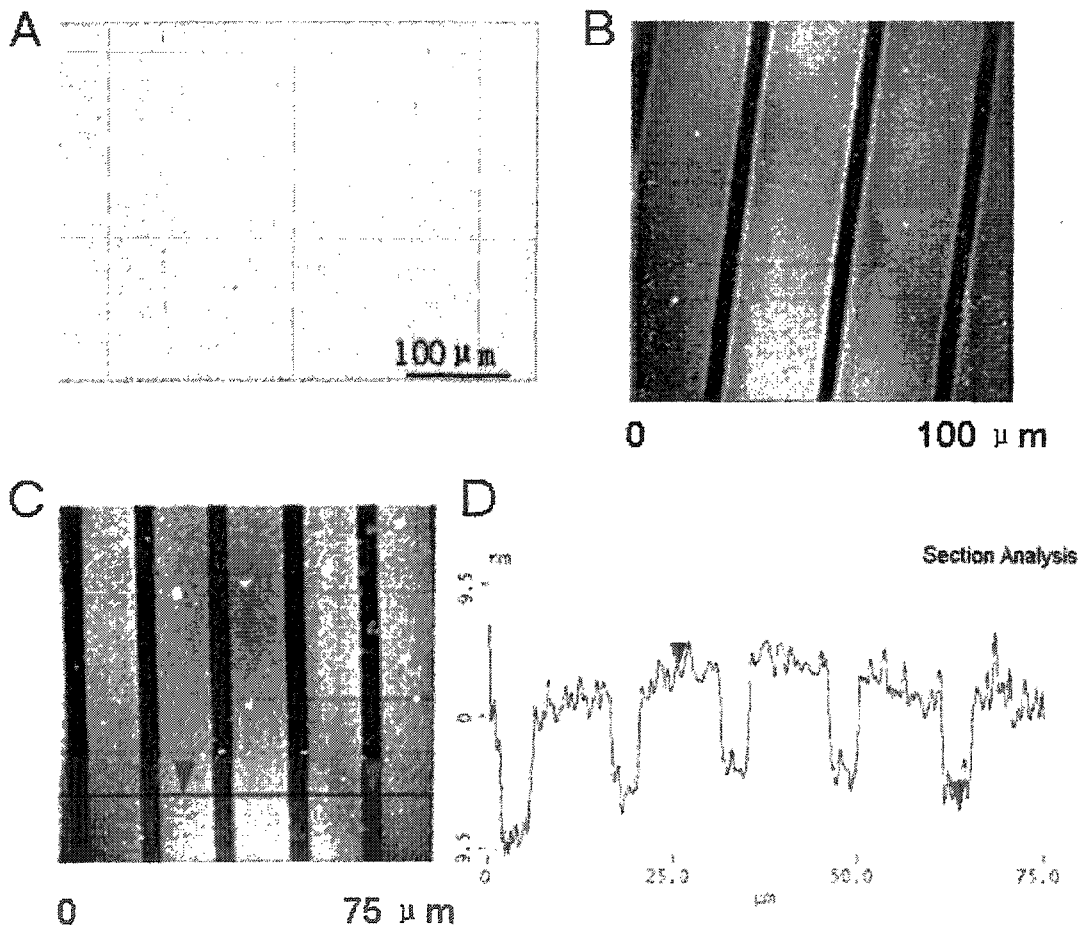

Figure 3.7 Polymer brush patterns generated from microchannel confined surface initiated polymerization: microscopy (A) and AFM image of poly-NIPAM brushes, AFM (C) and line section of poly-HEMA brushes.

NIPAM and HEMA were used to pattern the surface. As shown in Figure 3.7, poly-NIPAM brushes with thickness up to 100 nm can be patterned on surface. Figure 3.7C shows the patterned poly-HEMA brushes fabricated with μSIP. Line trace through the patterns clearly indicates that a uniform layer of polymer brushes formed inside the channel.

Generally, patterned polymer brushes were synthesized through polymerization from initiator patterns on surface, which can be generated through lithographic techniques.[27] For its simple experimental setup, soft lithography is most often used to pattern initiator SAMs on surface. However, with current soft lithography techniques, it is hard to pattern high density uniform initiator SAMs on surfaces in systems other than thiols on gold. Since the pattern is generated during the polymerization process, patterning of initiator is no longer a requirement in μSIP. Furthermore, as shown in Figure 3.3, it is possible to fabricate complex polymer brush patterns on surfaces with consecutive μSIP.

3.4 Conclusions

In summary, surface-initiated atom transfer radical polymerization can be carried out inside microchannels to produce flat, exposed gradient and patterned surfaces. Compared with regular surface-initiated polymerization in a flask, μSIP has several advantages: (1) As the microchannel height is only 300 μm, only a small amount of solution is necessary for the polymerization. (2) Since the flat surface in contact with the PDMS stamp retains initiating capacity, μSIP can be used to pattern the surface sequentially with the same or

block (co)polymer brushes. It is also possible to pattern the surface simultaneously with several brush configurations using multiple channels because the polymerization conditions can be varied from channel to channel. Patterns polymer brushes with dimension down to a few microns can be generated on surface with micro-patterned stamps. (3) By taking advantage of the composition gradients formed inside microchannels, it is possible to systematically investigate how the solution composition influences the formation of polymer brushes and synthesize statistical copolymer gradients, which can potentially served as platforms for combinatorial study of interactions between materials and polymer brushes.

Chapter IV

Synthesis of Gradient Copolymer Brushes via Surface Initiated Atom Transfer Radical Copolymerization

4.1 Introduction

Tethering surfaces with polymer brushes provides a versatile method to tailoring surface properties such as wettablility,[1] friction,[2] and protein/cell adhesion.[3] By polymerization from initiator moieties anchored on surfaces, surface initiated polymerization can provide high-density polymer brushes on surface. Different polymerization strategies, such as free radical,[4,5] cationic,[6] anionic,[7] and ring opening metathesis polymerization[8], were all demonstrated to form polymer brushes on surfaces. Among all types of polymerization methods, atom transfer radical polymerization (ATRP) attracts significant interest for its living/controlled character, tolerance of functional groups, and mild requirement on experimental conditions.[9]

Recently, modifying surface with copolymer brushes attracts growing interests. Statistical copolymer brushes provide one means to fine tune surface properties. By adjusting the composition of statistical copolymer brushes of styrene and methyl methacrylate, Russell *et al.* demonstrated that the interfacial energies and wetting behavior of polymers on surfaces could be precisely controlled.[10] Block copolymer brushes can form responsive surfaces. Selective solvent treatment preferentially exposes segments of polymer chain that miscible in the solvent to the surface. Therefore, the surface properties can be switched from one component of the copolymer to the other upon different solvent treatments.[11,12] This switching can also change the surface morphology, leading to the formation of a nano-structured surface.[13-16]

Gradient copolymers are the class of copolymers that have gradual composition variations from one end of the polymer chain to the other. Unlike block copolymers or

statistical copolymers, gradient copolymers possess their distinct properties.[17] Similar to block copolymers, for their composition inhomogenities along the polymer chains, gradient copolymer brushes will also have solvent response behavior. In addition, with precise control over gradient profiles of the polymer brushes, it is possible to tune the properties of surface after different solvent exposures. For block copolymer brushes, the outmost layer of the surface can be switched from one block to the other. However, there is no driven force to enforce the ordering within each block of the copolymer brushes. In contrast, for gradient copolymer brushes, as the gradual composition change extended throughout the polymer chains, it is possible for the total ordering within the polymer brush to be established once it was treated with solvent favoring one component of the brush. Simulation of the gradient copolymer brushes also predicts that there is a thermally-controllable zone that the free ends are excluded in gradient copolymer brushes.[18]

In this work, we report the synthesis of gradient copolymer brushes via surface initiated ATRP of methyl methacrylate (MMA) and 2-hydroxyethyl methacrylate (HEMA). Advances in controlled radical polymerization allowed precise syntheses of gradient copolymers.[18] Generally, gradient copolymers were synthesized through either spontaneous or forced method. For surface initiated ATRP without sacrificial initiator in solution, since there is nearly no consumption of monomer during the polymerization, only the forced method can be used to synthesize gradient polymer brushes from surfaces.

4.2 Experimental Section

4.2.1 Materials and Characterization

Deionized H_2O was obtained from a Barnstead EASYpure system. The initiator, 11-(2-bromo-2-methyl)propionyloxyundecenyltrichlorosilane, was synthesized according to the literature procedure.[1] Inhibitor was removed from methyl methacrylate (MMA, Aldrich, 99%) through a DHR-4 column (Scientific Polymer Products Inc.). 2-hydroxyethyl methacrylate (HEMA, ophthalmic grade, 99.5+ %, Polysciences), bipyridine (Aldrich, 99+ %) copper (II) bromide ($CuBr_2$, 99 %, Aldrich), Copper (I) chloride (CuCl, 99+ %, Aldrich), methanol (ACS grade, Aldrich), were used as received. BS-8000 programmable syringe pump (Braintree Scientific, Inc.) was used to control the injection rate of the reaction mixture.

4.2.2 Synthesis of initiator modified silicon surface

A fresh cut silicon wafer (1 cm × 3 cm) was first rinsed with acetone, dried, treated with Ultroviolet-Ozone for 30 min. Then it was quickly immersed into an initiator toluene solution (0.5mM) and kept overnight. After thoroughly rinsed with copious amount of toluene and acetone, the initiator-modified substrate was dried under a flow of nitrogen.

4.2.3 Synthesis of MMA-grad-HEMA brushes on surface.

To synthesize gradient copolymer brushes on the surface, we first prepared two solutions. Solution (A) had MMA as the monomer, and the other (B) had HEMA. For

both solutions, 2,2'-bipyridine (250 mg) and CuBr (114 mg) were added to a flask. Fitted with a rubber septum, each flask then underwent three cycles of evacuation and backfilling with argon. Followed by addition of degassed H_2O (1.6 mL), methanol (6.4 mL), and monomer (8 mL), the reaction mixtures were stirred at room temperature for 1 h to ensure complete dissolution of the catalyst. In a separated flask, an initiator modified silicon wafer was placed and capped with a septum. After the flask was degassed, 5 mL of solution A was quickly injected into the flask. At the same time, solution B was slowly pumped into the vial at a rate of 100 μL/min using a syringe pump with constant stirring of the mixture. After a certain period of reaction time, the introduction of HEMA was ceased. The wafer was then immediately taken out of the reaction vial, thoroughly rinsed with DMF and ethanol, and dried under a flow of nitrogen.

4.2.4 Solvent treatment of the surface

The substrate was first immersed solvent for 60 min. Then it is taken out from the solution and dried under a flow of nitrogen.

4.2.5 Characterization Methods

Polymer brush thickness was measured using a J. A. Woollam Co. Inc. VASE system. Surface water contact angle measurement was carried out with a Krüss G2 contact angle instrument. AFM images were collected on a Dimension 3100 system (Vecco Instruents).

4.3 Results and discussion

4.3.1 Synthesis of homo and copolymer brushes.

Aqueous ATRP, as demonstrated by Huck *et al.* and Kim *et al.*,[19] provides a facile route to fast synthesize thick polymer brushes from initiator SAMs modified surface. In this work, the same conditions utilized by Huck *et al.* for MMA polymerization were adopted and expanded to synthesize gradient copolymer brushes. For their close free radical copolymerization reactivity ratios,[20] MMA and HEMA were selected as monomers to synthesize gradient copolymer brushes from surface. In our approach, surface-initiated polymerization without the addition of sacrificial initiator, since the amount of monomer consumed in the polymerization process is extremely small, only forced method was used to grow gradient copolymer brushes from surface (Scheme 4.1).

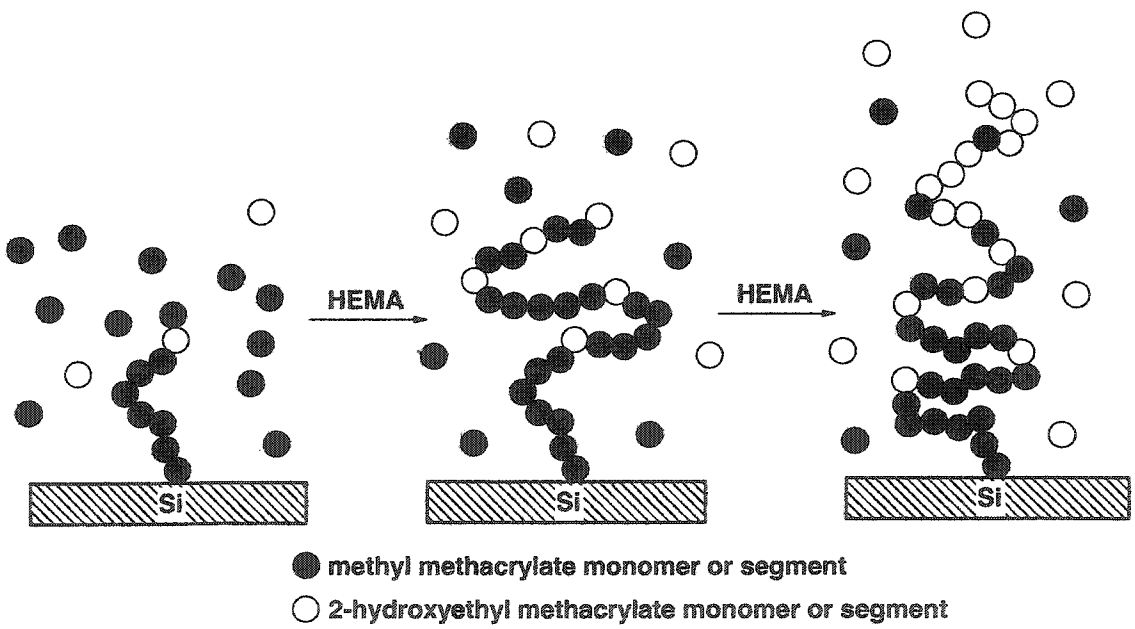

Scheme 4.1 Synthesis of gradient copolymer brushes on surface.

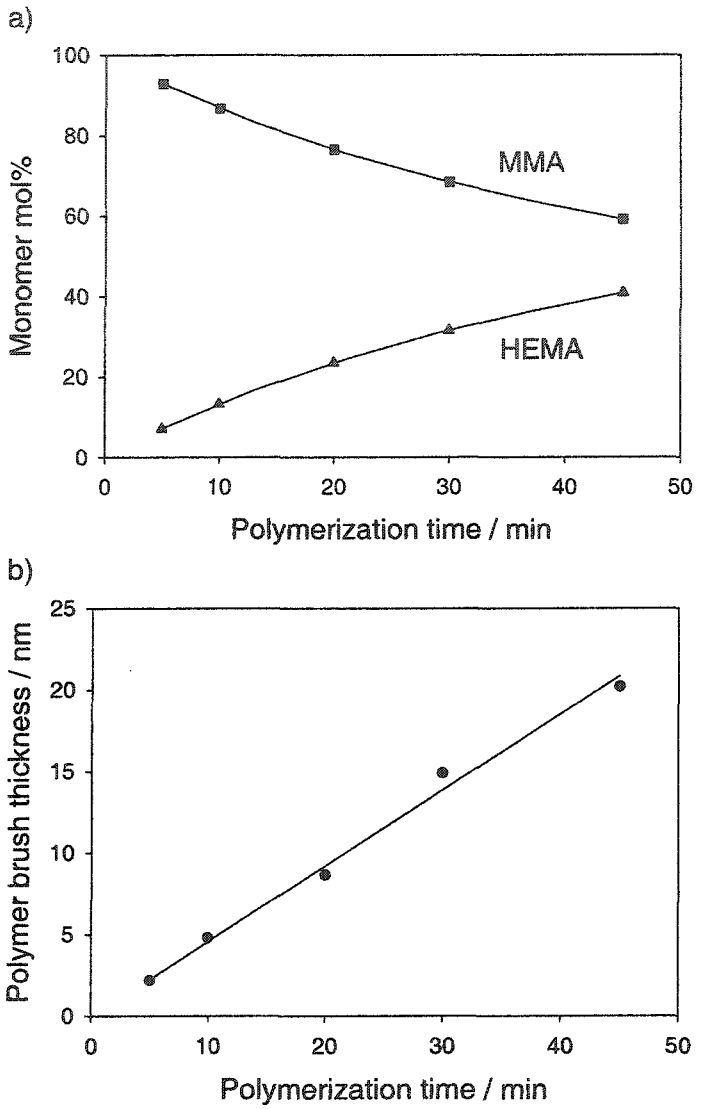

Figure 4.1 Synthesis of gradient copolymer brushes from surface. a) Calculated monomer molar percentage through the course of polymerization. ■: methyl methacrylate, ▲: 2-hydroxyl ethyl methacrylate. b) Growth of gradient copolymer brushes on surface.

At the beginning of the polymerization, MMA (5 mL) solution was first syringed into the reaction flask containing the initiator modified silicon slide. Simultaneously, pumping of HEMA solution into the reaction flask was started at a constant rate of 100 μL/min.

Figure 4.1 shows the change of monomers molar percentage as a function of reaction time. Initially, the only monomer accessible to the surface tethered initiators was MMA. As the HEMA solution was gradually introduced into the reaction mixture, the concentration of HEMA increased while the concentration of MMA decreased (Figure 4.1a). To form a gradient copolymer, it is essential that the polymerization is controlled. Removal of the silicon substrate from the polymerization mixture after different periods of polymerization time allows determination of how the copolymer brushes grow during polymerization process. As shown in Figure 4.1b, despite the gradual change in monomer composition, an almost linear increase in polymer brush thickness with polymerization time was observed. This result suggests that the polymerization was controlled and the surface-tethered propagating chain-ends remain active through the course of polymerization.

As a result, the polymer brushes have an MMA-rich bottom layer formed at the initial stage of polymerization and become increasingly HEMA rich as polymerization progresses. In these experiments, the only difference in the HEMA solution and MMA solution was the monomer, which allows controlled changes in the concentration of individual monomer without disturbing other polymerization conditions.

4.3.2 Solvent response of gradient copolymer brushes

The formation of gradient copolymer brushes was evidenced by contact angle characterization of the above samples with different polymerization time. Due to the composition variation inside polymer brushes, similar to block copolymer brushes, gradient copolymer brushes can also respond to selective solvent treatment. Two

solvents, methylene chloride and methanol, were chosen to treat the gradient copolymer brushes. Methylene chloride is a good solvent for MMA and a nonsolvent for HEMA while methanol is a better solvent for HEMA than MMA. After a 60 min immersion in solvent, the substrate was quickly dried with a flow of nitrogen and the static water contact angle of the polymer brush was measured. For homopolymer brushes synthesized with the same procedure, the static water surface contact angles measured are 70° for MMA and 46° for HEMA. For the gradient copolymer brush film synthesized, the surface would be expected to become more hydrophilic and the surface water contact angle would decrease with increasing HEMA composition in the polymer brushes. Figure 4.2a shows the result of contact angle measurements of samples removed from the reaction mixtures after different periods of polymerization time. For all surfaces, the contact angles fell between that of MMA and HEMA homo-polymer brushes. As anticipated, higher contact angles were observed for samples with shorter polymerization times. For example, after 5 min of reaction, the polymerization mixture contains only 8 mol% HEMA. The sample taken out at this time has water contact angle of 62° after methanol treatment and 68° after CH_2Cl_2 treatment. After 45 min, the HEMA concentration in the polymerization flask reached 44 mol% and the contact angles of the sample taken out at this time are 48° after methanol treatment 59° after CH_2Cl_2 treatment and. These changes in contact angles clearly reveal that the surfaces with longer polymerization time are more hydrophilic and contain higher HEMA composition. Therefore, the copolymer brushes synthesized are gradient copolymer brushes that have a MMA rich bottom layer and become progressively HEMA rich as the polymer chains extended from the surface.

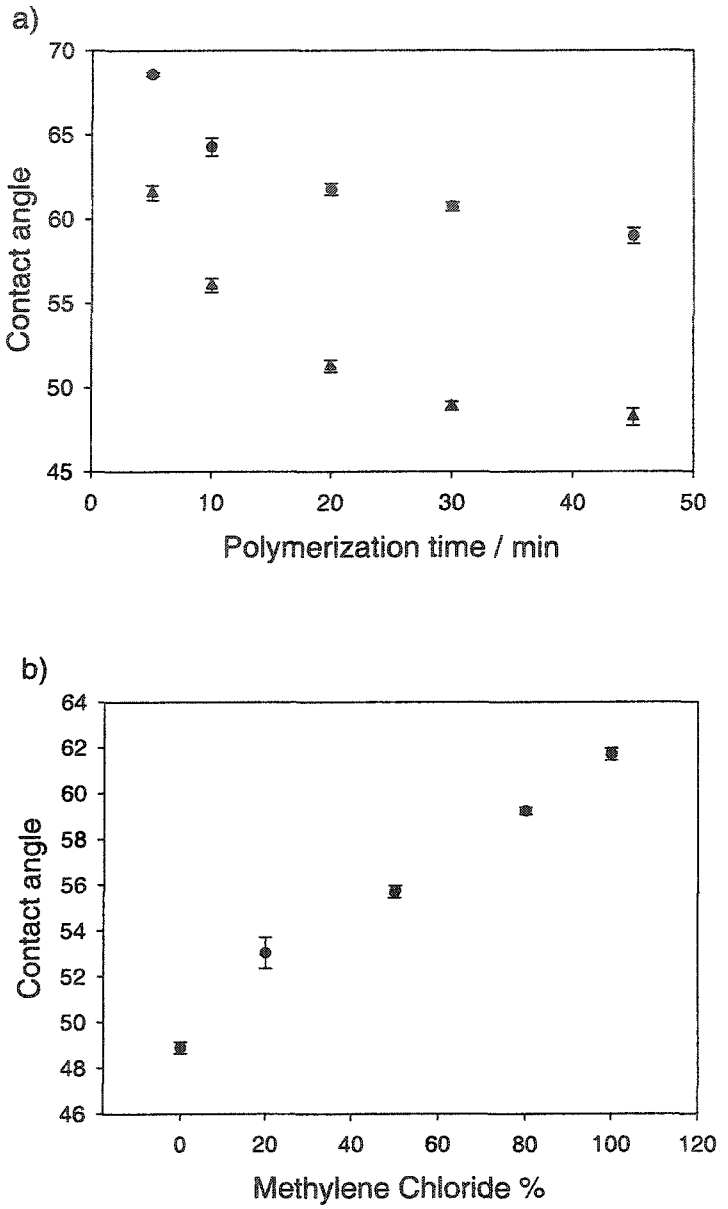

Figure 4.2 Contact angle measurement of the gradient copolymer brushes after selective solvent treatment. a) Comparison of polymer brushes with different periods of polymerization time after solvent treatment. ▲: after methanol treatment, ●: after methylene chloride treatment. b) Methanol and methylene chloride mixed solvent treatment of polymer brush with 30 min polymerization time.

As shown in Figure 4.2a, for the same gradient copolymer brushes, higher water contact angle was observed after CH_2Cl_2 treatment than after methanol treatment. Treating the polymer brushes with a mixed solvent of CH_2Cl_2 and methanol clearly revealed that the surface contact angle went up with increasing CH_2Cl_2 concentration (Figure 4.2b). The change of water contact angle was reversible as constant contact angle results were observed through several cycles of solvent treatment. We considered that the change of water contact angle should be attributed to the rearrangement of polymer brushes (Scheme 4.2). When the surface is treated with CH_2Cl_2, the MMA-rich segments of the polymer chains would move to the solvent interface while those HEMA-rich segments would migrate into the polymer film to avoid interaction with the solvent. After CH_2Cl_2 treatment, the water contact angles of samples with different polymerization time kept the same trend as those after methanol treatment.

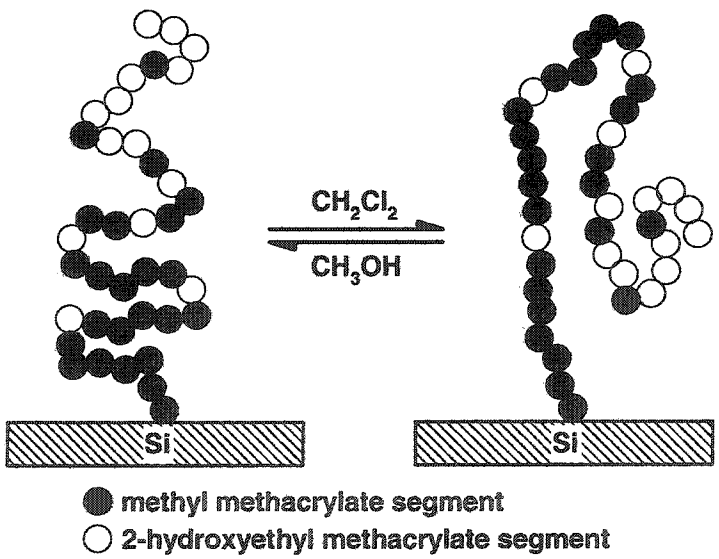

Scheme 4.2 Proposed rearrangement of gradient copolymer brushes upon solvent treatment.

It is also worth to note here that the contact angle of the gradient copolymer brushes cannot reach the value of pure MMA after CH_2Cl_2 treatment. Instead, it decreases with increase of polymer brushes thickness. After CH_2Cl_2 treatment, the bottom MMA rich segments tend to migrate to the surface. However, for any segment of the gradient copolymer chain exposed to the surface, it must be able to stretch from surface through a distance no less than the thickness of the polymer brushes. Therefore, polymer chains formed at the early stage of the polymerization may not be able to penetrate the thickness of the polymer brushes, even though they are more favored by the solvent. With increasing thickness of the polymer brushes, only polymer segments formed at later stage of the polymerization would be able to stretch enough distance to reach the surface. As a result, for the above gradient polymer brushes, their contact angles also gradually decrease with increased polymerization time after CH_2Cl_2 treatment.

Tapping mode atomic force microscopy (AFM) measurement of the polymer brushes formed with 30 min polymerization time also suggested the rearrangement of gradient copolymer brushes after solvent treatment. As shown in Figure 4.3, after methanol treatment, a rough surface was observed (Fig. 3a); after CH_2Cl_2 treatment, the surface became smoother (Fig. 3b). Besides topography difference, phase imaging of the sample revealed a surface composition change after solvent treatments. After methanol treatment, the phase image was dominated by bright area (Fig. 3c); after CH_2Cl_2 treatment, the phase image was almost evenly occupied by the dark and bright regions (Fig. 3d). After methanol treatment, surface areas high in topography corresponded to the bright area in phase image. In contrary, after CH_2Cl_2 treatment, surface areas high in topography appeared dark in phase image. We speculated that brighter regions in phase image

represented surface areas richer in HEMA while darker regions in phase image represented surface areas richer in MMA. Therefore, after methanol treatment, most of the surface areas were rich in HEMA composition. After CH_2Cl_2 treatment, the MMA rich segments moved to the surface and increased the surface contact angle.

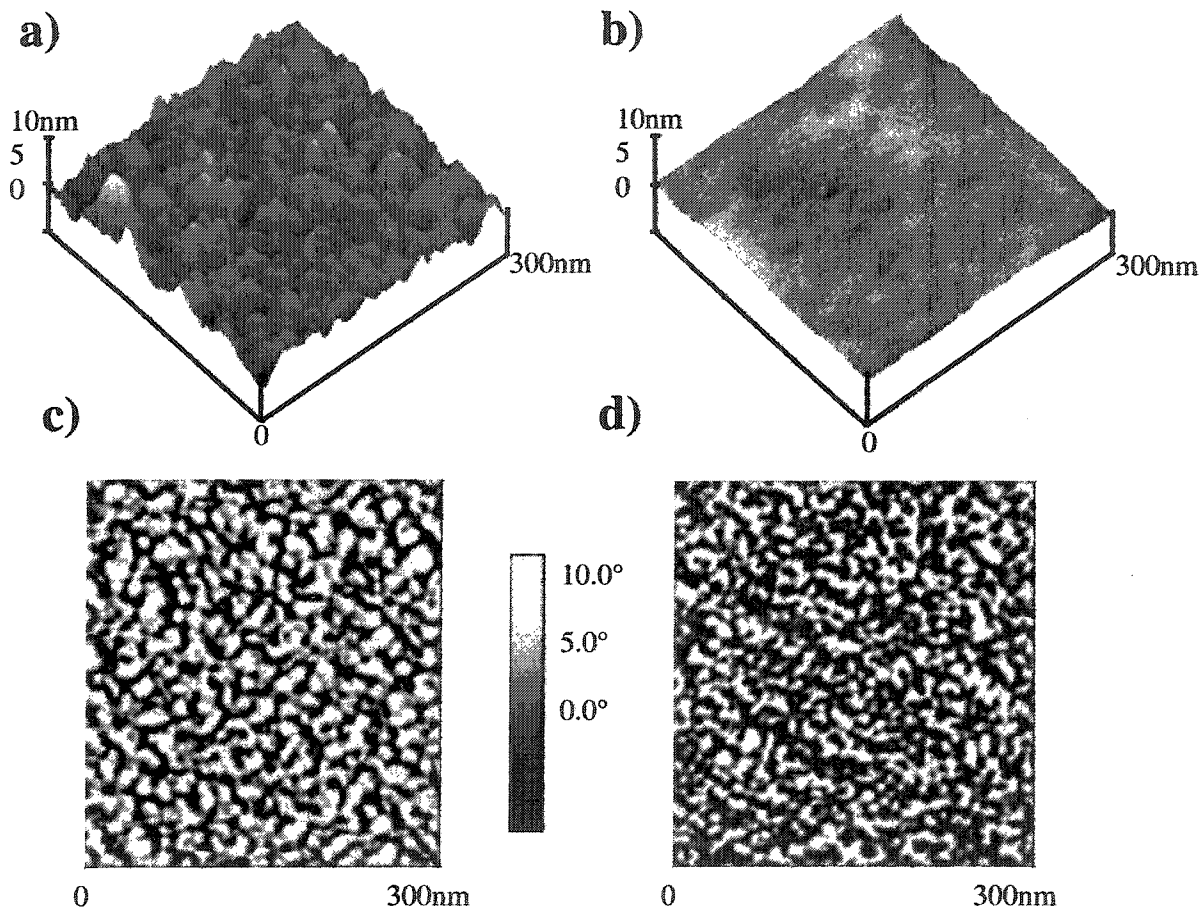

Figure 4.3 Atomic force image of gradient copolymer brushes with 30 min polymerization time after selective solvent treatment. a) Three dimensional view of topographic image after methanol treatment. b) Three dimensional view of topographic image after methylene chloride treatment. c) Phase image of the sample after methanol treatment. d) Phase image of the sample after methylene chloride treatment.

4.4 Conclusions

In summary, by gradually increasing HEMA concentration in the polymerization mixture, we synthesized poly-MMA-*grad*-HEMA copolymer brushes on surfaces via surface-initiated atom transfer radical copolymerization. Polymer segments formed at the later stage of the polymerization had increased HEMA composition, which is supported by the gradual decrease in water contact angle results. Due to the gradual composition change inside the polymer chains, the gradient copolymer brush formed can reversibly respond to selective solvent treatment. Treating the gradient copolymer brush with CH_2Cl_2, a good solvent of MMA, can bring MMA rich segments to the surface and increase surface contact angle. Treating the surface with methanol, a better solvent for HEMA, can bring HEMA rich segments to surface and reduce surface contact angle.

The rearrangement of the gradient polymer brushes was also supported by AFM results. The formation of gradient copolymer brushes on surface also provides a one-pot synthesis method to fabricate surface with switchable properties. The properties of the surface can be fine tuned by the gradient profile of the surface.

Chapter V

Grafted block copolymer brushes gradients: a combinatorial approach to study solvent response behavior of block copolymer brushes

5.1 Introduction

Grafting surface with polymer brushes provides a versatile way to modify surface properties.[1-3] One convenient method to graft polymer brushes on surfaces is surface-initiated polymerization.[4] In this approach, initiator molecules are first immobilized on the surface. Subsequent polymerization from those tethered initiator molecules leads to the formation of polymer brushes on surface. For its controlled/living character, tolerance of functional groups, and mild experimental requirements, surface-initiated atom transfer radical polymerization (ATRP)[5-7] has attracted the most attention among various types of polymerization methods.[5-13]

With the development of living surface-initiated polymerization, copolymers brushes with different architectures have been synthesized.[14-17] To form responsive surfaces, block copolymers were often used to modify the surfaces.[14, 16-18] Selectively treating block polymer brushes with solvents favoring one block exposes that specific block to the surface, resulting in changes of surface properties.

Previous theoretical and experimental results demonstrated that various factors, such as grafting density, thickness, chemical composition, solvents, and temperature, may affect the properties of polymer brushes.[19-28] Combinatorial approach, which has been widely used to accelerate the new drug discovery and process development in pharmaceutical and catalyst industry during the last decades,[29-31] was also explored to study polymer brushes. For example, with a polymer grafting density gradient polymer brushes, Genzer *et al.* studied how its grafting density affects its swelling properties.[19,20] In another example, with a gradient substrate that composed of two polymer brushes,

several groups has studied the effect of relative grafting densities on the solvent induced rearrangement of polymer brushes.[32-33]

In above cases, gradient substrates with systematic variations of parameters across the surfaces were synthesized and utilized as high-throughput platforms for further studies. Several methods have been developed to synthesize polymer brush modified substrates with gradient properties such as grafting density, molecular weight and chemical composition.[19, 34, 35] Recently, Genzer *et al.* demonstrated the synthesis of block copolymer brush gradients.[36] In their approach, a layer of gradient molecular weight 2-hydroxyethyl methylacrylate (HEMA) was first synthesized. In one example, a uniform second MMA layer was constructed. In another example, a second gradient layer was targeted to bring the overall thickness of polymer brushes even across the surface.

In this work, we used gradient substrates to combinatorially study the influence of relative block thickness on the solvent responsive behavior of diblock copolymer brushes. To achieve this goal, block copolymer brush gradients were synthesized via surface-initiated ATRP. The resulting polymer brushes had a uniform n-butyl metharylate (BMA) bottom block and gradient molecular weight 2-(N,N'-dimethylamino)ethyl methacrylate (DMAEMA) top block. With gradient samples of different BMA block thicknesses, copolymer brush libraries with controlled variation of individual block thickness were established. Those gradient substrates then were subjected to the selective solvent treatments. The response behavior of the block copolymer brushes was evaluated through water contact angle measurement.

5.2 Experimental Section

5.2.1 Materials

2-(dimethylamino)ethyl methacrylate (DMEAMA, 99%) was purchased from Polysciences. Copper (I) bromide (CuBr, 99%, Aldrich) was purified according to the literature procedures.[37] Copper (II) bromide ($CuBr_2$, 99%), 2,2'-bipyridyl (bpy, 99+%), n-butyl methacrylate (BMA, 99%), methylene chloride (99.9%, HPLC grade), hexane (98.5% ACS grade), diemthylformamide (DMF, 99.8%, HPLC grade), acetone (99.5%, ACS grade) anhydrous toluene (99.8%) were purchased from Aldrich. Isopropanol (HPLC grade) was ordered from J. T. Baker. Water was purified through a Millipore Rios 16 system. Single side polished silicon (100) wafers were purchased form Wafer World Inc, and the double side polished silicon (100) wafers were purchased from Silicon Inc. A BS-8000 programmable syringe pump (Braintree Scientific, Inc.) was used to control the injection rate of the reaction mixture.

5.2.2 Initiator SAMs modified silicon substrate

The formation of initiator SAMs on silicon surface was reported in a previous work.[38] Briefly, the initiator, 11-(2-bromo-2-methyl)propionyloxy-undecenyltrichlorosilane, was synthesized according to the literature procedures.[6] Then it was diluted with anhydrous toluene to a concentration of 0.5 mM. A fresh cut silicon wafer (1.6×3 cm^2 for uniform sample, 1.2×8 cm^2 for gradient sample) was rinsed with acetone and ultraviolet-ozone cleaned for 30 min. Then the slide was immersed into the initiator toluene solution and kept overnight to ensure the complete formation of initiator self-assembled monolayers

(SAMs) on surface. Following rinse of toluene and acetone, the slide was dried under a flow of nitrogen.

5.2.3 Preparation of polymerization solutions

CuBr (19.2 mg), $CuBr_2$ (3.3 mg), bpy (49.2 mg), and a stirring bar were added into a flask and capped with septum. After three cycles of vacuum and backfilling with argon, 4.5 mL degassed isopropanol, 0.5 mL degassed H_2O, and 5 mL degassed monomer (BMA or DMAEMA) were sequentially syringed into the flask. The polymerization mixture then was stirred for 1 hr.

5.2.4 Synthesis of surfaces with uniform polymer brushes

An initiator modified silicon substrate (1.6 x 3 cm^2) was placed in a flask and sealed with a rubber septum. Following three cycles of vacuum and backfilling with argon, the flask was quickly filled in with the above prepared polymerization mixture and the whole substrate was immersed by the polymerization solution. After a certain period of polymerization at room temperature, the substrate was taken out from the reaction mixture, thoroughly rinsed with DMF, and dried under a flow of nitrogen. To synthesize block copolymer brushes, the same procedures described above were applied with a polymer brush modified substrate.

5.2.5 Synthesis of polymer brush gradients.

An initiator/polymer modified silicon substrate (1.2 x 8 cm^2) was placed upright in a flask, sealed with a rubber septum and followed by three cycles of vacuum and argon.

The polymerization solution was transferred into a 10mL syringe, which then was mounted on the micro-pump. The polymerization solution was slowly pumped into the reaction flask along its sidewall at a rate of 100 μL/min. After a given period of time, the pumping process ceased. The substrate was removed from the flask, rinsed with DMF, and dried under a flow of nitrogen.

5.2.6 Solvent treatment of the surface

Hexane, methylene chloride, acetone, methanol, and water were used to treat the surface. For each solvent treatment, the substrate was immersed inside the solvent for 30 min. Then it was taken out from the solvent and immediately dried under a flow of nitrogen.

5.2.7 Measurement methods

VASE ellipsometry (Woolan Inc.) was used to measure the thickness of the SAMs and polymer brushes. Surface water contact angle was measured using a Krüss G2 contact angle instrument. Transmission FT-IR was measured on a Nicolet Magna-IR 860 sepectrometer at Brewster's angle of silicon (74°). Each spectrum was collected with 512 scans at a 8 cm^{-1} resolution.

5.3 Results and discussion

5.3.1 Surface-initiated atom transfer radical polymerization of BMA and DMAEMA.

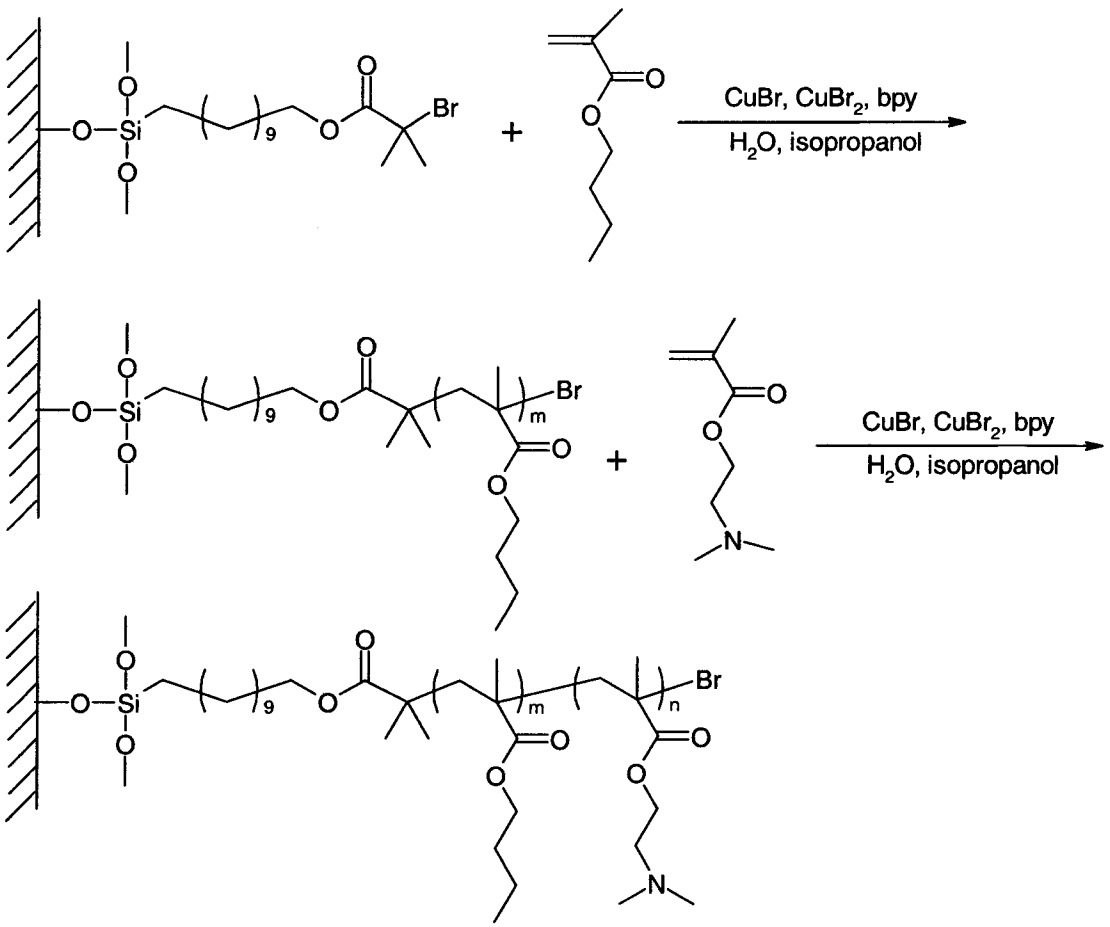

Figure 5.1 Synthesis of copolymer brushes of n-butyl methacrylate and 2-(dimethylamino)ethyl methacrylate via surface-initiated atom transfer radical polymerization.

Figure 5.1 outlines surface-initiated atom transfer radical polymerization (ATRP) of BMA and DMAEMA. The polymerization conditions used in this work were modified from solution ATRP of BMA and DMAMEA reported by Matyjaszewski *et al.*[37] The

only difference was the initiator, which was replaced by initiator SAMs modified substrates. Due to the extremely small amount of initiator moieties present in the polymerization, we did not assume that the surface-initiated polymerization was also controlled. The kinetics of surface-initiated polymerization of BMA and DMAEMA were first characterized.

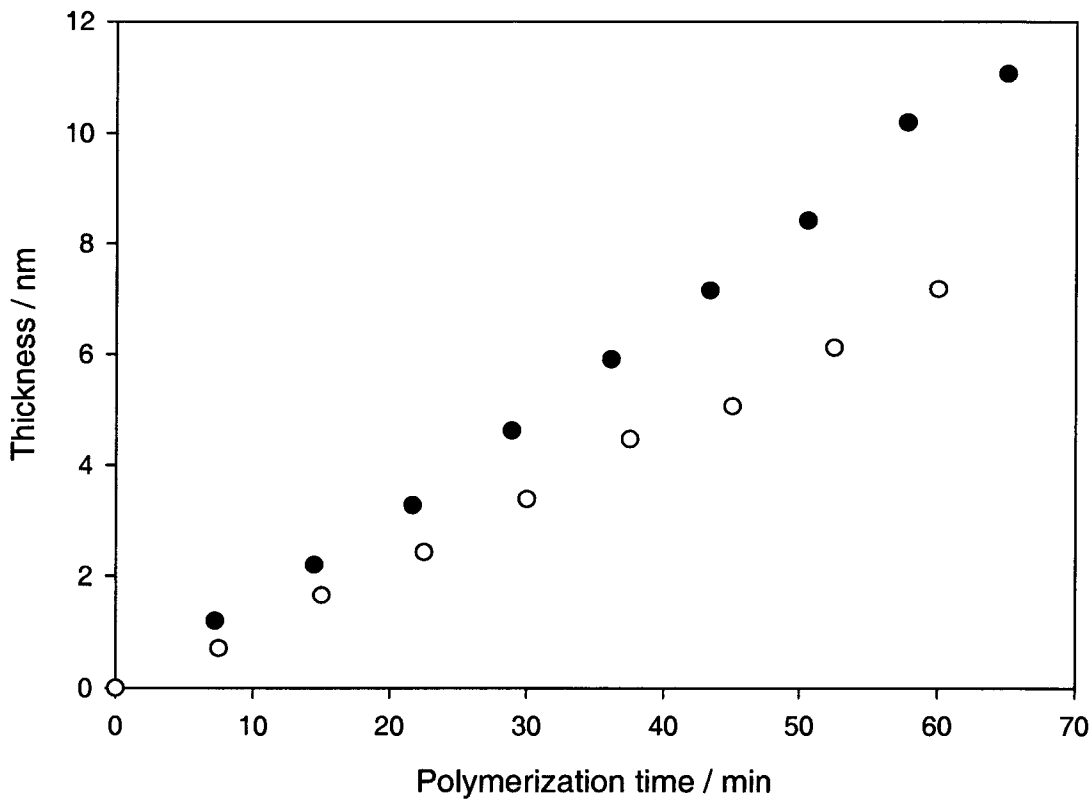

Figure 5.2 Kinetics of homopolymer brush's growth of. • poly (n-butyl methacrylate) (BMA), and ○ poly (2-(dimethylamino)ethyl methacrylate) (DMAEMA). Polymerization conditions: [CuBr] = 13.5 mmole, [$CuBr_2$] = 1.5 mmole, [bipyridine] = 30 mmole, monomer (BMA or DMAEMA) : isopropanol : H_2O = 50 : 45 : 5 (v : v : v).

Recently, it was demonstrated that the kinetics of surface-initiated polymerization could be combinatorially studied by varying the polymerization time at different locations of the substrate.[35] Similar approach was adopted in this study. During the polymerization, polymerization solutions were gradually pumped into the reaction flask at a controlled rate. As the solution level went up, the substrate was gradually immersed. After a certain period of time, the whole substrate was removed from the polymerization solution. Therefore, areas located at the bottom of the flask had longer polymerization time than those at the top. Figure 5.2 shows the results of such polymerization of both BMA and DMAEMA. For both monomers, linear growth of polymer brush thickness with polymerization time was observed. These results suggested that the polymerization processes were controlled under current conditions and the thickness of the polymer brushes could be readily controlled with polymerization time.

5.3.2 Block copolymer brushes synthesis

Prior to the synthesis of block copolymer brush gradients, we synthesized uniform block copolymer brushes of BMA and DMAEMA. The chemistry of the resulting polymer brushes was characterized by transmission FT-IR. Here, double side polished silicon wafers were used to prevent light from scattering at the rough surfaces.

To synthesize block copolymer brushes, the initiator modified substrate was first polymerized in BMA solution for 40 min and the film thickness increased by 7 nm. Subsequent polymerization of DMAEMA for 1 hr added extra 8 nm to the total film

thickness. Under the same conditions, 8 nm thick PDMAEMA homopolymer brushes were synthesized from initiator modified substrate.

IR spectra for substrates with initiator self-assembled monolayers only, PBMA, PDMAEMA, and PBMA-b-PDMAEMA brushes were shown in Figure 5.3 from top to bottom. The characteristic peak for the C=O group was at 1736 cm^{-1}, peaks at 1254 and 1159 cm^{-1} were attributed to C-O stretching. The peaks at 2854 and 2927 cm^{-1} were assigned to the C-H symmetric and asymmetric vibration modes, respectively, of the -CH_2- groups. The clear existence of peaks for C=O, CH_2, and C-O in the sample with SAMs only confirmed that initiator was immobilized on the Si wafer surfaces. After the polymerization of either BMA or DMAEMA, the intensity of these characteristic peaks increased, indicating the growth of methacrylate-based polymers on the surface. The n-butyl group inside PBMA brush contributed to the much higher intensity of peak at 2980 cm^{-1} ($\nu_{as}(CH_3)_{n\text{-butyl}}$). The spectrum of PDMAEMA sample clearly showed the two extra peaks at 2819 and 2769 cm^{-1}, which were attributed to C-H vibrations of $-N(CH_3)_2$. The IR spectrum of the PBMA-b-PDMAEMA brush contained all characteristic peaks of both homopolymer brushes. Furthermore, its peak intensities matched well with the sum of corresponding peaks in the spectra of the homopolymer brushes. Thus, in addition to the ellipsometry results, IR spectra further confirmed the successful synthesis of block copolymer brush on surfaces.

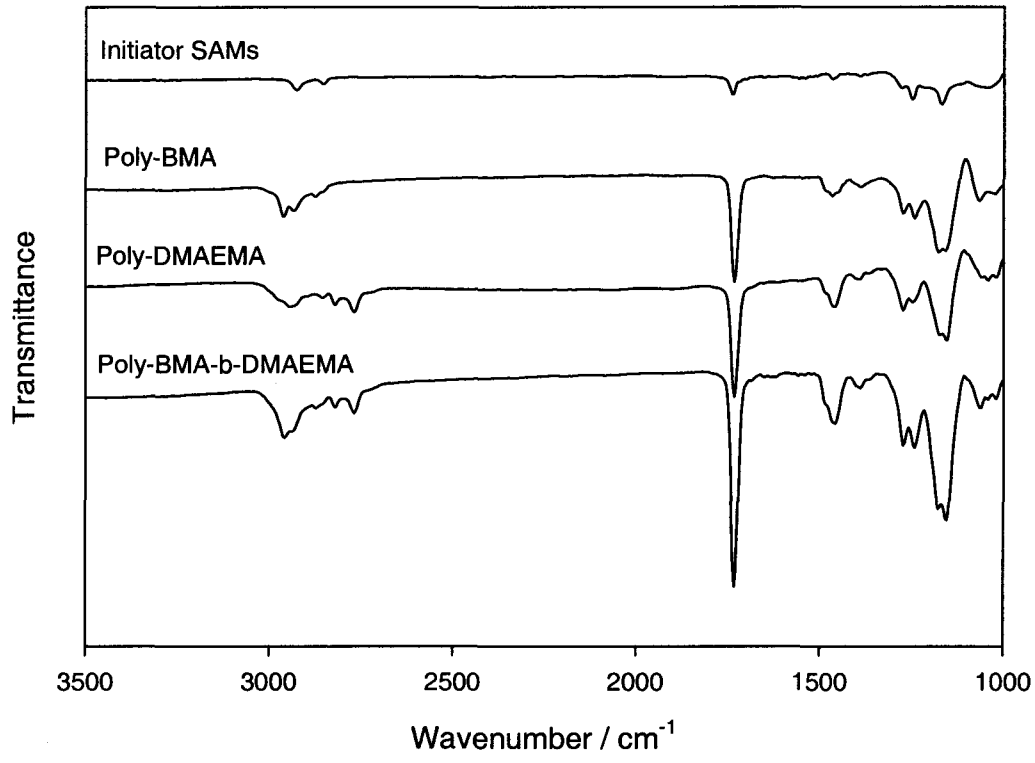

Figure 5.3 FT-IR of (co)polymer brushes synthesized from surface initiated polymerization. 1) initiator self-assembled monolayers, 2) n-butyl methacrylate (BMA), 3) 2-(dimethylamino)ethyl methacrylate (DMAEMA), 4) poly-BMA-b- DMAEMA.

5.3.3 Block copolymer brush gradient and its solvent response behavior

The block copolymer brush gradient was synthesized in two steps. First a uniform layer of PBMA brush (9.8 nm) was synthesized. With the same technique used to synthesize the homopolymer brush gradient, subsequent polymerization from the homogeneous PBMA brushes resulted in the block copolymer brush gradient. As shown

in Figure 5.4, the PDMAEMA block thickness increased linearly from 0 nm at one end of the substrate to 12 nm at the other.

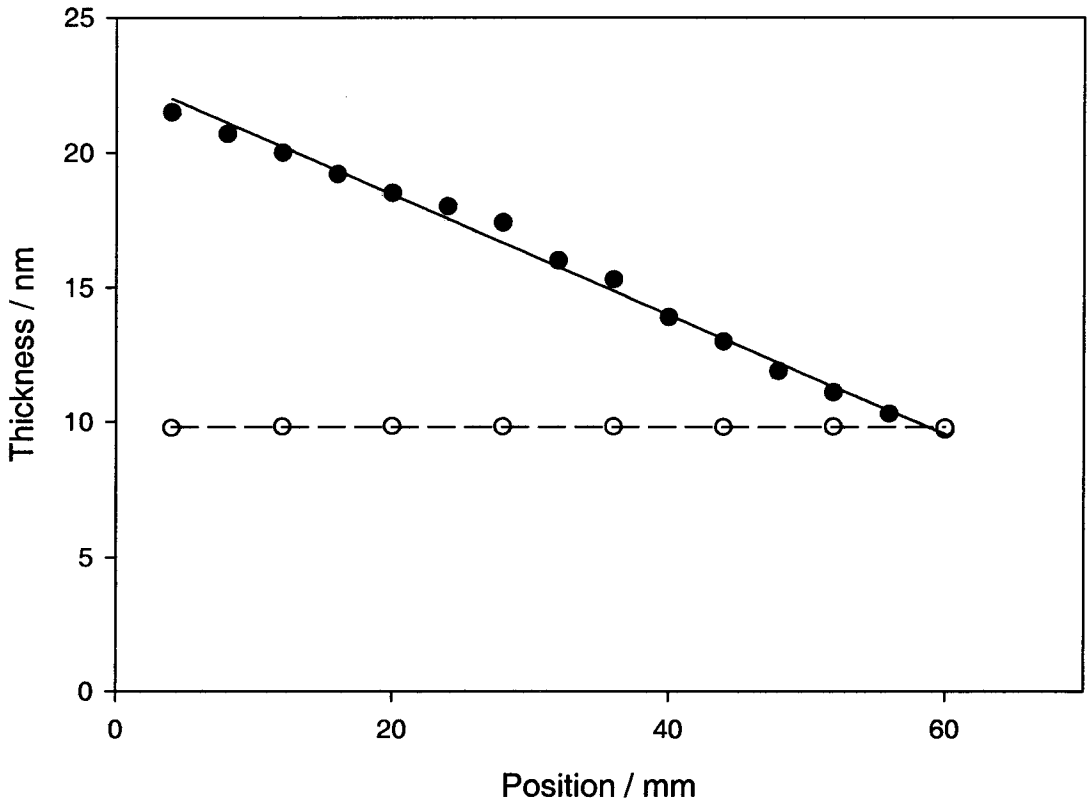

Figure 5.4 Profile of block copolymer brush gradient synthesized. ○ thickness of the first PBMA block, ● thickness of the overall block copolymer brush thickness after polymerization of PDMAEMA.

Here, the block copolymer brush gradient libraries synthesized provided a high throughput pathway to elucidate how relative block thicknesses affect the properties of the block copolymer brushes. Hexane and water were chosen to treat the gradient surfaces. To facilitate the rearrangement of the block copolymer segments, methylene

chloride, acetone and methanol were used as intermediate solvents. For example, to check the surface properties after water treatment, the sample was sequentially immersed in methylene chloride, acetone, and methanol before the sample was treated with water. For hexane treatment, the reverse sequence was applied.

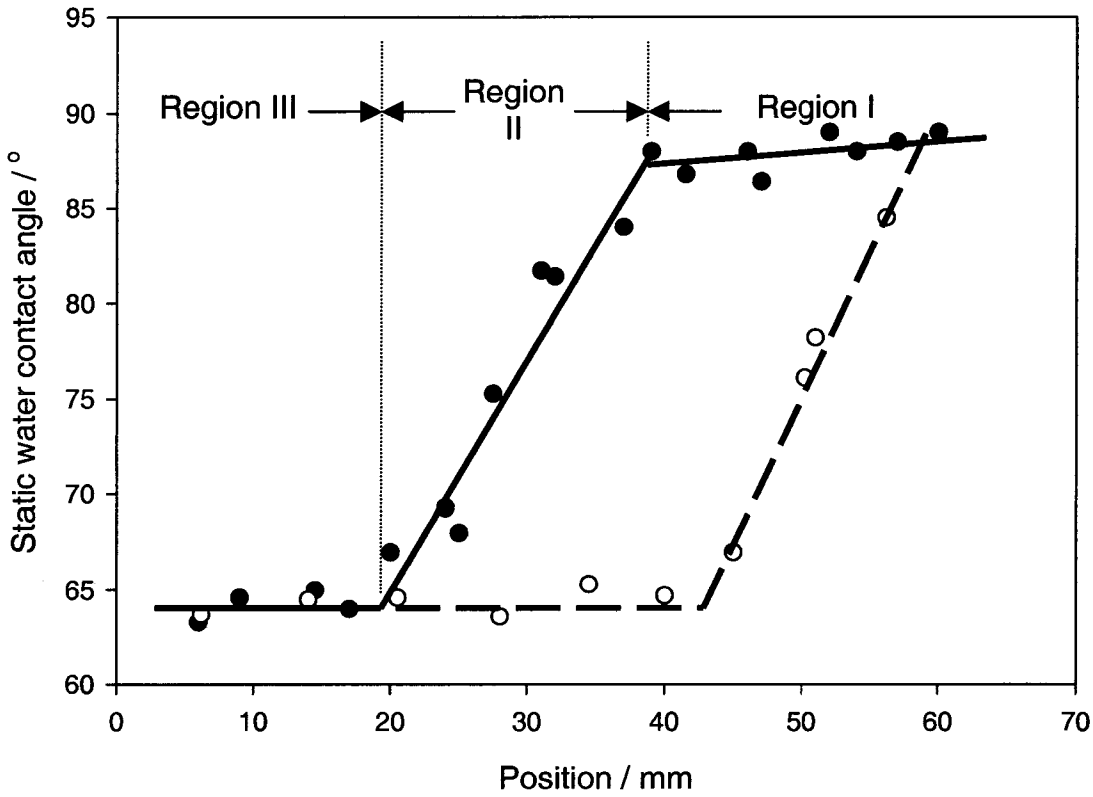

Figure 5.5 Surface water contact angle after hexane • and water ○ treatment of copolymer brushes gradient surface with uniform 9.8 nm bottom PBMA block.

WCA mapping results of the gradient surface after solvent treatments were shown in Figure 5.5. For homopolymer brushes of PBMA and PDMAEMA, the contact angles were 89° and 65°, respectively. After water treatment, the introduction of a PDMAEMA

block over the PBMA layer quickly changed the surface properties. With increasing PDMAEMA thickness, the WCA of the surface decreased quikly until the thickness of the PDMAEMA block reached 2.5 nm, where the WCA results became the characteristic value of PDMEAMA. Beyond this point, further increase of the PDMEAMA thickness didn't affect the surface WCA.

After hexane treatment, the presence of a thin PDMAEMA layer on PBMA block hardly changed the surface WCA, which resembled that of homo PBMA brushes. However, after the PDMAEMA block thickness reached ~4.5 nm, a sharp decrease of surface WCA with increase of PDMAEMA block thickness was observed. This decrease of WCA continued until the PDMAEMA thickness reaches ~10 nm, where the characteristic WCA value of PDMAEMA was observed.

The surface wetting properties depend on not only its chemical composition but also the surface roughness. Atomic force microscopy (AFM) images of the surface indicated that the surface was homogenous and. surface roughness was less than 1 nm after both water and hexane treatment. No nanostructure appeared on surfaces after hexane treatment. The appearance of homogeneous surfaces was probably due to the small χ interaction parameter between PBMA and PDMAEMA. Therefore, variations of surface contact angle mostly reflected the surface composition changes, which could be calculated from the Cassie equation:[39]

$$\cos\theta = \varphi\cos\theta_A + (1-\varphi)\cos\theta_B$$

where θ is the surface WCA, θ_A and θ_B are the WCA of homopolymer brushes of PBMA and PDMAEMA, and φ is the fraction of surface covered by PBMA. Therefore, the increase of the surface contact angle would indicate the increase of PBMA segments on the surface.

Water is a better solvent for PDMAEMA than for PBMA. Water treatment of the polymer brushes brings the PDMAEMA to the surface. Therefore, PDMAEMA block dominated surface if it was thicker than 3 nm. If the PDMAEMA block is thinner than 3 nm, it couldn't effectively shield PBMA from surface, resulting in higher.

Hexane is a better solvent for PBMA than PDMAEMA. While PDMAEMA block collapse and avoid contact with the hexane, PBMA tend to migrate to the surface during hexane treatment. Based on surface WCA results after hexane treatment, the block copolymer brush gradient can be divided into three regions (Figure 5.6). Region I covers areas with relatively short PDMAEMA block. In this region, the PBMA block can effectively accommodate the collapsed PDMAEMA block and dominate the surface. In region II, with the increased PDMEMA block thickness, it is hard for the collapsed PDMAEMA block to be fully covered by the PBMA. Both PBMA and PDMAEMA segments co-exist on the surface. The amount of PBMA segments exposed on surfaces decreases with increase of PDMAEA block thickness. In region III, the PDMAEMA block is so thick that the PBMA segment no longer be able to be exposed to the surface. Surface is totally occupied by PDMAEMA segments.

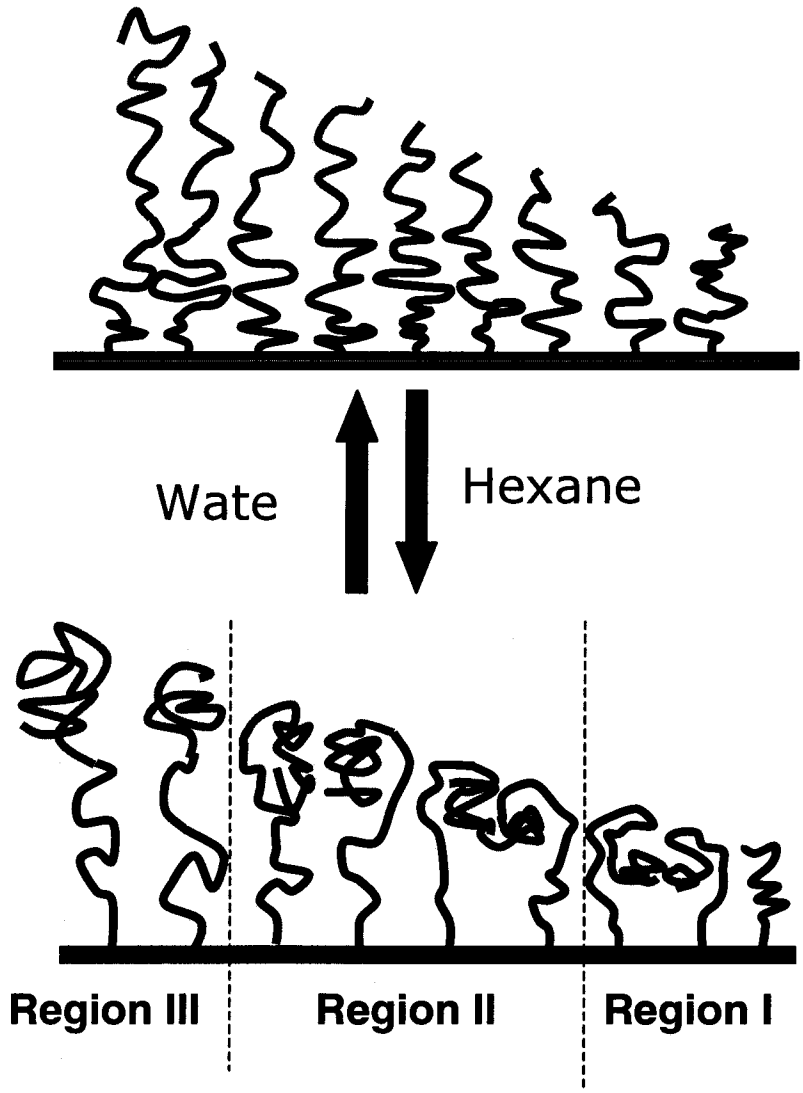

Figure 5.6 Schematic illustration of three regions of the block copolymer brushes after hexane treatment.

5.3.4 Effects of bottom layer thickness on re-initiation

Before tuning the uniform PBMA block thickness of the block copolymer gradients, we assessed how the first PBMA block thickness affects the growth of the second DMAEMA block. For this purpose, a molecular weight gradient PBMA substrate with linear thickness variation from 0 nm at one end to 23 nm at the other end was synthesized. Then the whole substrate was immersed into a polymerization solution of DMAEMA. After 2 hrs of polymerization, the whole substrate was removed from the polymerization solution. Therefore, different regions on surface had the same polymerization time for DMAEMA. As shown in Figure 5.7a, polymer brush thickness substantially increased all over the gradient surface. The bare initiator SAMs modified surface, which was not exposed to the first BMA polymerization solution, provided an ideal internal standard to address the reinitiating efficiency for the second PDMAEMA block. Figure 5.7b show the percentage growth of the second PDMAEMA block on the gradient substrate with respect to the bare initiator SAMs areas. Generally, the growth of second block gradually slowed down with the increase of the PBMA block thickness. However, high reinitiating efficiency was maintained across the gradient. With 23 nm PBMA block, the growth of PDEMAEMA remained 80% of that of initiator SAMs. For surface areas with PBMA thickness less than 15 nm, more than 90% growth of PDMAEMA block was retained. In this region, the small and gradual change in reinitiating efficiency allowed us to independently study how the bottom PBMA block affected block copolymer brush properties.

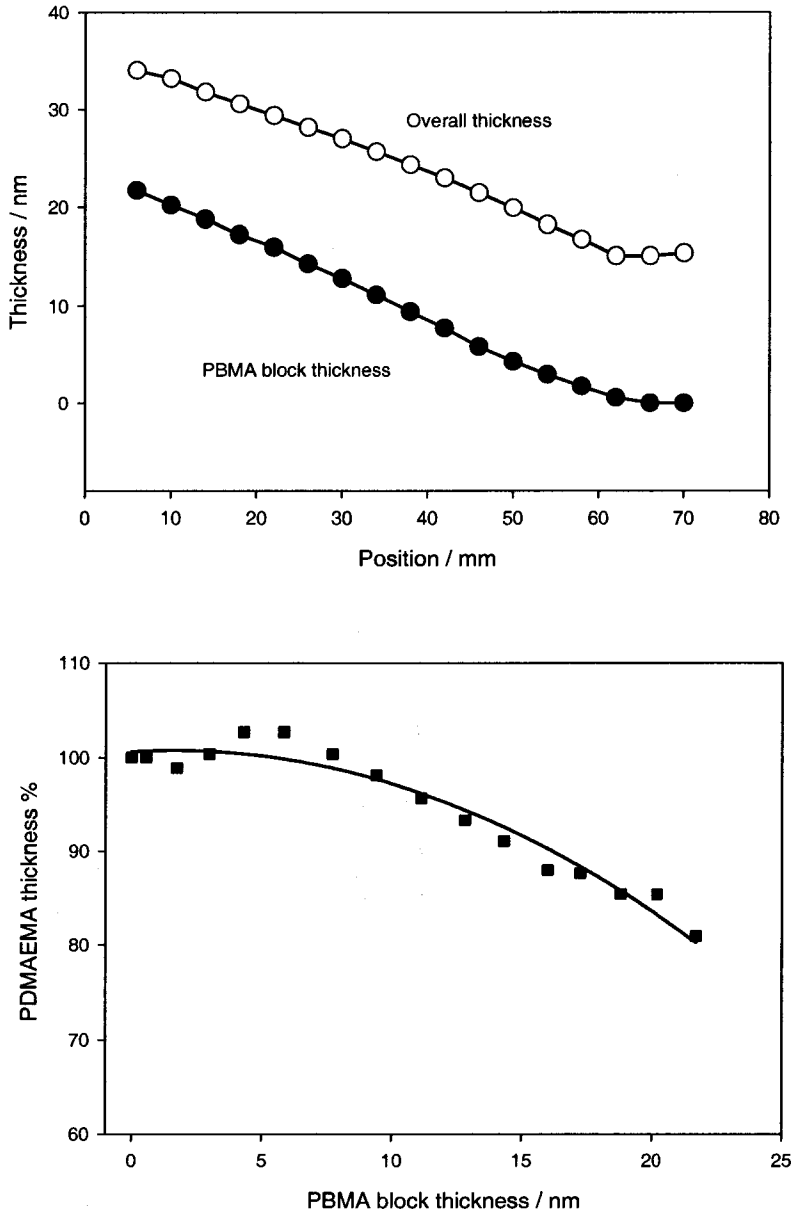

Figure 5.7 Effect of first poly (n-butyl methacrylate) (PBMA) block thickness on the growth of second poly (2-(dimethylamino)ethyl methacrylate) (PDMAEMA) block. a) Polymer brush thickness after • polymerization of PBMA and ○ subsequent polymerization of PDMAEMA. B) Percentage growth of PDMAEMA block on the gradient surface with respect to surface with initiator self-assembled monolayers only.

5.3.5 Effects of lower block thickness on solvent response behavior

With block copolymer gradients of different PBMA layer thickness, we explored how bottom layer thickness affected the solvent response behavior of the copolymer brushes. Two more substrates with uniform PBMA block and gradient PDMAEMA block were synthesized. One had 4.5 nm and the other had 14.1 nm PBMA bottom layer. Their solvent response behaviors were studied and compared with the previous sample of 9.8 nm PBMA block. Figure 5.8 shows the results of such comparison. After water treatment, similar properties were observed for all three different gradients. Introducing a thin PDMAEMA block over the PBMA layer immediately changed surface wetting behavior. The surface WCA quickly reduced with increasing PDMAEMA block thickness. The presence of 2~3 nm or more PDMAEMA completely changed the surface WCA to that of PDMAEMA homopolymer brushes.

On the contrary, after hexane treatment, the surface wetting behaviors were greatly influenced by the PBMA block thickness. Extension of the PBMA block effectively expanded regions I and II. Within region II, higher WCA was observed for the substrate with thicker PBMA blocks. For the sample with a 4.5 nm PBMA block, the presence of PDMAEMA immediately decreased the surface WCA. Only 6 nm PDMAEMA block was necessary to bring the surface into region III. For substrate with 14.1 nm PBMA block, region I covered areas with top PDMAEMA block thickness up to 6 nm thick. In region II, even 15 nm PDMAEMA block still could not prevent the PBMA layer from being exposed to the surface.

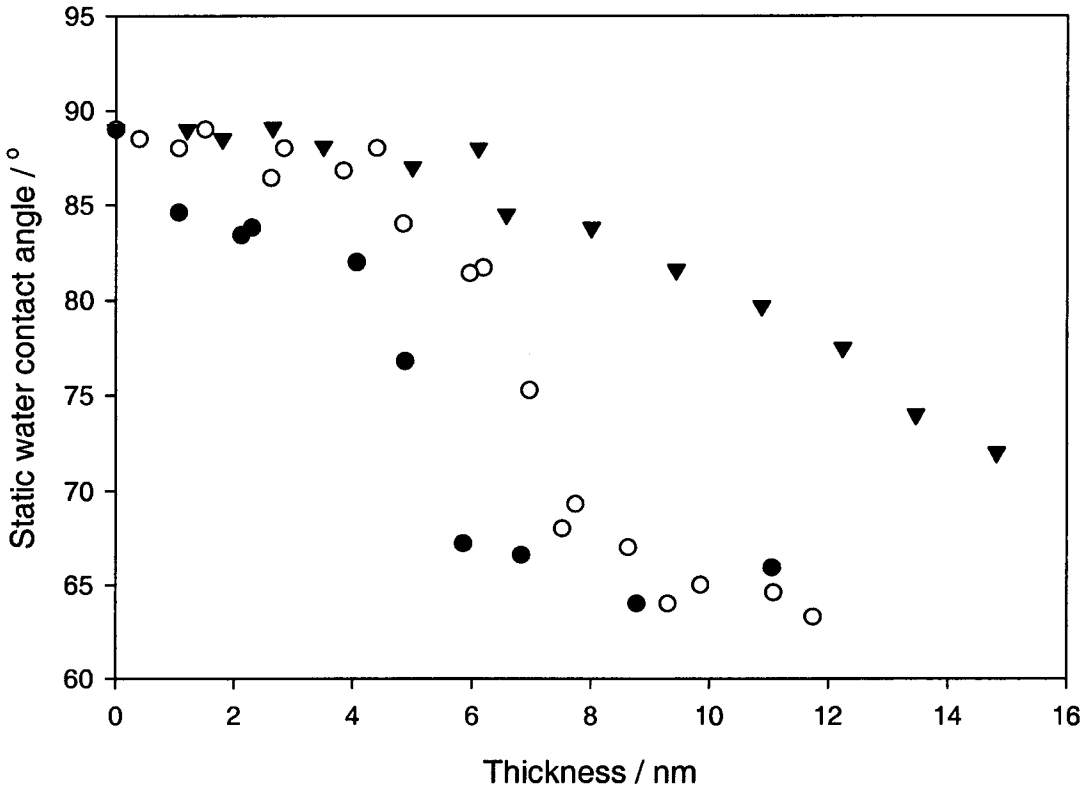

Figure 5.8 Effect of bottom poly (n-butyl methacrylate) (BMA) block thickness on the gradient properties of the surface after hexane treatment. The thicknesses of the PBMA block are ● 4.5, ○ 9.8 nm, and ▼14.1 nm, respectively

Because PBMA end of the block copolymer brushes is anchored on surface, to be exposed at the air interface during hexane treatment, the PBMA segment must stretch long enough to overcome the thickness barrier of the top DMAEMA block. Moreover, it is much easier for longer PBMA segments to accommodate the inversion of collapsed PDMAEMA block. As a result, with increase of PBMA block thickness, regions I and II expand. On the other side, such barrier doesn't exist for the upper PDMAEMA block at

the free end of the copolymer brushes. Therefore, after water treatment, the WCA is almost independent of the PBMA block thickness.

5.4 Conclusions

In summary, we systematically studied the influence of individual block thickness on the solvent response behavior of poly-BMA-b-DMAEMA brushes. To achieve this goal, homo and block (co)polymer brush gradients were utilized as combinatorial libraries. Block copolymer brushes BMA and DMAEMA were synthesized via sequential atom transfer radical polymerization. The successful syntheses of homo and block copolymers were confirmed by ellipsometry and transmission FT-IR measurements of the surface.

The block copolymer brush gradients synthesized here had uniform first PBMA blocks and molecular weight gradient second PDMAEMA blocks. After water treatment, the presence of 2~3 nm or more PDMAEMA block reduced surface WCA of the block copolymer brushes close to that of PDMAEMA brushes. After hexane treatment, three regions were observed. In region I, the PBMA block dominated the air interface and surface WCA was close to that of PBMA homopolymer. In region II, PBMA and PDMAEMA segments co-exist at the air interface. Increasing PDMAEMA block thickness reduces the surface WCA and suppresses rearrangement of the chains to allow the PBMA chains to occupy the air interface after solvent treatment. In region III, PBMA no longer be able to occupy the surface and the surface WCA of PDMAEMA is observed.

With gradient substrates of different uniform bottom PBMA block thickness, we also investigated how the bottom block thickness affects the solvent response behavior of the block copolymer brushes. The surface WCA is irrelevant to the thickness of the PBMA block thickness after water treatment. However, surface WCA is greatly influenced by the bottom PBMA block thickness after hexane treatment. After hexane treatment, the regions I and II expand. Within the region II, increase of bottom block thickness increases surface WCA. This change is explained by the PBMA segment's abilities to stretch from surface and cover the collapsed domains of PDMAEMA.

Chapter VI

Using Surfaces to Control Porphyrin Nanoparticle Morphology

6.1 Introduction

Porphyrins and their related macrocycles are well known to have catalytic, photonic, and magnetic properties that can be modulated by choice of metalo derivative and the hierarchical structure of the material.[1-3] Additionally, many of these properties can be gated or altered by wavelengths of light corresponding to the electronic spectra. Given the rich chemical and physical properties, porphyrins are remarkably robust. Thus it is not surprising that the interaction of materials containing these chromophores with surfaces also has profound consequences on the porphyrin function(s). Since many applications of porphyrinic materials – especially electronic, photonic and magnetic – require them to reside on and interact with surfaces, it is important to develop deposition methods that result in predictable and controllable morphologies.[3-5] Nanoscaled structures, films and aggregates of most dyes such as the porphyrinoids have properties found neither in the individual macrocycle nor in larger crystalline or amporphous materials.[6-13] Supramolecular chemistry is an efficient means to construct nanoscaled porphyrinic materials with desired hierarchical structures in solution,[14] but there is no *a priori* reason that the supramolecular structure will be maintained upon surface deposition.[4]

The deposition and characterization of inorganic colloidal nanoprticals continues to be an active arena of research, but much less work on the formation, deposition and properties of nanoparticles of organic dyes has been reported because of the aforementioned structural rearrangements and agglomeration. The latter problem can be addressed by the use of stabilizing agents or surfactants to form colloidal suspensions of

porphyrin nanoparticles.[15] In this approach, the hydrophobic porphyrins are first dissolved in a water-miscible (host) solvent such as DMF, THF, DMSO, and acetonitrile and this solution added to water (guest solvent) with vigorous mixing. The PEG stabilizing agent can be covalently attached to the porphyrin or can be present in the guest solvent. Conversely, hydrophilic porphyrins in water can be added to an organic guest solvent. The size of the porphyrin nanoparticles can be somewhat controlled by the ratio between the host/guest solvents.[15]

Presently, we demonstrate that surface properties, in this case hydrophobicity, can be used to control the morphology and aggregation of porphyrinic nanoparticles composed of a pentacationic cationic porphyrin bearing four PEG moieties: Fe(III)TPEGPP (Figure 6.1).

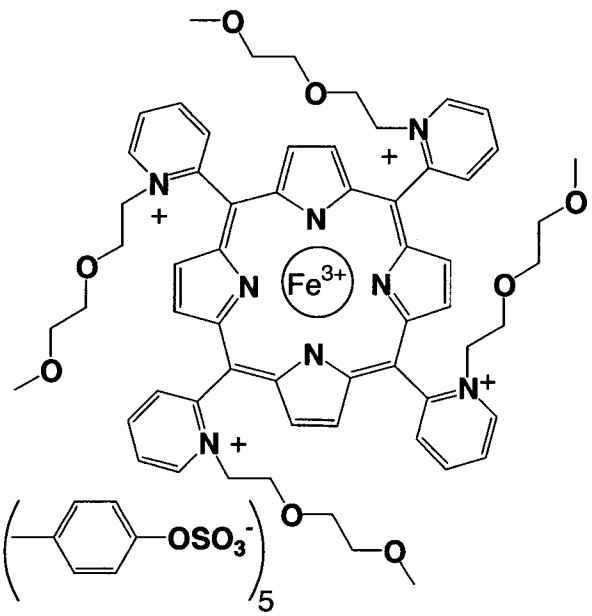

5,10,15,20-Tetrakis-{1-[2-(2-methoxy-ethoxy)-ethyl]-pyridin-2-ium}-porphyrinatto Fe(III)

Figure 6.1: Fe(III)TPEGPP

6.2 Experimental Section.

6.2.1 Synthesis of porphyrin nanoparticles

A stock solution of porphyrin nanoparticles was prepared by adding 5 mL acetonitrile to 50 μL of a ~1 mM solution of Fe(III)TPEGPP water with vigorous stirring.[15] Before the nanoparticles were applied onto surfaces, the stock solution was diluted 50 times with acetonitrile. The average diameter of the porphyrin nanoparticles in the final solution was 110 nm, as determined by dynamic light scattering (DLS) measurements.

6.2.2 Preparation of surfaces with different hydrophilicities

Surfaces with different affinities for water were prepared. Hydrophilic surfaces were prepared by ultraviolet ozone cleaning of a freshly cut silicon wafer (2 x 3 cm^2) for 30 min. Hydrophobic substrates were constructed of octadimethylchlorosilane (ODS) self-assembled monolayers (SAMs) on silicon slides, formed by vapor deposition of ODS molecules onto a ultroviolate ozone cleaned surface. The static surface water contact angle is less than 10° for ultraviolet ozone cleaned hydrophilic substrates, and is 107° for hydrophobic substrates of ODS SAMs.

6.2.3 Deposition of porphyrin nanoparticle on surfaces

Nanoparticles were transferred to the surface by drop-casting 15 μL of the diluted solution onto the substrates. To allow the nanoparticles to interact with the surface and to avoid agglomeration, the rate of solvent evaporation was retarded by placing the substrate

inside a confined space. After complete evaporation of the solvent from the surface, the samples were imaged using tapping atomic force microscopy (AFM, Park Instruments).

6.3 Results and Discussion

6.3.1 Morphology of porphyrin nanoparticle on UV-ozone cleaned surface

On hydrophilic surfaces the nanoparticle solution spreads around most of the surface area available. As the solvent evaporates, the solution boundary gradually recedes and visibly disappears in about 2 min. Generally, porphyrin aggregates were observed throughout the surface that was in contact with the solution.

Two different morphologies of porphyrin aggregates with heights much less than the diameter of original nanoparticles in solution were observed (Figure 6.2). One type aggregate is particle like (Figure 6.2a) while the other type has a disk-shape. Generally, for particle-shaped structures, their heights are less than 20 nm, and in most cases, between 1 to 10 nm. Most disk-shape structures have heights less than 2 nm and spread across several hundred nm^2 on the surface, which is substantially different from the 110 nm average diameter of the original nanoparticles in solution. The thinnest disk observed in our study was about 0.4~0.6 nm thick (Figure 6.2b), which corresponds to a monolayer film of porphyrin molecules laying flat on the surface. In addition to the two main morphologies, aggregates with intermediate morphologies were also observed. One such intermediate structure is shown in Figure 6.2b; where a particle is imbedded in a disk-shaped film. These intriguing intermediate structures suggest that the disk like aggregates

may result from the collapse of the large particles found in solution and possibly the melding of neighboring materials.

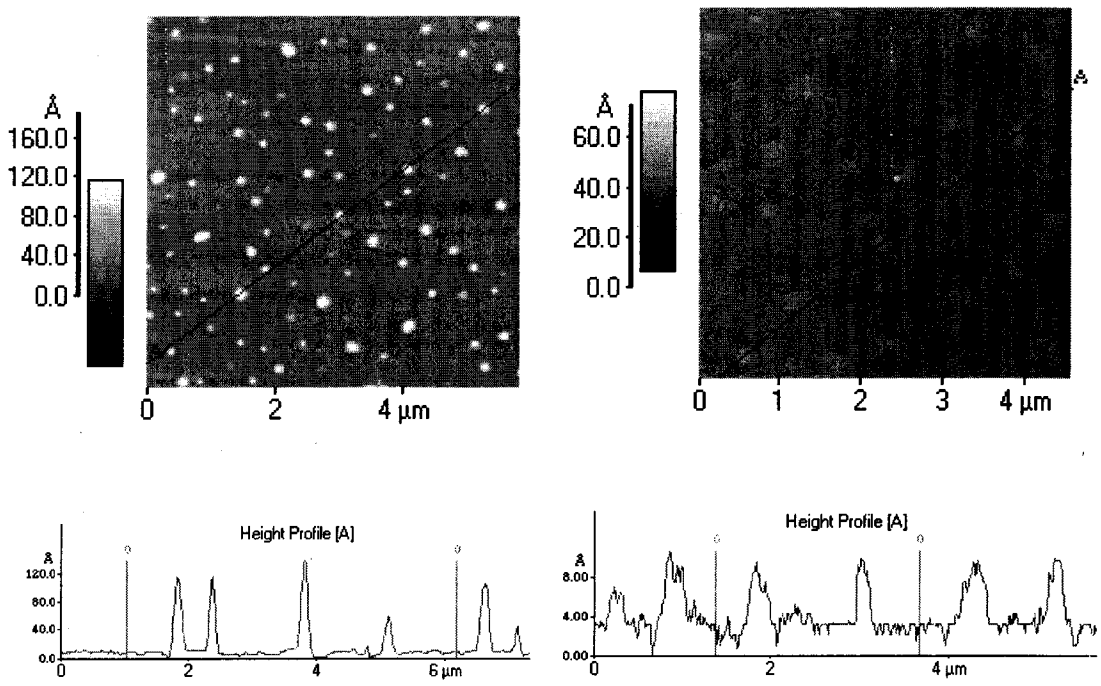

Figure 6.2 Fe(III)TPEGPP aggregates on an UV ozone cleaned hydrophilic surface.

Other structures with various degrees of organization were also observed (Figure 6.3). For example, doughnut arrangements of nanoparticles on hydrophilic surfaces are also observed (Figure 6.3a and 6.3b). Figures 6.3b and 6.3c illustrate trails of porphyrin molecules on surface, which likely indicates that large nanoparticles are shedding porphyrin clusters as they traverse the surface during solvent evaporation.[8,16,17] This hypothesis is supported by the tadpole-shaped structure in Figure 6.3d. Thus on hydrophilic surfaces, structures ranging from hundreds of nm to tens of microns of various morphologies are observed to cover most of the surface.

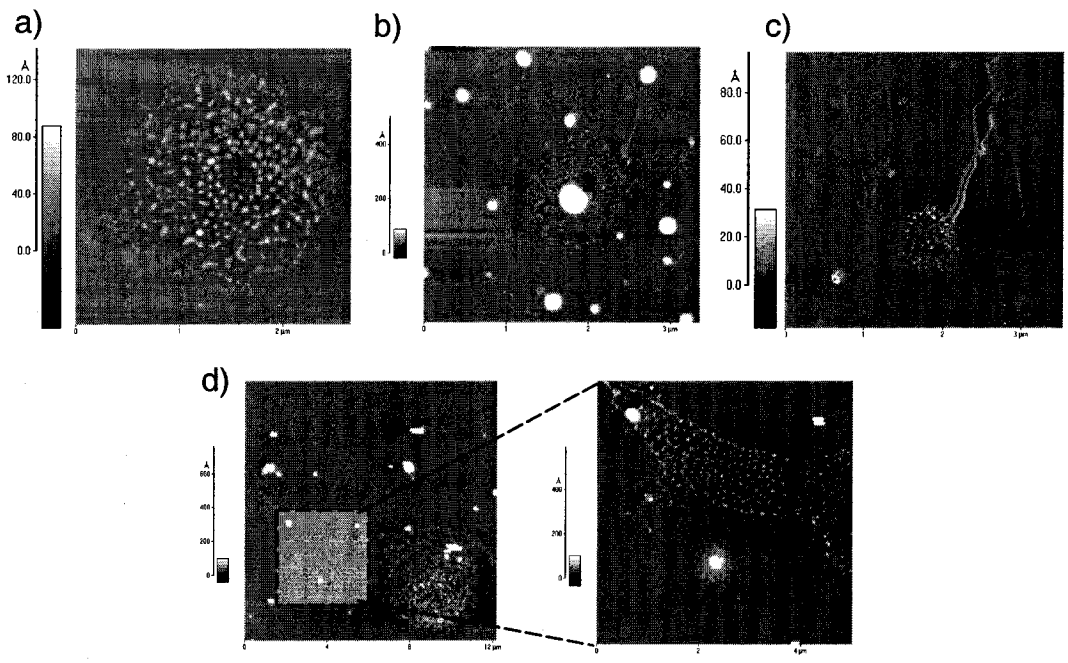

Figure 6.3 Examples of other self-reorganized patterns of Fe(III)TPEGPP nanoparticles on UV-ozone cleaned hydrophilic surfaces. a) doughnut assembly, 2.5 x 2.5 μm image b) large and small particles and lines of small porphyrin aggregates, 3.3 x 3.3 μm image, c) circular and linear patterns of porphyrin aggregates, d) a tadpole-shaped pattern of self-reorganized porphyrinic material.

6.3.2 Morphology of porphyrin nanoparticle on ODS surface

On hydrophobic ODS SAMs, the nanoparticle solution spreads over a smaller surface area than on hydrophilic surfaces; therefore, the solvent evaporates at a slower rate and it takes about 10 min for the solvent to visibly disappear. After solvent evaporation, AFM images of the surface indicate that most of the porphyrin nanoparticles on the surface correlate to the original particle size found in solution (Figure 6.4a). However, some disk-like aggregates were also observed. As shown in Figure 6.4b, the top of the disk is flat and the height of the disk is around 4 nm. Figure 6.4c shows a disk-like aggregate with one layer of materials on top of the other. The line trace of this aggregate indicates that both the top and bottom layer of the aggregate have the same height – around 4 nm. These disk structures generally have a surface area of several square microns. The volumes of the smaller disks are about the same as the average volume of a single nanoparticle in solution, which suggests that the porphyrin nanoparticles rearrange structurally, but do not completely disassemble on hydrophobic surfaces. The larger disks are likely due to the melding of more than on nanoparticles.

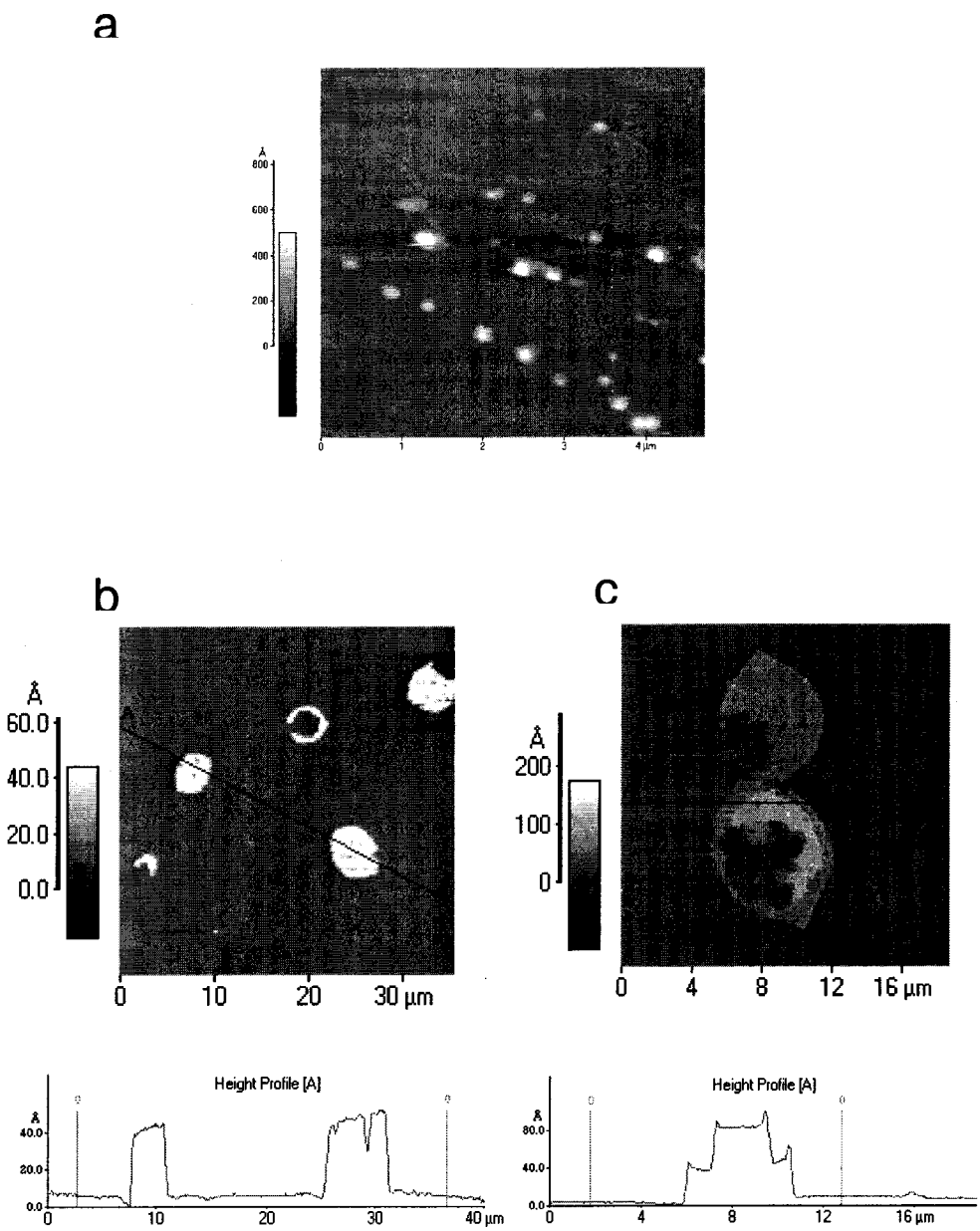

Figure 6.4 Aggregates and patterns of Fe(III)TPEGPP on ODS covered, hydrophobic surfaces. a) Self-organized structures are patterned into lines at the edge of the solvent boundary as it evaporates, b) and c) Self-reorganized, flattened discs of porphyrins found toward the center of the area covered by the solution results from the melding and reorganization of several nanoparticles; the contour plots are below.

6.3.3 Mechanisms for transformation of porphyrin nanoparticle on surfaces

Based on the observations above, we proposed the following mechanisms for the transformation of the colloidal nanoparticles upon surface deposition. The nanopartilces used in this work are composed of water soluble Fe(III)TPEGPP. It is expected that these molecules have much stronger affinity towards hydrophilic surfaces than hydrophobic surfaces. On hydrophilic surfaces, the observed small porphyrin aggregates result from the partial disassembly of the larger nanoparticles in solution, because the strong interactions between Fe(III)TPEGPP and the surface are greater than the various intermolecular forces holding the aggregate together. Preliminary density and cross-section studies indicate that the nanoparticles in solution are composed of sub-domains of up to a few hundred porphyrins, *i.e.* the nanoparticles are not optimally packed. If the interactions between sub-domains are weak, the reorganization of the nanoparticles upon removal of the solvent and surface deposition is likely.

The Brownian motion of nanoparticles and solution dynamics allow the particles to randomly collide into the surface. The nanoparticle then either resides on or bounces back from the surface. Because of the significant substrate-porphyrin interactions on hydrophilic surfaces, the sub-domain(s) that made contact with the surface are then pealed away from the nanoparticles as it moves across the surface (Figure 6.5). As the solvent evaporates and the solvent boundary recedes, the nanoparticles in solution have less room to move and are more likely to move along a direction perpendicular to the receding solvent front. In the latter case, nanoparticles may roll or be dragged on the surface, leaving trails of sub-domains behind. It is also possible that the directional

solvent flow can generate sheering forces that are strong enough to disaggregate the sub-domains in the nanoparticle (Figure 6.5b). The small porphyrin aggregates on the surface can undergo further transformations to maximize surface-molecule interactions, and if they are mobile, can re-organize by merging into disc-like structures. The radial distributions of smaller aggregates results from disaggregating nanoparticles and solvent dynamics. The tadpole-shaped assembly shown in Figure 6.3d may result from both lateral motion of nanoparticles and solvent spreading. Thus solvent flow during evaporation can dictate surface patterns. All of the structures of the final porphyrin aggregates on hydrophilic surfaces are stable in air for many weeks.

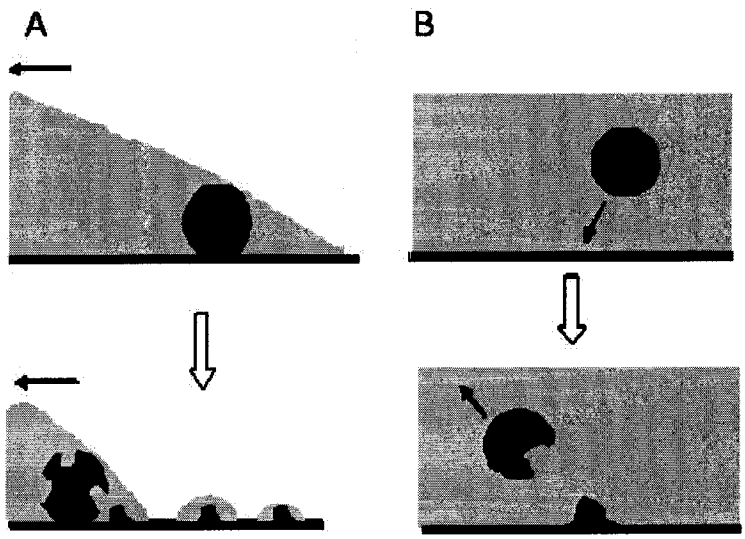

Figure 6.5 Proposed mechanisms for porphyrin nanopartice reorganization on UV-ozone treated hydrophilic surfaces involve a convolution of solution dynamics and Brownian motion. a) Processes dominated by solvent dynamics induce the deposition of sub-domains of porphyrin nanoparticles in linear arrays – in this case by the receding solvent front. b) Processes dominated by Brownian motion of nanoparticles and solvent induce a random deposition of porphyrin nanoparticles.

On hydrophobic surfaces, where the interaction between the Fe(III)TPEGPP nanoparticles and the ODS surface are significantly weaker, most of the large nanoparticles in solution retain their structure integrity upon deposition and solvent evaporation. Since most nanoparticles remain in solution and thus concentrate as the solvent dries, the nanoparticles are found to aggregate along the final lines of evaporation. Secondly, while the solvent slowly evaporates from the surface, the nanoparticles can reorganize to optimize the interaction between the porphyrin molecules, without competing surface-molecule interactions. These rearrangements are clearly indicated by the unique 4 nm thick by micron^2 disc structures formed on hydrophobic surface. Note that the final morphology the Fe(III)TPEGPP aggregates on either surface also depends on the rate of evaporation of the solvent. On hydrophilic surfaces, if the evaporation rate is fast, intermediate morphologies with larger average heights are observed.

6.4 Conclusions

In summary, the morphology of porphyrin nanoparticles on surfaces depends on the complex interplay between the forces holding the porphyrins together into sub-domains, the inter-sub-domain interactions, molecule-substrate interactions, and solution dynamics during evaporation. On hydrophilic surface, due to strong interaction between both the solvent and solute molecules with the surface, porphyrin nanoparticles disaggregate into smaller particles that may correspond to sub-domains in the nanoparticles. These smaller aggregates may, in turn, reorganize as the solvent evaporates. The circular assemblies of the small aggregates suggest the collapses of the solution-formed nanoparticles assisted by solvent spreading on the surface. Fluid dynamics on the micro and nanoscale can dictate the patterns observed on the surface. In contrast, these types of complex patterns of re-organized porphyrin nanoparticles are not observed on hydrophobic surfaces, whereon there is a greater degree of structural fidelity to the colloidal particles in solution, and only occasional nanoparticle reorganization into disc shaped structures. These considerations can be used in the formation of complex patterns of nanostructured materials on surfaces and suggests that the dynamics of controlled solvent evaporation[8,16,17] and flow can be exploited to reorganize, transport, and pattern nanomaterials of organic dyes.

Reference

Chapter I

1. Rubinstein, I.; Steinberg, S.; Tor, Y.; Shanzer, A.; Sagiv, J. Nature 1988, 332, 426.
2. Ulman, A. *Adv. Mater.* **1990**, 2, 573.
3. Ulman, A. *An Introduction to Ultrathin Organic Films*; Academic Press: Boston, 1991.
4. Zhao, B.; Brittain, W.J. *Prog. Polym. Sci.* **2000,** 25, 677.
5. Ulman, A.; *Chem. Rev.* **1996,** 96, 1533.
6. Bigelow, W. C.; Pickett, D. L.; Zisman, W. A. *J. Colloid Interface Sci.* **1946,** 1, 513.
7. Nuzzo, R. G.; Allara, D. L. *J. Am. Chem. Soc.* **1983,** 105, 4481
8. Smith, K. R.; Lewis, P. A.; Weiss, P. S *Prog. in Surf. Sci.* **2004,** 75, 1.
9. Zhao, B.; Brittain, W. J. *Macromolecules,* **2000**, *33*, 8813.
10. Shah, R. R.; Merreceyes, D.; Husemann, M.; Rees, I.; Abbott, N. L.; Hawker, C. J.; Hedrick, J. L. *Macromolecules* **2000** *33,* 597.
11. Zhao, B.; He, T. *Macromolecules* **2003**, *36*, 8599.
12. Tu, H.; Heitzman, C. E.; Braun, P. V.; *Langmuir* **2004,** *20,* 8313.
13. Allara, D. L.; Parikh, A. N.; Rondelez, F.; *Langmuir* **1995,** 11, 2357.
14. Parikh, A. N.; Schivley, M. A.; Koo, E.; Seshadri, K.; Aurentz, D.; Mueller, K.; Allara, D. L. *J. Am. Chem. Soc.* **1997,** 119, 3135.
15. Bain, C. D.; Troughton, Y. T.; Tao, Y. T.; Evall, J.; Whitesides, G. M.; Nuzzo, R. G. *J. Am. Chem. Soc.* **1989,** 111, 321.

16. Laibinis, P. E.; Fox, M. A.; Folkers, J. P.; Whitesides, G. M. *Langmuir,* **1991,** 7, 3167.

17. Allara, D. L.; Nuzzo, R. G. *Langmuir* **1985,** 1, 45.

18. Chaudhury, M. K.; Whitesides, G. M. *Science* **1992**, 256, 1539.

19. Silberzan, P.; Leger, L.; Ausserre, D.; Benattar, J. J. *Langmuir* **1991**, 7, 1647.

20. Tripp, C. P.; Hair, M. L. *Langmuir* **1992**, 8, 1120.

21. Angst, D. L.; Simmons, G. W. *Langmuir* **1991**, 7, 2236.

22. Wasserman, S. R.; Tao, Y. -T.; Whitesides, J. M. *Langmuir* **1989**, 5, 1074.

23. Brandriss, S.; Margel, S. *Langmuir* **1993**, *9,* 1232.

24. Prucker, O.; Ruhe, J. *Macromolecules* **1998,** 31, 592.

25. Dowson, D. *History of Tribology*; Longman: London, 1979.

26. Maboudian, R. *Surf. Sci. Rep.* **1998** 30, 207.

27. Binnig, G.; Quate, C. F.; Gerber, C. *Phys. Rev. Lett.* **1986**, 56, 930.

28. Bhushan, B.; Israelachvili, J. N.; Landman, U. *Nature* **1995**, 374, 607.

29. Krim, J. *Sci. Am.* **1996**, 275, 74.

30. *Fundamentals of Friction: Macroscopic and Microscopic Processes*; Singer, I. L., Pollock, H. M., Eds.; Kluwer: Dordrecht, 1992.

31. *Physics of Sliding Friction*; Persson, B. N. J., Tosatti, E., Eds.; Kluwer: Dordrecht, 1996.

32. Frisbie, C. D.; Rozsnyai, L. F.; Noy, A.; Wrighton, M. S.; Lieber, C. M. *Science* **1994**, 265, 2071.

33. Xiao, X.-D.; Hu, J.; Charych, D. H.; Salmeron, M. *Langmuir* **1996**, 12, 235.

34. Marti, A.; Hahner, G.; Spencer, N. D. *Langmuir* **1995**, 11, 4632.

35. Johnson, K. L.; Kendall, K.; Roberts, A. D. *Proc. R. Soc. London A* **1971**, 324, 301.

36. Hadziioannou, G.; Patel, S.; Granick, S.; Tirrel, M. J. Am. Chem. Soc. 1986, 108, 2869.

37. Dan, N.; Tirrell, M. *Macromolecules* **1993,** 26, 4310.

38. Belder, G. F.; ten Brinke, G.; Hadziioannou, G. *Langmuir* **1997,** 13, 4102.

39. Yerushalmi-Royen, R.; Klain, J.; Fetters, L. *Science* **1994,** 263, 793.

40. Reiter, G. *Europhys. Lett.* **1996,** 33, 29.

41. Jordan, R.; Graf, K.; Riegler, H.; Unger, K. K. *J. Chem. Soc. Chem Commun.* **1996,** 9, 1025.

42. Tsubokawa, N.; Hosoya, M..; Yanadori, K.; Sone, Y. J. *Macromol. Sci. Chem.* **1990,** A27, 445.

43. Ben Ouada, H.; Hommel, H.; Legrand, A. P.; Balard, H.; Papirer, E. *J. Colloid Interface Sci.* **1994,** 122, 441.

44. Sun, F.; Grainger, D. W.; Castner, D. G.; Leach-Scampavia, D. K. *Macromolecules* **1994,** 27, 3053.

45. von Werne, T.; Patten, T. E. *J. Am. Chem. Soc.* **2001,** 123, 7497.

46. Kong, H.; Gao, C.; Yan, D. *J. Am. Chem. Soc.* **2004,** 126, 412.

47. Yao, Z.; Braidy, N.; Botton, G. A.; Adronov, A. *J. Am. Chem. Soc.* **2003,** 125 16015.

48. Prucker, O.; Ruhe, J. *Macromolecules* **1998,** 31, 592.

49. Huang, X.; Wirth, M. J. *Anal. Chem.* **1997,** 69, 45477.

50. Kong, X.; Kawai, T.; Abe, J.; Iyoda, T. *Macromolecules* **2001,** 34, 1837.

51. Boven G.; Folkersma R.; Challa G.; Schouten A. *J. Polym. Commun.* **1991,** 32, 50.

52. Jordan, R.; Ulman, A.; Kang, J. F.; Rafailovich, M. H.; Sokolov, J. *J. Am. Chem. Soc.* **1999,** 121, 1016.

53. Zhou, Q.; Fan, X.; Xia, C.; Mays, J.; Advincula, R. *Chem. Mater.* **2001,** 13, 2465.

54. Zhao, B.; Brittain, W. J. *Macromolecules* **2000,** 33, 342.

55. Zhao, B.; Brittain, W. J. *J. Am. Chem. Soc.***1999,** 121 3557.

56. Husseman, M.; Malmstrom, E. E.; McNamara, M.; Mate, M.; Mecerreyes, D.; Benoit, D. G.; Hedrick, J. L.; Mansky, P.; Huang, E.; Russell, T. P.; Hawker, C. J. *Macromolecules* **1999,** 32, 1424.

57. Otsu, T.; Yoshida, M.; Makromol. Chem., Rapid Commun. **1982,** 3, 127.

58. Patten, T. E.; Xia, J.; Abernathy, T.; Matyjaszewski, K. *Science* **1996,** 272, 866.

59. Matyjaszewski, K.; Xia, J. *Chem. Rev.* **2001,** 101, 2921.

60. Kamigaito, M.; Ando, T.; Sawamoto, M. *Chem. Rev.* **2001,** 101, 3689.

61. Fischer, H. *Chem. Rev.* **2001,** 101, 3581.

62. Matyjaszewski, K.; Miller, P. J.; Shukla, N.; Immaraporn, B.; Gelman, A.; Luokala, B. B.; Siclovan, T. M.; Kickelbick, G.; Vallant, T.; Hoffmann, H.; Pakula, T. M*acromolecules* **1999,** 32, 8716.

63. Matyjaszewski, K.; Ziegler, M. J.; Arehart, S. V.; Greszta, D.; Pakula, T. *J. Phys. Org. Chem.* **2000**, 13, 775.

64. Wang, J. S.; Matyjaszewski, K. *J. Am. Chem. Soc.* **1995**, 117, 5614.

65. Matyjaszewski, K.; Wang, J. S. WO Pat. 9630421, U.S. Pat. 5,763,548.

66. Mandal, T. K.; Fleming, M. S.; Walt, D. R. *Nano Lett.* **2002**, 2, 3.

67. Jones, D. M.; Huck, W. T. S. *Adv. Mater.* **2001,** 13, 1256.

68. Jones, D. M.; Smith, J. R.; Huck, W. T. S.; Alexander, C. *Adv. Mater.* **2002,** 1130

69. Huang, W.; Kim, J.-B.; Bruening, M. L.; Baker, G. L. *Macromolecules* **2002,** 35, 1175.

70. Kim, J.-B.; Huang, W.; Bruening, M. L.; Baker, G. L. *Macromolecules* **2002,** 35 5410.

71. Osborne, V. L.; Jones, D. M.; Huck, W. T. S. *Chem. Commun.* **2002,** 1838.

72. W. Huang, W.; Baker, G. L.; Bruening, M. L. *Angew. Chem. Int. Ed.* **2001,** 40, 1510.

73. Lee, S. B.; Koepsel, R. R.; Morley, S. W.; Matyjaszewski, K.; Sun, Y.; Russell, A. *Biomacromolecules,* **2004,** 5, 877.

74. Sun, T.; Wang, G.; Feng, L.; Liu, B.; Ma, Y.; Jiang, L.; Zhu, D. 2004, 43, 357.

75. Zhao, B.; Brittain, W. J.; Zhou, W.; Cheng, S. Z. D. *Macromolecules* **2000,** 33, 8821.

76. Ruardy, T. G.; Schakenraad, J. M.; van der Mei, H. C.; Busscher, H. *J. Surf. Sci. Rep.* **1997,** 29, 1.

77. Genzer, J.; Kramer, E. J. *Europhys. Lett.* **1998,** 44, 180.

78. Bhat, R. R.; Fisher, D. A.; Genzer, J. *Langmuir* **2002,** 18, 5460.

79. Genzer, J. "Molecular gradients: Formation and application in soft condensed matter science", Encyclopedia of Materials Science, Elsevier, Oxford, **2002.**

80. Tomlinson, M. R.; Genzer, J. *Macromolecule* **2003**, 36, 3449.

81. Wu, T.; Efimenko, K.; Genzer, J. *J. Am. Chem. Soc.* **2002,** 124, 9394.

82. Tomlinson M. R.; Genzer, J. *Chem. Commun.* 2003, 12, 1350.

Zhao, B. *Langmuir* **2004,** 20, 11748

Chapter II

1. Jost, H.P.; *Wear* **1990** *136,* 1.
2. Carpick, R.W.; Salmeron, M.; *Chem. Rev.* **1997** *97,* 1163.
3. Maboudian, R.; *Surf. Sci. Rep.* **1998** *30,* 207.
4. Maboudian, R.; Ashurst, W.R.; Carraro, C.; *Sensors and Actuators A* **2000** *82,* 19
5. Frisbie, C. D.; Rozsnyai, L. F.; Noy, A.; Wrighton, M. S.; Lieber, C. M. *Science* **1994**, *265*, 2071.
6. Overney, R. M.; Meyer, E.; Frommer, J.; Brodbeck, D.; Luthi, R.; Howald, L.; Guntherodt, H.-J.; Fujihara, M.; Takano, H.; Gotoh, Y. *Nature* **1992**, *359*, 133.
7. Meyer, E.; Howald, L.; Overney, R.; Brodbeck, D.; Luthi, R.; Haefke, H.; Frommer, J.; Guntherodt, H.-J. *Ultramicroscopy* **1992**, *42*-44, 274.
8. Meyer, E.; Overney, R.; Luthi, R.; Brodbeck, D.; Howald, L.; Frommer, J.; Guntherodt, H.-J.; Wolter, O.; Fujihira, M.; Takano, H.; Gotoh, Y. *Thin Solid Films* **1992**, *220*, 132.
9. Overney, R. M.; Meyer, E.; Frommer, J.; Guntherodt, H. J. *Langmuir* **1994**, *10*, 1281.
10. Overney, R. M.; Leta, D. P. *Tribol. Lett.* **1995**, *1*, 247.
11. Greenwood, J.A.; Williamson, J.B.P.; *Proc. Roy. Soc. Lond. A* **1966** *295,* 300.
12. Komvopoulous, K.; *Wear* **1996** *200,* 305.
13. Wei, Z.; Wang, C.; Bai, C. *Langmuir* **2001,** *17,* 3945-3951.
14. Grinevich, O.; Mejiritski, A.; Neckers, D. C. *Langmuir* **1999**, *15*, 2077.

15. Tsukruk, V. V.; Bliznyuk, V. N. *Langmuir* **1998**, *14*, 446.

16. Ton-That, C.; Campbell, P. A.; Bradley, R. H. *Langmuir* **2000**, *16*, 5054.

17. Tsukruk, V. V.; Bliznyuk, V. N.; Wu, J.; Visser, D. W. *Polym. Prepr. (Am. Chem. Soc., Div. Polym. Chem.)* **1996**, *37*, 575.

18. Ito, T.; Madoka, N.; Buhlmann, P.; Umezawa, Y. *Langmuir* **1997**, *13*, 4323.

19. Nakagawa, T.; Ogawa, K.; Kurumizawa, T. *J. Vac. Sci. Technol., B* **1994**, *12*, 2215.

20. Nakagawa, T.; Ogawa, K.; Kurumizawa, T.; Ozaki, S. *Jpn. J. Appl. Phys.* **1993**, *32*, L294.

21. Nakagawa, T. *Jpn. J. Appl. Phys.* **1997**, *36*, L162.

22. Barrat, A.; Silberzan, P.; Bourdieu, L.; Chatenay, D. *Europhys. Lett.* **1992**, *20*, 63

Chapter III

1. Prucker, O.; Ruhe, J., *Macromolecules* **1998,** *31*, 592-601.

2. Jordan, R.; Ulman, A., *J. Am. Chem. Soc.* **1998,** *120*, 243-247.

3. Zhao, B.; Brittain, W. J., *Progress in Polymer Science* **2000,** *25*, 677-710.

4. Jordan, R.; Ulman, A.; Kang, J. F.; Rafailovich, M. H.; Sokolov, J., *J. Am. Chem. Soc.* **1999,** *121*, 1016-1022.

5. Juang, A.; Scherman, O. A.; Grubbs, R. H.; Lewis, N. S., *Langmuir* **2001,** *17*, 1321-1323.

6. Matyjaszewski, K.; Miller, P. J.; Shukla, N.; Immaraporn, B.; Gelman, A.; Luokala, B. B.; Siclovan, T. M.; Kickelbick, G.; Vallant, T.; Hoffmann, H.; Pakula, T., *Macromolecules* **1999,** *32*, 8716-8724.

7. Huang, X.; Wirth, M. J., *Macromolecules* **1999,** *32*, 1694-1696.

8. Husseman, M.; Malmstrom, E. E.; McNamara, M.; Mate, M.; Mecerreyes, D.; Benoit, D. G.; Hedrick, J. L.; Mansky, P.; Huang, E.; Russell, T. P.; Hawker, C. J., *Macromolecules* **1999,** *32*, 1424-1431.

9. Patten, T. E.; Xia, J. H.; Abernathy, T.; Matyjaszewski, K., *Science* **1996,** *272*, 866-868.

10. Matyjaszewski, K.; Patten, T. E.; Xia, J. *J. Am. Chem. Soc.* **1997,** *119*, 674-680.

11. Patten, T. E.; Matyjaszewski, K., *Adv. Mater.* **1998,** *10*, 901-915.

12. Harrison, C.; Chaikin, P. M.; Huse, D. A.; Register, R. A.; Adamson, D. H.; Daniel, A.; Huang, E.; Mansky, P.; Russell, T. P.; Hawker, C. J.; Egolf, D. A.; Melnikov, I. V.; Bodenschatz, E., *Macromolecules* **2000,** *33*, 857-865.

13. Huang, E.; Pruzinsky, S.; Russell, T. P.; Mays, J.; Hawker, C. J., *Macromolecules* **1999,** *32*, 5299-5303.

14. Mansky, P.; Russell, T. P.; Hawker, C. J.; Pitsikalis, M.; Mays, J., *Macromolecules* **1997,** *30*, 6810-6813.

15. Wu, T.; Efimenko, K.; Genzer, J., *J. Am. Chem. Soc.* **2002,** *124*, 9394-9395.

16. Wu, T.; Efimenko, K.; Vlcek, P.; Subr, V.; Genzer, J., *Macromolecules* **2003,** *36*, 2448-2453.

17. Tomlinson, M. R.; Genzer, J., *Macromolecules* **2003,** *36*, 3449-3451.

18. Tomlinson, M. R.; Genzer, J., *Chem. Comm.* **2003,** *12*, 1350-1351.

19. Kenis, P. J. A.; Ismagilov, R. F.; Takayama, S.; Whitesides, G. M.; Li, S.; White, H. S., *Acc. Chem. Res.* **2000,** *33*, 841-847.

20. Junker, D.; Schmid, H.; Bernard, A.; Caelen, I.; Michel, B.; Rooij, N.; Delamarche, E., *J. Micromech. Microeng.* **2001,** *11*, 532.

21. Kenis, P. J. A.; Ismagilov, R. F.; Whitesides, G. M., *Science* **1999,** *285*, 83-85.

22. Feldmann, A.; Claussnitzer, U.; Otto, M., *J. Chromatogr., B* **2004**, *803*, 149-157.

23. Huang, W. X.; Kim, J. B.; Bruening, M. L.; Baker, G. L., *Macromolecules* **2002,** *35*, 1175-1179.

24. Jones, D. M.; Huck, W. T. S., *Adv. Mater.* **2001,** *13*, 1256-1259.

25. Harrison, C.; Cabral, J. T.; Stafford, C. M.; Karim, A.; Amis, E. J. *J. Micromech. Microeng.* **2004,** 14, 1563-158.

26. Bird, R.B.; Stewart, W.E.; Lightfoot, E.N. *Transport Phenomena* John Wiley & Sons, New York, **1960**.

27. Xia, Y. N.; Whitesides, G. W. *Angew. Chem. Int. Ed.* **1998,** 37, 550-575.

Chapter IV

1. T. Sun, G. Wang, L. Feng, B. Liu, Y. Ma, L. Jiang, D. Zhu *Angew. Chem. Int. Ed.* **2004,** 43, 357-360

2. U. Raviv, S. Glasson, N. Kampf, J. Gohy, R. Jérôme, J. Klein *Nature,* **2003,** 425, 163-165

3. H. Ma, J. Hyun, P. Stiller, A. Chilkoti *Adv. Mater.* **2004,** 16, 338-341

4. O. Prucker, J. Ruhe *Langmuir* **1998**; *14,* 6893-6898.

5. K. Matyjaszewski, P. J. Miller, N. Shukla, B. Immaraporn, A. Gelman, B. B. Luokala, T. M. Siclovan, G. Kickelbick, T. Vallant, H. Hoffmann, T. Pakula *Macromolecules* **1999,** 32, 8716-8724.

6. B. Zhao, W. J. Brittain *Macromolecules*, 2000, **33**, 342–348.

7. R. Jordan, A. Ulman, M. H. Rafailovick, J. Sokolov *J. Am. Chem.Soc.*, 1999, **121**, 1016–1022.

8. A. Juang, O. A. Scherman, R. H. Grubbs, N. S. Lewis *Langmuir* **2001,** 17, 1321-1323. 1265–1269.

9. K. Matyjaszewski, J. Xia, *Chem. Rev.* **2001**; *101*(9); 2921-2990.

10. P. Mansky, Y. Liu, E. Huang, T. P. Russell, C. Hawker *Science* **1997,** 275, 1458-1460

11. B. Zhao, W. J. Brittain *Macromolecules* **2000,** 33, 8813-8820

12. J-B. Kim, W. Huang, M. L. Bruening, G. L. Baker, *Macromolecules* **2002,** 5410-5416

13. B. Zhao, W. J. Brittain, W. Zhou, S. Z. D. Cheng *J. Am. Chem. Soc.* **2000,** 122, 2407-2408

14. B. Zhao, W. J. Brittain, W. Zhou, S. Z. D. Cheng *Macromolecules* **2000,** 33, 8821-8827

15. S. G. Boyes, W. J. Brittain, X, Weng, S. Z. D. Cheng *Macromolecules* **2002,** 35, 4960-4967

16. W. Huang, J-B. Kim, G. L. Baker, M. L. Bruening *Nanotechnology* **2003,** 14, 1075-1080

17. G. T. Pickette *J. Chem. Phys.* 2003, 118, 3898-3903

18. K. A. Davis, K. Matyjaszewski *Adv. in Poly. Sci.* 2002, 29, 1-157

19. Jones, D. M.; Huck, W. T. S. *Adv. Mater.* **2001,** 13, 1256.

20. J. Brandrup, E. H. Immergut, E. A. Grulke, *Polymer Handbook, 4th Edition,* Wiley-Interscience, 1999.

Chapter V

1. Halperin, A.; Tirrell, M.; Lodge, T. P. *Adv. Polym. Sci.* **1991**, *100*, 31-71.
2. Sanchez, I. C. *Physics of Polymer Surfaces and Interfaces*; Butterworth: London, 1992.
3. Alexander, S. *J. Phys. (Paris)* **1977**, *38*, 977.
4. Zhao, B.; Brittain, W.J. *Prog. Polym. Sci.* **2000,** *25,* 677-710.
5. Matyjaszewski, K.; Xia, J. *Chem. Rev.* **2001,** *101,* 2921-2990.
6. Matyjaszewski, K.; Miller, P. J.; Shukla, N.; Immaraporn, B.; Gelman, A.; Luokala, B. B.; Siclovan, T. M.; Kickelbick, G.; Vallant, T.; Hoffmann, H.; Pakula, T. M*acromolecules* **1999,** *32,* 8716-8724.
7. Huang, X.; Wirth, M. J. *Macromolecules* **1999**, *32*, 1694-1696.
8. Prucker, O.; Ruhe, J. *Macromolecules* **1998**, *31*, 592-601.
9. Jordan, R.; Ulman, A. *J. Am. Chem. Soc.* **1998**, *120*, 243-247.
10. Zhao, B.; Brittain, W. J. *Prog. Polym. Sci.* **2000**, *25*, 677-710.
11. Jordan, R.; Ulman, A.; Kang, J. F.; Rafailovich, M. H.; Sokolov, J. *J. Am. Chem. Soc.* **1999**, *121*, 1016-1022.
12. Juang, A.; Scherman, O. A.; Grubbs, R. H.; Lewis, N. S. *Langmuir* **2001**, *17*, 1321-1323.

13. Husseman, M.; Malmstrom, E. E.; McNamara, M.; Mate, M.; Mecerreyes, D.; Benoit, D. G.; Hedrick, J. L.; Mansky, P.; Huang, E.; Russell, T. P.; Hawker, C. J. *Macromolecules* **1999**, *32*, 1424-1431.

14. Zhao, B.; Brittain, W. J. *J. Am. Chem. Soc.* **1999**, *121*, 3557-3558.

15. Xu, C.; Wu, T.; Drain, C. M.; Batteas, J. D.; Beers, K. L. *Polym. Preprints* **2004,** *45,* 677-688.

16. Boyes, S. G.; Brittain, W. J.; Weng, X.; Cheng, S. Z. D. *Macromolecules* **2002**, *35*, 4960-4967.

17. Kim, J.-B.; Huang, W.; Bruening, M. L.; Baker, G. L. *Macromolecules* **2002**, *35,* 5410-5416.

18. Zhao, B.; Brittain, W. J.; Zhou, W.; Cheng, S. Z. D.; *J. Am. Chem. Soc.* **2000,** *122,* 2407-2408.

19. Wu, T.; Efimenko, K.; Genzer, J. *J. Am. Chem. Soc.* **2002**, *124,* 9394-9395.

20. Wu, T.; Efimenko, K.; Vlcek, P.; Subr, V.; Genzer, J. *Macromolecules* **2003**, *36,* 2448-2453.

21. Pik Yin Lai, Avi Halperin *Macromolecules* **1992,** *25,* 6693-6695.

22. Roters, A.; Schimmel, M.; Ruhe, J.; Johannsmann, D. *Langmuir* **1998,** *14,* 3999-4004.

23. Liu, G.; Zhang, G. *J. Phys. Chem. B.* **2005,** *109,* 743-747.

24. Yim, H.; Kent, M. S.; Huber, D. L.; Satija, S.; Majewski, J.; Smith, G. S. *Macromolecules* **2003,** *36,* 5244-5251.

25. Tu, H.; Heitzman, C. E.; Braun, P. V. *Langmuir* **2004,** *20,* 8313-8320.

26. Kaholek, M.; Lee, W.-K.; LaMattina, B.; Caster, K. C.; Zauscher, S. *Nano Lett.* **2004**, *4*, 373-376.

27. Zhu, X.; DeGraaf, J.; Winnik, F. M.; Leckband, D. *Langmuir* **2004,** *20,* 1459-1465.

28. E.P.K. Currie, A.B. Sieval, G.J. Fleer, M.A. Cohen Stuart, *Langmuir* **2000**, *16,* 8324-8333.

29. Jandeleit, B.; Schaefer, D. J.; Powers, T. S.; Turner, H. W.; Weinberg, W. H. *Angew. Chem., Int. Ed.* **1999**, *38,* 2494-2532.

30. Meredith, J. C.; Karim, A.; Amis, E. J. *MRS Bull.* **2002**, *27,* 330-335.

31. Crosby, A. J. *J. Mater. Sci.* **2003**, *38,* 4439-4449.

32. Ionov, L.; Houbenov, N.; Sidorenko, A.; Stamm, M.; Luzinov, I.; Minko, S. *Langmuir* **2004,** *20,* 9916-9919.

33. Zhao B. *Langmuir* **2004,** *20,* 11748-11755.

34. Tomlinson, M. R.; Genzer, J. *Macromolecules* **2003**, *36,* 3449-3451.

35. Xu, C.; Wu, T.; Drain, C. M.; Batteas, J. D.; Beers, K. L. unpublished results

36. Tomlinson, M. R.; Genzer, J. *Chem. Commun.* **2003**, *12,* 1350-1351.

37. Lee, S. B.; Russell, A. J.; Matyjaszewski, K. *Biomacromolecules* **2003,** *4* 1386-1393.

38. Xu, C.; Wu, T.; Drain, C. M.; Batteas, J. D.; Beers, K. L. *Macromolecules* **2005,** *38*, 6-8.

39. Cassie, A. *Discuss. Faraday Soc.* **1948**, 3, 11.

Chapter VI

1. C. M. Drain, I. Goldberg, I. Sylvain, A. Falber, *Topics in Current Chemistry* **2004**, *245*, 55–88.
2. C. M. Drain, X. Chen., in *Encyclopedia of Nanoscience & Nanotechnology, Vol. 9* (Ed.: H. S. Nalwa), American Scientific Press, New York, **2004**, pp. 593-616.
3. C. M. Drain, G. Smeareanu, J. Batteas, S. Patel, in *Dekker Encyclopedia of Nanoscience and Nanotechnology, Vol. 5* (Eds.: J. A. Schwartz, C. I. Contescu, K. Putyera), Marcel Dekker, Inc., New York, **2004**, pp. 3481-3502.
4. T. Milic, J. C. Garno, G. Smeureanu, J. D. Batteas, C. M. Drain, *Langmuir* **2004**, *20*, 3974-3983.
5. C. M. Drain, T. Milic, J. C. Garno, G. Smeureanu, J. D. Batteas, *ACS Polymer Reprints* **2004**, *45*, 346-347.
6. C. Nitschke, S. M. O'Flaherty, M. Kroll, W. J. Blau, *J. Phys. Chem. B* **2004**, *108*, 1287-1295.
7. C. Li, J. Ly, B. Lei, W. Fan, D. H. Zhang, J. Han, M. Meyyappan, M. Thompson, C. W. Zhou, *J. Phys. Chem. B* **2004**, *108*, 9646-9649.
8. C. Jeukens, M. C. Lensen, F. J. P. Wijnen, J. Elemans, P. C. M. Christianen, A. E. Rowan, J. W. Gerritsen, R. J. M. Nolte, J. C. Maan, *Nano Letters* **2004**, *4*, 1401-1406.
9. C. Nitschke, S. M. O'Flaherty, M. Kroell, A. Strevens, S. Maier, M. G. Ruether, W. J. Blau, *Proc. SPIE* **2003**, *4991*, 124-132.
10. E. Iengo, E. Zangrando, E. Alessio, *Eur. J. Inorg. Chem.* **2003**, *2003*, 2371-2384.
11. S. I. Stupp, M. U. Pralle, G. N. Tew, L. Li, M. Sayar, E. R. Zubarev, *MRS Bull.* **2000**, 42-48.

12. C. M. Drain, *Proc. Natl. Acad. Sci., USA* **2002**, *99*, 5178-5182.

13. C. M. Drain, J. D. Batteas, G. W. Flynn, T. Milic, N. Chi, D. G. Yablon, H. Sommers, *Proc. Natl. Acad. Sci., USA* **2002**, *99*, 6498-6502.

14. S. Leininger, B. Olenyuk, P. J. Stang, *Chem. Rev.* **2000**, *100*, 853-908. Self-assembly of discrete cyclic nanostructures mediated by transition metals

15. X. Gong, T. Milic, C. Xu, J. D. Batteas, C. M. Drain, *J. Am. Chem. Soc.* **2002**, *124*, 14290-14291.

16. . R. L. P. N. Jeukens, F. J. P. Wijnen, J. A. A. W. Elemans, P. C. M. Christianen, A. E. Rowan, J. W. Gerritsen, R. J. M. Nolte, J. C. Maan, *Nano Lett.* **2004**, *4*, 1401-1406.

17. M. C. Lensen, K. Takazawa, J. Elemans, C. Jeukens, P. C. M. Christianen, J. C. Maan, A. E. Rowan, R. I. M. Nolte, *Chem . Eur. J.* **2004**, *10*, 831-839.